ADAPTIVE RESOURCE ALLOCATION STRATEGIES

FOR DYNAMIC HETEROGENEOUS TRAFFIC

IN TD-CDMA/TDD SYSTEMS

By

RAJPAMAL R. PETHURAJ

Bachelor of Engineering
Bharathiar University
Coimbatore, India
1999

Master of Science
Oklahoma State University
Stillwater, Oklahoma
2001

Submitted to the Faculty of the Graduate College of the
Oklahoma State University in partial fulfillment of
the requirements for the Degree of
DOCTOR OF PHILOSOPHY
May, 2006

ADAPTIVE RESOURCE ALLOCATION STRATEGIES

FOR DYNAMIC HETEROGENEOUS TRAFFIC

IN TD-CDMA/TDD SYSTEMS

Dissertation Approved:

Dr. Jong-Moon Chung

Dissertation Adviser

Dr. Keith A. Teague

Dr. Charles F. Bunting

Dr. Louis G. Johnson

Dr. David B. Pratt

Dr. Gordon A. Emslie

Dean of the Graduate College

PREFACE

The radio frequency spectrum for commercial wireless applications has become an expensive commodity. So, radio access techniques are required that enable efficient exploitation of these resources. A flexible air-interface that provides good spectral efficiency is also needed. The nature of the emerging multimedia traffic consists of different classes and each class has its own quality-of-service (QoS) where the bandwidth between uplink and downlink is asymmetric and dynamic. Time division duplex (TDD) is preferred to frequency division duplex (FDD) with regard to applications in which the traffic in the transmission and reception directions is asymmetric. FDD and static time division duplex (S-TDD) may result in poor frequency utilization in these cases as the transmission bandwidth is fixed in both modes. But dynamic time division duplex (D-TDD) can support dynamic and asymmetric traffic by adapting its transmission bandwidth according to the traffic variations. This is one of the unique features of D-TDD systems. But this unique feature is also the cause of one the serious problems in D-TDD systems, namely, interference. A D-TDD system is subject to severe interference from the co-channel cells that are in downlink transmission when the reference cell is in uplink reception. The statistical multiplexing gain that can be achieved due to the unique feature of D-TDD may not be achieved due to the interference.

Code division multiple access (CDMA) is an efficient multi-user access system in a cellular system. If D-TDD is combined with CDMA, the additional interference due to D-TDD proves to be a very significant issue of consideration. This problem can be solved

if a hybrid time division duplex access (TDMA)/CDMA (TD-CDMA) air interface is used as this TDMA component provides an additional degree of freedom that can be used to avoid interference. But, to reduce interference, dynamic channel allocation (DCA) algorithms are required in place of fixed channel allocation (FCA) algorithms. Interference can also be reduced by making use of sectored antennas and spatial filters at the base station (BS) and mobile station (MS) sites.

In [1] it was shown that significant reduction in interference and corresponding increase in the capacity of TD-CDMA/TDD systems can be achieved by making use of a centralized DCA algorithm called the time slot (TS)-opposing algorithm.

In [3], the signal-to-interference ratio (SIR) outage probability of a TDMA/D-TDD system employing omni-directional and smart antennas at the BS and MS sites was studied. It was seen that the performance of the system degraded rapidly when the boundary between the uplink and downlink duty cycles was made variable. The usage of smart antennas gave promising results in suppressing the interference and improving the performance.

TS allocation algorithms that are part of DCA algorithms were proposed in [5] to reduce the interference in TDMA/D-TDD systems.

The TS-opposing algorithm, from [1], used in TD-CDMA/D-TDD systems to reduce interference, is reviewed as part of the background study for this research. The performance of D-TDD in TDMA systems is analyzed next. Initially omni-directional antennas are used both at the BS and MS sites and the dynamic boundary between the uplink and downlink is varied. It will be seen that the SIR outage increases as the number of extra uplink TSs in the reference cell increases. Then, sectored antennas will be used at

the BS and MS sites to suppress the interference. The use of sectored antennas reduces the interference but a large amount of sectors might be needed to achieve a significant reduction in interference. This can be alleviated by making use of time slot allocation algorithms. The *Max* {SIR} algorithm from [5] is combined with sectored antennas and a significant reduction in interference and hence an improvement in performance can be obtained for a lesser number of sectors. In this dissertation, we extend the *Max* (SIR) algorithm and apply it to a multi-cell environment. We call this algorithm the extended *Max* {SIR} algorithm. This algorithm co-ordinates the information from all the cells present in the system to assign the best mobile station to the extra uplink time slot. Also, an analytical model of SIR in D-TDD systems is derived.

In order to conduct a realistic analysis, a real Ethernet data model has to be applied. Ethernet data and wireless data were found to be highly self-similar [16], [17], and [28]. Also, wireless data services have asymmetrical traffic in the transmission and reception directions. This self-similar and asymmetrical data is obtained from [34] and [35]. The data traffic from [34] and [35] was shown to be self-similar in [16] and [21] respectively. The exact distribution of traffic might be hard to obtain and hence [53] made use of simple truncated Gaussian traffic model to study the effects of traffic dynamics between uplink and downlink on the spectral efficiency in TDD systems.

The data set from [34] and [35] is proven to be self-similar. The traffic is then modeled to follow the simple truncated Guassian model and the spectral efficiency of the S-TDD and D-TDD modes under this modeling is studied and compared. In this dissertation, the dataset from [34] is modeled using ON-OFF traffic modeling. The

modeled ON-OFF traffic is applied to a D-TDD system employing the *Max* {SIR} algorithm and the results obtained were comparable to the simulation results.

ACKNOWLEDGMENTS

I wish to express my deep and sincere thanks and gratitude to my advisor Dr. Jong-Moon Chung for his supervision, support, critical suggestions, and inspiration without whom this dissertation would not have been possible. . My appreciation and thanks are also due to my committee members, Dr. Charles F. Bunting, Dr. Louis G. Johnson, and Dr. David B. Pratt for their invaluable support, assistance, encouragement and guidance throughout my graduate studies here at Oklahoma State University.

I would like to thank the Advanced Communication Systems Engineering Laboratories (ACSEL) at the Oklahoma State University for supporting resources. I would like to thank my group members for their contribution. I would also like to thank other members of the ACSEL laboratories for their recommendations and support and my friends who made my dissertation work an enjoyable and pleasant one.

Finally, I would like to thank my parents and my sister for their support and encouragement.

TABLE OF CONTENTS

Chapter Page

LIST OF TABLES

Table Page

LIST OF FIGURES

Figure Page

Figure Page

Figure Page

NOMENCLATURE

3G	Third Generation
AP	Access Point
ATM	Asynchronous Transfer Mode
BCA	Borrowing Channel Assignment
BS	Base Station
CB	Common Band
CCI	Co-Channel Interference
CDMA	Code Division Multiple Access
CIR	Carrier Power to Interference Power Ratio
CTMC	Continuous Time Markov Chain
DCA	Dynamic Channel Allocation
DD	Decorrelating Detector
DL	Downlink
D-TDD	Dynamic-Time Division Duplex
DTMC	Discrete Time Markov Chain
FCA	Fixed Channel Allocation
FDD	Frequency Division Duplex
FDMA	Frequency Division Multiple Access
HPBW	Half Power Beam Width
IMT	International Mobile Telecommunications

IP	Internet Protocol
IT	Information Technology
LAN	Local Area Network
MLS	Maximum Likelihood Sequence
MMSE	Minimum Mean Squared Error
MP	Maximum Packing
MPEG-4	Motion Picture Experts Group -4
MS	Mobile Station
MUD	Multi-User Detection
PDF	Probability Density Function
PE	Polynomial Expansion
PSTN	Public Switched Telephone Network
QoS	Quality of Service
RF	Radio Frequency
RNC	Radio Network Controller
SDMA	Space Division Multiple Access
SIR	Signal Power to Interference Power Ratio
SNR	Signal Power to Noise Power Ratio
S-TDD	Static Time Division Duplex
TD-CDMA	Time Division Multiple Access/Code Division Multiple Access
TD-CDMA/D-TDD	TD-CDMA/Dynamic-TDD
TD-CDMA/TDD	TD-CDMA /Time Division Duplex
TDD	Time Division Duplex

TDMA	Time Division Multiple Access
TS	Time Slot
TSA	Time Slot Allocation
UMTS	Universal Mobile Telecommunication System
UL	Uplink
VoD	Video on Demand
WCDMA	Wideband CDMA
WWW	World Wide Web
ZF-DF	Zero Forcing-Decision Feedback

1 INTRODUCTION

1.1 Motivation

The last decade of the 20th century and the first several years of the 21st century have been characterized by the digital revolution. During these years, the computer and wireless information technology (IT) have emerged as a mass product and has led to the tremendous growth of the Internet. The various types of Internet services that require high data rates like video conferencing and transfer of huge multimedia (movie, or TV programs) files have been supported by the wired Internet while integrated packet, voice and data services are offered by wireless IT systems accessing the Internet [5]. During this current ongoing third generation (3G) of mobile communication, the efforts are concentrated on supporting high quality integrated data and voice services [26].

The popularity of wired Internet services has ignited the demand for broadband services. As the need for broadband digital video and audio grows, the demand on broadband access from subscribers is expected to increase manifold in both the wired and wireless networks [5], [26].

The traffic in broadband applications consists of different classes and these classes can be characterized roughly into two different groups: delay sensitive and delay tolerant data traffic. The delay sensitive traffic has static bandwidth requirements for uplink and downlink transmission on an average sense and the delay constraint at the reception of information requires a strict resource allocation strategy to guarantee the

quality-of-service (QoS) requirements. The delay tolerant traffic, on the other hand, is bursty and has asymmetric bandwidth requirements in the uplink and downlink directions. When wireless networks deliver the integrated traffic, the spectral efficiency might be poor when the bandwidth between the uplink and downlink transmissions is fixed.

Figure 1-1 shows the communication between a wireless access network and an Internet Protocol (IP) backbone network. The mobile hosts (cell phones and hand-held computers) within the cells communicate with the access points (APs) which in turn communicate with the edge nodes of the IP backbone network.

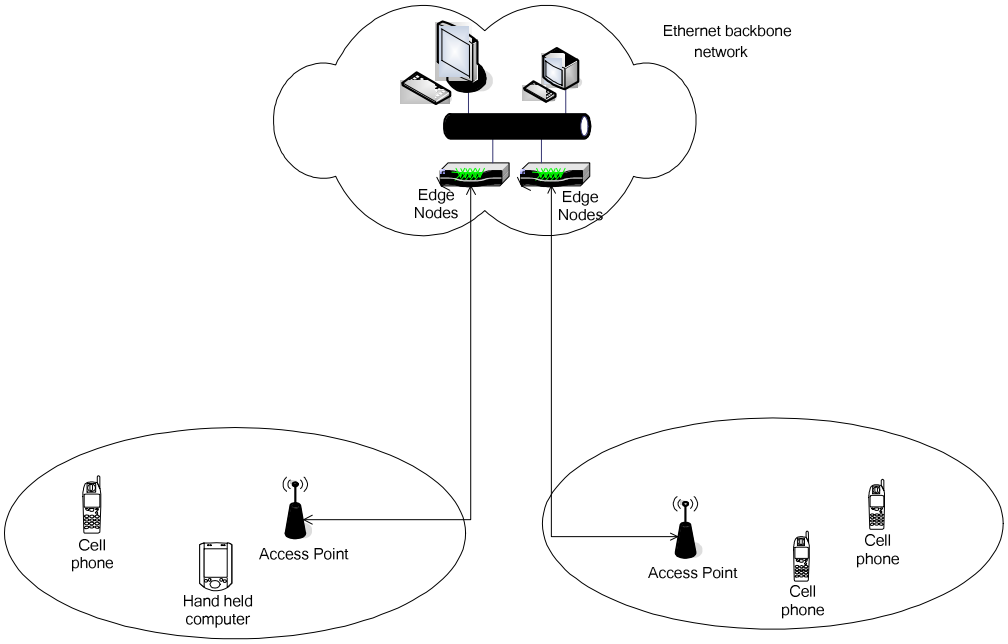

Figure 1-1: Diagram showing an IP backbone network and wireless access networks.

1.1.1 Dynamic Time Division Duplex Systems

In conventional wireless systems, frequency division duplex (FDD) is used for the separation of uplink and downlink transmissions [3]. The downlink transmission uses a radio frequency (RF) carrier and the uplink uses a different RF carrier. Downlink (DL) is used to refer to the direction of transmission from the base station (BS) to the mobile station (MS) and uplink (UL) is used to refer to the direction of transmission from the mobile station to the base station. The most important advantage of FDD is that there is no interference between uplink and downlink transmissions due to the orthogonal nature [3] of the frequency bands. FDD is best suited for symmetrical uplink and downlink traffic. But FDD is highly disadvantageous with respect to asymmetrical traffic between the uplink and downlink as this might either lead to a huge waste of bandwidth or the

service requirements will not be satisfied as the amount of traffic in one direction will exceed the amount of capacity already allocated in that direction [3].

Time division duplex (TDD) is different from FDD in that the same RF carrier is used for downlink and uplink directions. One of the important advantages of TDD over FDD is that the boundary between the uplink and downlink cycles can be adjusted dynamically and this makes the D-TDD system suitable to handle varying uplink and downlink traffic. For example, in wireless Internet services, where mostly the mobile host is downloading information from websites, D-TDD systems will be best suited. D-TDD enables efficient asymmetric services which increases the spectral efficiency of the network. But this dynamic boundary is also the cause for one of the serious problems in D-TDD as explained next.

In FDD systems, when a reference cell is in downlink or uplink transmission, all the other cells are also in downlink or uplink transmission and the interference at the reference cell occurs only from the base stations or mobile stations in the other cells respectively. But, in D-TDD systems there can be interference from downlink transmission in other cells when the reference cell is in uplink cycle or vice versa. This interference can be very high at times that can lead to a reduction in capacity of the cell.

1.1.2 Self-similarity of Internet Traffic

Network traffic was assumed to be modeled as a Poisson process that was challenged by papers like [16] and [17]. The modeling assumed that the packet and connection arrival times are Poisson process. But [16] showed that LAN traffic can be modeled as a statistically self-similar process whose theoretical properties are much different from Poisson process. For self-similar traffic there is no natural length of a burst

and traffic bursts occur on a wide range of time scales. If traffic was modeled as a Poisson or Markovian arrival process, it would have a characteristic burst length that would tend to be smoothed by averaging over a long enough time scale. But measurement of real traffic indicated that significant traffic variance (burstiness) is present over a wide range of time scales [18].

Traffic that is bursty on many or all time scales can be statistically described using self-similarity. Self-similarity is the property associated with one type of fractal, which is an object whose appearance is unchanged regardless of the scale at which it is viewed [18]. When applied to stochastic objects like time series, self-similarity is used in the distributional sense: when viewed at varying time scales, the object's co-relational structure remains unchanged and so the time series exhibits bursts over wide range of time scales. This leads to the observance of long-range dependence in the time series, where the values at any instant are non-negligibly positively correlated with values at all future instants. When using self-similar models for time series, the degree of self-similarity of the time series can be expressed in terms of only one parameter, namely the Hurst parameter (H). This parameter expresses the speed of decay of the autocorrelation function of the time series.

1.2 Organization

The asymmetric nature of traffic in mobile communications is a very important issue. It is estimated that by the year 2008 the required traffic in the downlink will be four times that of the uplink [26]. The data rates are equal in the uplink and downlink for voice traffic but this is not the case for the World Wide Web (WWW) and video on demand (VoD). Thus, to support the wireless services in next generation mobile

communication systems, an efficient allocation scheme that can handle the asymmetric data traffic is needed. The traffic properties of a wireless network can include a wide range of dynamic properties that have a huge impact on the capacity of the BS and the wireless network on the whole [16], [27]. The number of wireless channels is limited and they are reused and this reuse leads to co-channel interference. This degrades the signal-to-noise ratio (SNR) and consequently the throughput of the entire network. The aim of dynamic channel allocation (DCA) algorithms is to allocate channels dynamically to the network so that it minimizes the interference at the same time meeting the traffic demands of the network and consequently improving the capacity of the network.

Network traffic was found to exhibit self-similar characteristics from [16] and [29]. But the traffic measurements in [16] and [29] were performed on wired networks. The authors of [28] have shown that the traffic in wireless networks exhibit self-similar behavior as well and indicated the end of "simple traffic models" [30], [31]. Self-similarity has emerged as one of the most important characteristics that need to be captured by traffic models [16], [29]. Traditional traffic models provide limited insight into the true nature of genuine traffic data but characteristics observed in measured traffic data can be captured with long-range dependent (self-similar) process defined by one parameter-the Hurst parameter [28].

The following have been done as part of background research for this thesis.

- The need for DCA algorithms to improve the capacity of cellular systems is shown.
- A DCA algorithm called the time slot (TS)-opposing algorithm that improves capacity in time division-code division multiple access/dynamic time division

duplex (TD-CDMA/D-TDD) networks is reviewed and the improvement in system capacity of D-TDD in comparison with FDD systems is documented.

- An analytical model of SIR in D-TDD systems is derived.
- The probability of outage of signal-to-interference ratio (SIR) was analyzed in time division multiple access/ dynamic TDD (TDMA/D-TDD) systems.
- The SIR probability outage analysis was done for the following different scenarios.
    - Omni-directional antennas are used both at the subscriber site and the base station site.
    - Sectored antennas are used both at the subscriber site and the base station site.
    - Sectored antennas combined with time slot allocation algorithms are used both at the subscriber site and the base station site.

It was concluded that the combination of sectored antennas with time slot allocation strategies provide the best performance with regards to the SIR probability outage ratio. The time slot allocation algorithm used was called as the *Max* {SIR} [5] algorithm and this is an example of a dynamic channel allocation algorithm.

- The truncated Gaussian traffic model for dynamic TDD and static TDD systems was analyzed and the spectral efficiency equations for both the systems assuming the truncated Gaussian traffic model were studied.
- The properties of self similarity are studied and the self-similar nature of the two different data types is verified through the estimation of the Hurst parameter. The Hurst parameter is estimated using the following three methods:

- Aggregate variance method
- Range-Statistics method
- Wavelet method

The two types of data traffic used are:

- Arrival of a million packets on an Ethernet at the Bellcore Morristown Research and Engineering facility.
- Motion Picture Experts Group -4 (MPEG-4) video. The video is of a high quality *Jurassic Park 1* movie.

As a follow-up to the above research, the following are the contributions from this research.

- Multi-cell coordinated D-TDD resource allocation for multi-cell environments was analyzed.
- The *Max* {SIR} algorithm was expanded and applied to multiple cells. The algorithm is called the extended *Max* {SIR} algorithm. The analysis was done for the following four cases.
    - The boundary between the uplink and downlink traffic is fixed and there are no extra uplink time slots. This is similar to a FDD system
    - The boundary between the uplink and downlink traffic is made variable and the maximum number of extra uplink time slots is three.
    - The boundary between the uplink and downlink traffic is made variable and the maximum number of extra uplink time slots is six.
    - The boundary between the uplink and downlink traffic is made variable and the maximum number of extra uplink time slots is twelve.

The multi-cell D-TDD application algorithm was combined with sectored antennas at the BS and high-gain antenna at the MS. The following cases were discussed.

- Four-sectored antennas were used at the BS and high-gain antennas were used at the MS.
- Fifteen-sectored antennas were used at the BS and high-gain antennas were used at the MS.

The SIR outage probability was improved when the multi-cell D-TDD application algorithm was used when compared with the *Max* {SIR} algorithm.

- Priority of subscribers was introduced in the D-TDD systems. The subscribers in the D-TDD system were divided into groups based on priority and the SIR outage probability was compared with and without the application of the *Max* {SIR} algorithm.
- Traffic available from [34] was modeled as an ON-OFF traffic source and applied to a TDMA/D-TDD system employing the *Max* {SIR} algorithm. The results obtained were compared with the results obtained when the number of extra uplink time slots was modeled using the uniform density function. The results were comparable in both the cases.

The remainder of the document is organized as follows. In chapter 2, the time-slot opposing algorithm that reduces interference in a TD-CDMA/D-TDD system is explained. An analytical expression for SIR outage probability in TDMA/D-TDD systems is derived. The *Max* {SIR} algorithm from [5] is introduced. In chapter 3, the three methods used in evaluating the self-similarity of time series are given. The truncated Gaussian traffic model for dynamic TDD and static TDD systems is then

applied. ON-OFF traffic modeling is applied to a TDMA/D-TDD system and the performance of the system using the *Max* {SIR} algorithm is analyzed. In chapter 4, the multi-cell coordinated D-TDD resource allocation for multi-cell environments is presented. In chapter 5, the conclusion and future research directions are given.

2 DYNAMIC CHANNEL ASSIGNMENT ALGORITHMS IN TD-CDMA/TDD AND TDMA/TDD SYSTEMS

Systems like the Universal Mobile Telecommunication System (UMTS) make use of time division-code division multiple access/time division duplex (TD-CDMA/TDD) air interface. A CDMA system is severely interference limited and so a reduction in interference in such a system by any means produces an increase in the capacity of the system. The reduction of interference in a TD-CDMA/TDD is made possible due to the additional component of TDD. Dynamic TDD (D-TDD) is employed as the flow of traffic is normally not symmetric in the uplink (UL) and downlink (DL) direction. Also, dynamic channel allocation (DCA) algorithms are used instead of fixed channel allocation (FCA) algorithms to obtain a reduction in the interference level. In this chapter, a DCA algorithm called the time slot (TS)-opposing algorithm presented in [1] is reviewed and the improvement in the capacity of the system over a FCA algorithm is noticed. The performance of D-TDD in time division multiple access (TDMA) systems is analyzed. An analytical expression for SIR in TDMA/D-TDD systems is derived. Different scenarios were analyzed and it was found that TDMA/D-TDD systems using a combination of sectored antennas and time slot allocation algorithms gave the best performance in regards to the reduction of the co-channel interference.

The rest of the chapter is organized as follows. In Section 2, the conventional duplex schemes are explained and the need for D-TDD is emphasized. This is followed

by a review of the existing co-channel interference management schemes emphasizing the need for DCA. In section 3, the TS-opposing algorithm is reviewed and the results and observations are documented. In section 4, the signal-to-interference ratio outage probability in TDMA/D-TDD systems is analyzed under various scenarios.

2.1 The need for Dynamic Time Division Duplex Systems and Dynamic Channel Allocation Algorithms in Wireless Telecommunications

The huge popularity of wireless systems has necessitated the need for multiple users to share the same frequency and this is known as the TDD multiple access system. The frequency spectrum or bandwidth allocated to a certain system is a limited resource. The maximum possible number of users needs to be accommodated (capacity) within this limited resource while keeping the interference among the users at a tolerable level. The separation of users can be done in the following four dimensions – frequency, time, space, and code and this leads to the four types of multiple access systems – frequency division multiple access (FDMA), time division multiple access (TDMA), space division multiple access (SDMA), and code division multiple access (CDMA). In FDMA systems the total bandwidth available is divided into separate channels and each channel can be allocated to a user for transmission. In other words, some of the bandwidth can be used by a user all the time. In TDMA systems, the entire available bandwidth spectrum is allocated to a user for a certain amount of time and then it is switched to the next user and so on. In other words, all of the available bandwidth can be used by a user at some periods of time. In CDMA systems, the available bandwidth spectrum can be used by all the users at all the times and the different users are separated by a special code. Unique codes are assigned to every user which is used to spread the user's data stream and the

receiver uses the same code to transform the spread-spectrum signal back into the original user's data stream. The bandwidth needed per user for a CDMA system is much greater than that required for a TDMA or FDMA system due to the spreading.

The concept of a cellular system is explained. In conventional wireless systems a mobile station (MS) is linked to a base station (BS). BSs are connected to a radio network controller (RNC) which is connected to the public switched telephone network (PSTN). The concept is explained in figure 2-1.

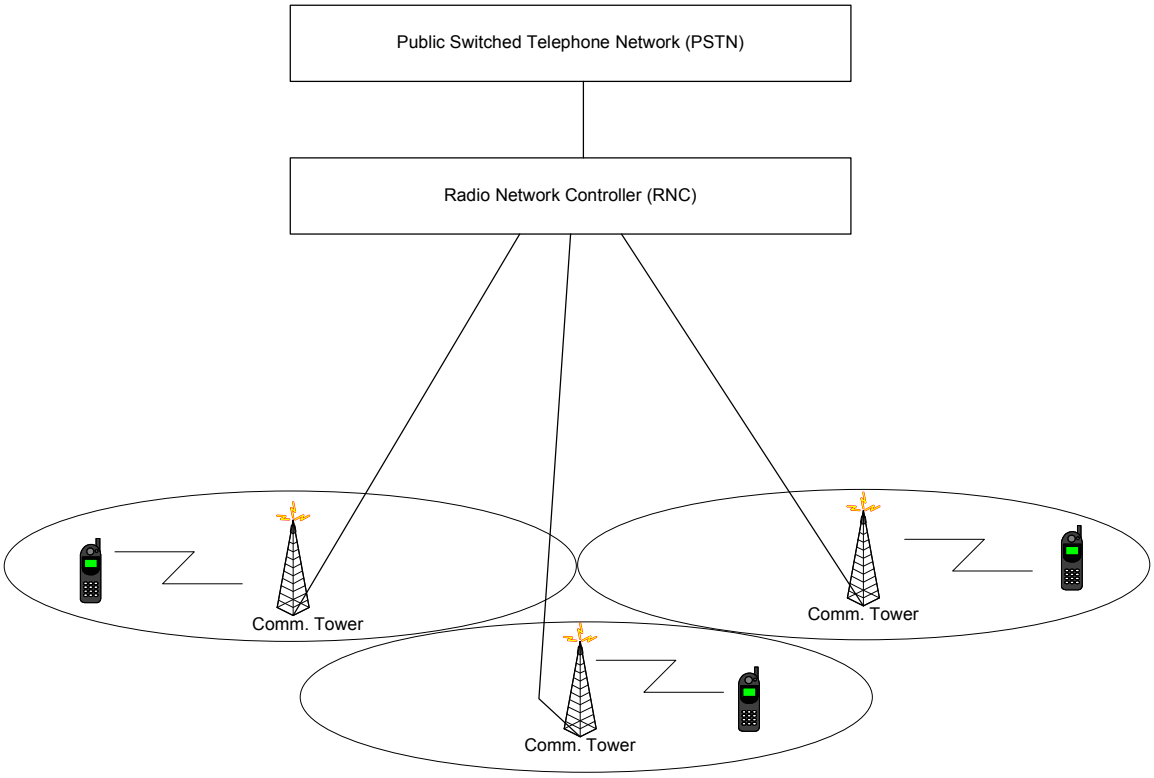

Figure 2-1: A cellular wireless system.

2.1.1 Conventional Duplex Schemes – FDD and TDD

There are three basic modes for operating a communication channel: simplex, half-duplex, and full-duplex. In a simplex channel, information is passed from one communication entity to another without any acknowledgement from the receiving entity. Examples of simplex communication include television and radio. In a half-duplex channel an entity can transmit as well as receive but not at the same time. One entity transmits at a time while the other entity listens and vice versa. Examples of half-duplex communication include talk-back radio and the Citizen-Band (i.e., common band (CB)) radio, where only one person can talk at a time. In a full-duplex channel, information passes in both the directions simultaneously. An example of full-duplex communication is the telephony system. These three modes are explained in figure 2-2.

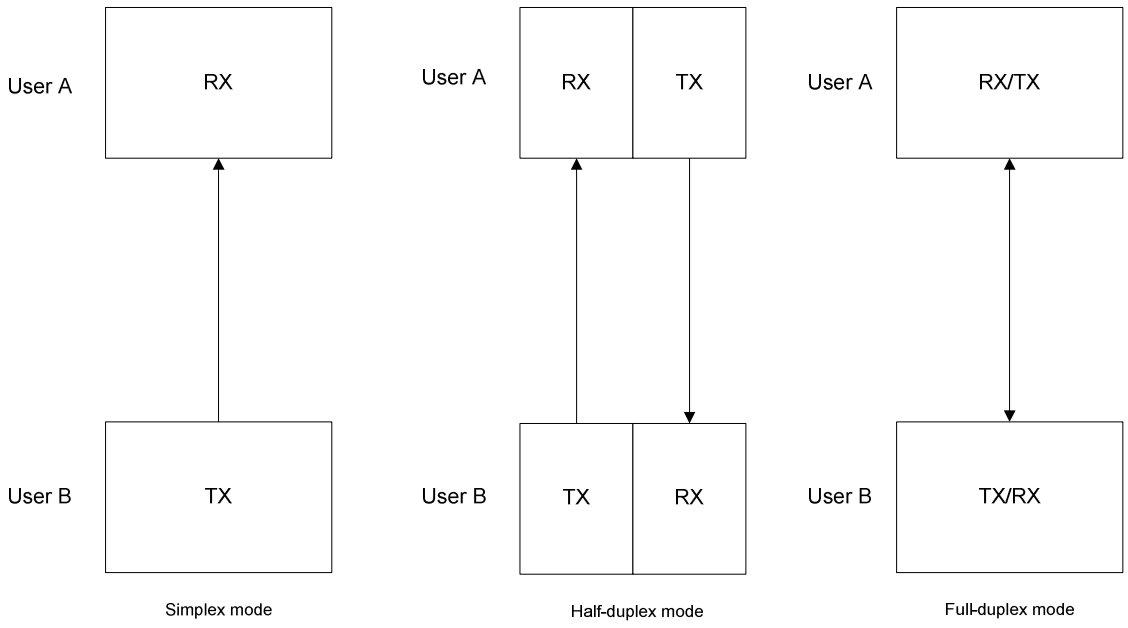

Figure 2-2: Channel operation methods.

In wireless communication systems, two methods are used to achieve a full duplex channel – frequency division duplex (FDD) and time division duplex (TDD). If

the transmit and receive slots of a half-duplex channel are repeated periodically in short intervals of time a full-duplex channel can be emulated by a half-duplex channel and this is the mechanism used in TDD. But, in FDD both the directions are separated in the frequency domain and so the full-duplex channel is accomplished by two independent simplex channels. The basic mechanism of TDD and FDD are explained in figure 2-3.

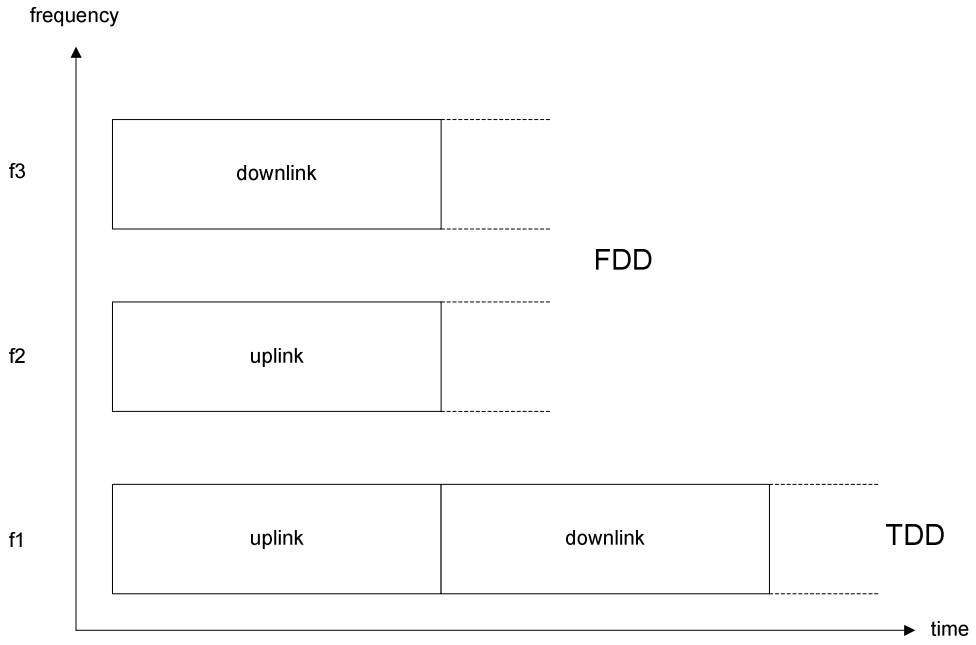

Figure 2-3: The FDD and TDD mechanisms.

FDD has an advantage in that it represents a true full duplex channel and does not require any coordination between the uplink and downlink transmission. In an FDD system, the uplink (UL) and downlink (DL) transmission are on separate carrier frequencies and so there is no interference between these two directions. When the reference user is in downlink transmission all the other (interfering) users are also in downlink transmission and so the interference seen at the reference mobile station (MS) comes only from the power transmitted by the other base stations (BS). Similarly, when the reference user is in UL transmission, all the other users are also in UL transmission

and the interference at the reference BS comes only from the power transmitted from the other MS. This is referred to as the other entity interference [1]. One major disadvantage of an FDD system is that the transmission is usually not symmetric in both the directions and so this leads to a waste of resources in FDD systems.

TDD is better suited for asymmetric services and this was the motivation of proposing TDD in some International Mobile Telecommunications (IMT) - 2000 systems and in wireless asynchronous transfer mode (ATM) systems. Also, based on the received signal, the TDD transmitter can determine the fast fading status of the multi-path channel and this helps in open loop power control between the transmitter and the receiver. Transmission diversity can also be applied with diversity antennas (i.e., space diversity). As an example, based on the uplink reception at the BS, the best antenna can be chosen for downlink transmission.

2.1.2 Dynamic TDD

TDD systems have a higher flexibility to handle the dynamic uplink and downlink traffic as the TDD operation can be divided into two different modes – static TDD (S-TDD) and dynamic TDD (D-TDD). In S-TDD, the boundary between uplink and downlink transmission is fixed but this boundary can be adjusted dynamically in D-TDD systems. So, D-TDD systems are suitable for asymmetrical traffic in the downlink and uplink directions as in wireless data services. But, one major drawback of this dynamic boundary in D-TDD systems is the additional co-channel interference mechanisms present in these systems when compared to FDD systems.

In figure 2-4, the time slot allocation in a D-TDD system for two users is shown.

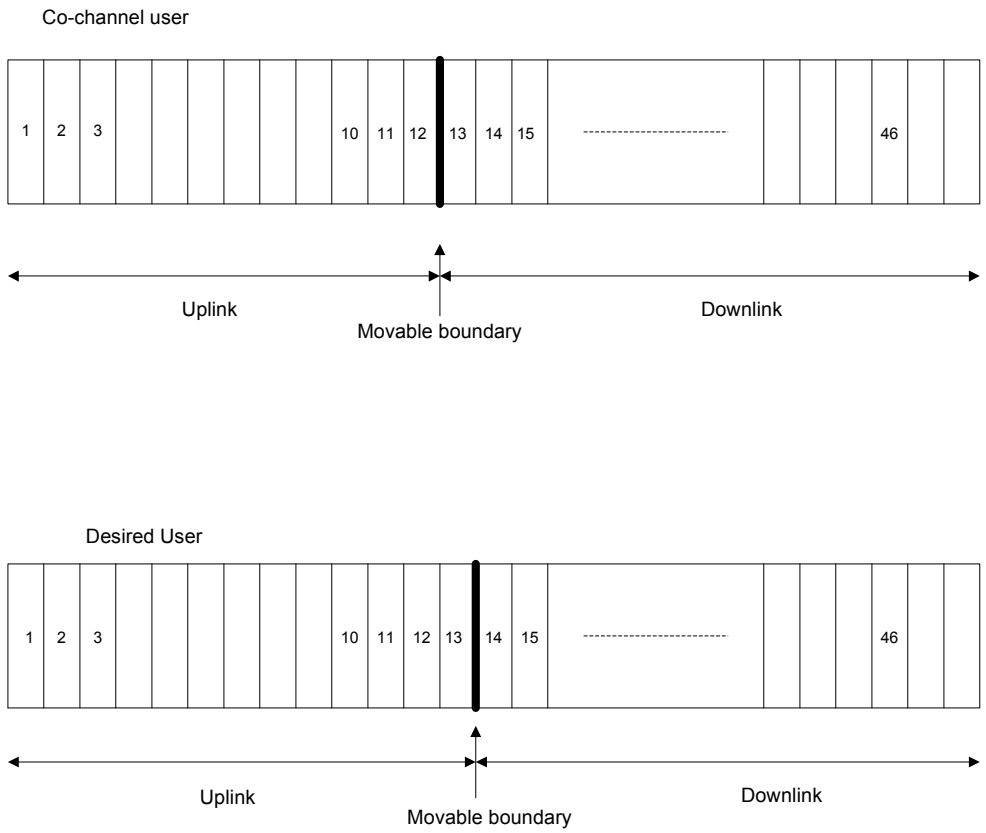

Figure 2-4: A dynamic TDD frame with the boundary movable between the uplink and downlink.

In figure 2-4, there are two user groups, namely the desired user group and the co-channel user group. The co-channel user group uses the same frequency as the desired user group. Each user has some time slots (TSs) that are used for uplink and some that are used for downlink. It can be seen that from TSs 1 to 12 both the user groups are in uplink (transmission from mobile station to base station) and so the interference seen at the BS of the desired user group comes from MS of the co-channel user group and this interference is similar to the other-entity interference observed in FDD systems. But in TS 13, the desired user group is in uplink but the co-channel user group is in downlink and so the interference occurring at the BS of the desired user group comes from the BS

of the co-channel user group and this interference is termed as the same-entity interference [1]. So, in a D-TDD system, the interference at the BS comes from the neighboring MSs (similar to FDD) as well as from the neighboring BSs (not present in FDD). Similarly, the interference at the MS comes from the neighboring BSs (similar to FDD) as well as from the neighboring MSs (not present in FDD). So, a D-TDD system is subject to additional co-channel interference mechanisms compared to an FDD system. The interference between MSs can be severe when the distance between the two entities is very small. It was shown in [1] that the interference between BSs can be very strong when the path loss between the BSs is very low.

To avoid the same-entity interference in the above figure, the frames of both user groups must be synchronized and the same rate of asymmetry must be employed by both the user groups which is clearly a disadvantage. It was shown in [49] that ideal synchronization is not necessary to achieve maximum capacity in a TD-CDMA/TDD system and this finding is exploited by the DCA algorithm in [1].

If the interference power from the co-channel cells is greater than the power of the desired user, then the user may not be able to obtain the required carrier power to interference power ratio (CIR) and consequently experience outage. Hence there is a great need to avoid this co-channel interference present in cellular systems.

2.2 Co-channel interference management techniques

The following methods are used in the management of co-channel interference (CCI).

- Co-channel interference suppression.
- Co-channel interference cancellation.

- Co-channel interference avoidance.

The three co-channel interference management schemes are explained in the next section.

2.2.1 Co-channel interference suppression

In order to reduce the CCI, techniques like sectorization and power adaptation are used. The distance between two co-channel cells can also be increased to decrease the interference but this reduces the system efficiency [37]. The increase of distance also necessitates the need for more power leading to costlier devices. The antenna can be down tilted mechanically on the coverage pattern and this method reduces CCI when the number of frequency cells is fixed but is not advisable when the CCI is high due to the presence of side lobes in the radiation pattern of the antenna. CCI can also be reduced by lowering the height of the base station but this reduces the reception level at the mobile unit.

The reduction of CCI by sectoring is explained with the help of figures 2-5 and 2-6. Figure 2-5 shows the co-channel interference in a cellular system without any sectoring. Figure 2-6 is an illustration of 120^0 sectoring. In figures 2-5 and 2-6, the reference cell is the cell at the center labeled as R and the co-channel cells are the six surrounding hexagons labeled from A to F. From Figure 2-5, all the users present anywhere in the co-channel cell interfere with the users in the reference cell. According to 120^0 sectoring, only the users present in one third of the total area of each co-channel cell will interfere with the users in the reference cell. From figure 2-6, only the users present within the dotted area in each co-channel cell interferes with the reference cell. In

60^0 sectoring only the users present in one sixth of the total area of each co-channel cell will interfere with the users in the reference cell.

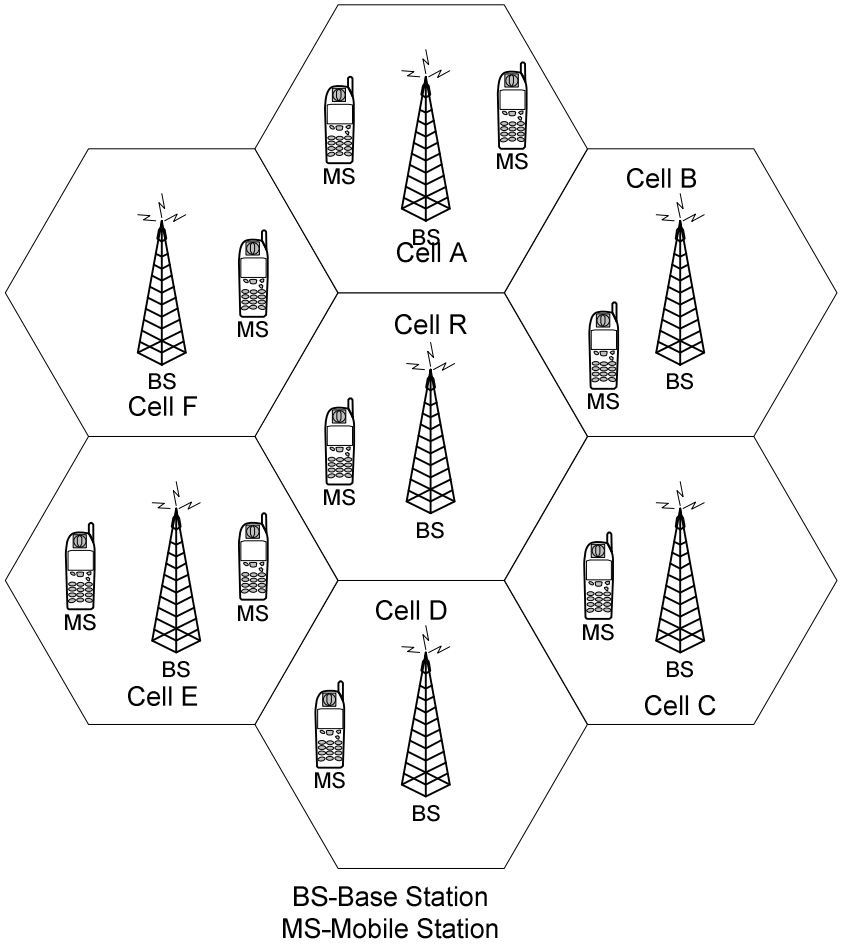

Figure 2-5: Co-channel interference in a cellular system.

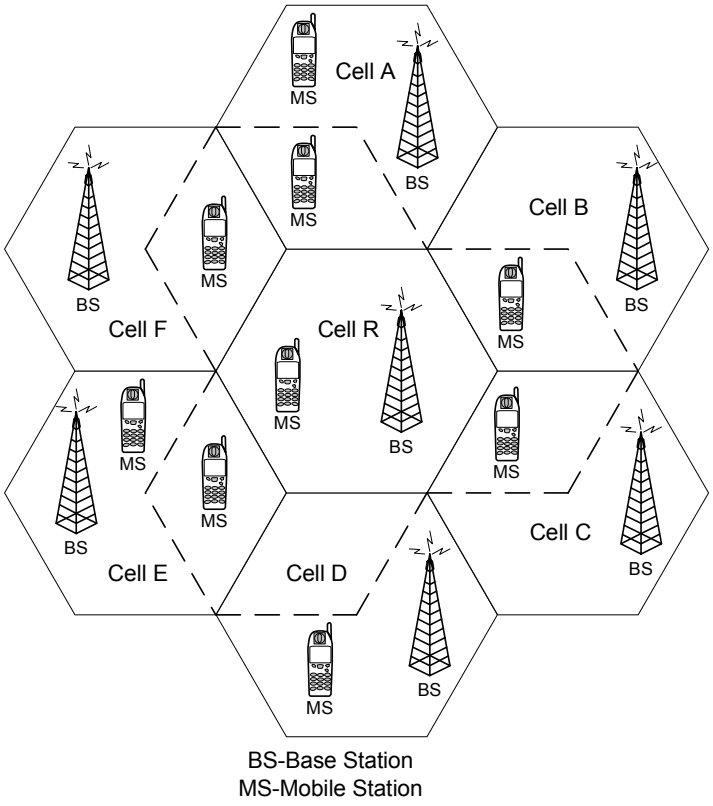

Figure 2-6: Co-channels for 120 degree sectoring scheme.

Smart antenna techniques are used in [38] and [39] to reduce CCI. Multiple antenna elements can be used at the transmitter or receiver to form an antenna array and space-time processing of the received signal at the antenna array reduces interference.

2.2.2 Co-channel interference cancellation

The most popular technique for CCI cancellation is the multi-user detection (MUD). Conventional CDMA detectors employ single-user detection strategy where each user is detected separately without regard to the other users. But in MUD, information about multiple users is used to improve detection of multiple users [40]. Some of the MUD techniques are maximum likelihood sequence (MLS) detection, linear detectors like decorrelating detector (DD), minimum mean squared error (MMSE) detector and

polynomial expansion (PE) detectors. The linear detectors apply a linear mapping to the soft output of a conventional detector to reduce the interference seen by each user [41].

Another group of detectors using MUD are the subtractive interference cancellation detectors. The principle of these detectors is the creation of the separate estimates of the interference contributed by each user at the receiver in order to cancel out some or all of the interference seen by each user [41]. Some detectors employing this technique are the successive interference cancellation detector, parallel interference cancellation detector and zero forcing decision feedback (ZF-DF) detector.

Some of the advantages of MUD scheme are the significant improvement in capacity, efficient uplink spectrum utilization and more efficient power control.

Some of the disadvantages of MUD scheme are as follows. In a CDMA system, the interference at a reference user occurs from other users present in the same cell (same-cell interference) as well as from users present in the neighboring co-channel cells (other-cell interference). If this other-cell interference is not included in the MUD algorithm, the potential gain in capacity reduces considerably. For an ideal system, there is no same-cell interference but the other-cell interference is still present. It has been shown in [9] that the maximum capacity gain factor using MUD algorithm would be 2.8. Also, due to the issues of cost, power consumption and size being much larger concern for mobile stations than for base stations, it was not practical to include the MUD algorithm in mobiles in the past. Therefore, MUD processors were mainly used in the BSs (for uplink reception of mobiles) where the detection of multiple users is required in any case. But, an increase in the capacity in the uplink without an increase in the downlink does not improve the overall capacity of the system. Also, MUD requires

knowledge of channel parameters which is difficult to obtain in a rapidly changing environment.

2.2.3 Co-channel interference avoidance

Co-channel interference avoidance can be accomplished by using dynamic resource and channel allocation methods. Dynamic channel allocation (DCA) algorithms, based on the interference margin in a system or carrier-to-interference ratio (CIR), are used. In DCA, channels are assigned dynamically over the cells in a service area to meet traffic requirements [42]. Two basic DCA schemes – centralized and non-centralized - can be distinguished [1]. A centralized DCA scheme collects the information for channel assignment from the associated BSs and MSs and this scheme operates at the higher hierarchical level of the mobile network architecture. As an example, a DCA algorithm can be located at the RNC that connects several BSs [43]. One disadvantage of the centralized DCA scheme is that a large amount of signaling is required to supply information about the load, channel status and interference level. In contrast, in decentralized DCA scheme, the channel assignment is made by the BSs or MSs based on information available locally. This reduces the huge signaling required for centralized DCA schemes but the decisions are made based on limited information of the channel state.

The borrowing channel assignment (BCA) is a type of DCA scheme that does not require system-wide information [42]. BCA uses some FCA scheme as a normal assignment condition. When all the fixed channels are occupied, the cell attempts to borrow a channel from the adjacent cell [44].

A DCA scheme is proposed in [48] where calls are accepted if a channel can be assigned that provides a minimum CIR. In [45], a DCA scheme is proposed based on the interference seen at the BS. Channels are assigned if the corresponding interference margin is less than the allowed interference. These two mechanisms are based on the assumption that the CIR is changing during operation which is not the case in practical systems. A DCA scheme which assumes that the CIR is constant during operation is proposed in [1]. In this scheme, the direction of transmission in co-channel cells is adjusted so that the interference seen at the desired cell decreases and so its capacity increases. A DCA algorithm based on TS allocation methods was proposed in [5]. In the TS allocation based algorithm, the MSs are assigned extra uplink TSs with the objective of increasing the CIR over these extra TSs.

CDMA has been seen to provide good multiple accesses in a cellular environment. But, what happens if a CDMA system is combined with TDD to produce a CDMA/TDD interface. Will the performance of CDMA, being a highly interference limited system, be affected by the TDD interface as it introduces additional interference scenarios? The answer to this lies in the access modes of UMTS.

The Universal Mobile Telecommunication System (UMTS) has been defined in the following two access modes: FDD and TDD. The FDD access is based on Wideband CDMA (WCDMA) allowing multiple user access in the code domain [3]. In TDD mode, a combination of TDMA and CDMA is specified. This hybrid interface of TDMA/CDMA (TD-CDMA) provides the solution to the question problem as the TDMA component provides an additional degree of freedom to reduce interference [1]. But, this requires DCA algorithms. DCA are different from FCA in that the allocation of resources

to various users is done dynamically based on requirements. The TS-opposing algorithm which is a DCA algorithm is reviewed in this chapter.

2.3 TS-Opposing Algorithm

In this section, the mathematical framework that describes the input and output parameters of the TS-opposing algorithm are presented and then the algorithm is explained and the simulation results are shown.

2.3.1 Mathematical Framework

As a hybrid time division-code division multiple access air interface is assumed several users are accommodated within one time slot (TS). Also, the network is assumed to be synchronized, where the frames and the TSs between the adjacent cells are aligned in time. So, the users belonging to different TSs do not interfere with each other.

The set of L cells connected to the radio network controller (RNC) is defined as

$$C \overset{def}{=} \{c_1, c_2, ..., c_L\} \tag{2.1}$$

Each cell consists of one base station (BS) and as there are L cells, the set of BSs gives

$$B \overset{def}{=} \{b_1, b_2, ..., b_L\} \tag{2.2}$$

Also, several mobile stations (MSs) are allocated to one BS that results in L sets of MS given by

$$M_i \overset{def}{=} \{m_1, m_2, ..., m_{|M_i|}\} \quad i = 1, 2, \ldots, L \tag{2.3}$$

where $|.|$ is the cardinality (number of members) of the respective set.

A single radio frequency carrier is assumed. Due to the TDMA component, a frame is divided into a maximum number of Q TSs and each TS can be used either for

uplink or downlink traffic. This enables a time division multiple access-time division duplex system to flexibly adapt to different traffic loads in the uplink and downlink. But, if two neighboring cells are not using the same TSs for uplink or downlink traffic, respectively, it follows that MSs ($MS \leftrightarrow MS$) and BSs ($BS \leftrightarrow BS$) interfere with each other. It is assumed that the adjacent cells are synchronized in time (frame synchronization) and so the following two states can be distinguished.

1. TSs between neighboring cells are used in a synchronous manner.
2. TSs between neighboring cells are used in an asynchronous manner.

For each of the TS, the above property can be modeled by a symmetric "synchronization matrix" defined as follows:

$$\alpha = \begin{pmatrix} 0 & \alpha_{1,2} & \ldots & \alpha_{1,L} \\ \alpha_{2,1} & 0 & \ldots & \alpha_{2,L} \\ \ldots & \ldots & \ldots & \ldots \\ \alpha_{L,1} & \alpha_{L,2} & \ldots & 0 \end{pmatrix} \tag{2.4}$$

The matrix in equation (2.4) is a L x L symmetric matrix as there are L cells that are considered to be attached to the RNC. In equation (2.4),

$$\begin{aligned} \alpha_{i,j} &= 0, \quad \text{if synchronous transmission} \\ &= 1, \quad \text{if opposed transmission} \end{aligned} \tag{2.5}$$

As α consists only of binary elements a complementary matrix $\bar{\alpha}$ can be found so that

$$\bar{\alpha} = \begin{pmatrix} 0 & 1 & \ldots & 1 \\ 1 & 0 & \ldots & 1 \\ \ldots & \ldots & \ldots & \ldots \\ 1 & 1 & \ldots & 0 \end{pmatrix} - \alpha \tag{2.6}$$

As the use of a TS as uplink or downlink can be chosen, the actual elements of the matrix defined above can be altered as part of a DCA procedure and this is utilized by the TS-opposing algorithm presented.

The downlink and uplink directions are distinguished by the following method. Symbols followed by the superscript "*u*" are associated with the uplink channel and symbols followed by the superscript "*d*" are associated with the downlink channel. For each set of MSs, M_i, and each TS, *n*, a vector of transmitted powers can de defined as

$$\mathrm{Pc}_i^u = (Pc_1^u, Pc_2^u, ..., Pc_{|M_i|}^u) \qquad i=1,\ldots, L \tag{2.7}$$

Given that *L* cells are connected to an RNC,

$$\mathrm{Pc}^u = (\mathrm{Pc}_1^u, ..., \mathrm{Pc}_L^u) \tag{2.8}$$

Similarly, a vector for the power transmitted by the *L* BSs can be denoted as

$$\mathrm{Pc}^d = (P_1^d, ..., P_L^d) \tag{2.9}$$

Four interference scenarios can be ascertained in a TDD system ($\mathrm{MS} \leftrightarrow \mathrm{MS}$, $\mathrm{BS} \leftrightarrow \mathrm{BS}$, $\mathrm{MS} \leftrightarrow \mathrm{BS}$, $\mathrm{BS} \leftrightarrow \mathrm{MS}$). The cases where the same entities interfere with each other are given here as *same-entity interference* and the cases where different entities interfere with each other are called as *other-entity interference*. So, four path loss matrices between the respective entities of different cells can be established. The path loss matrices will be used to determine the co-channel interference with a frequency reuse of 1. The entries on the main diagonal of the above matrices will be zero as the entities within the same TS and the same cell do not contribute to other cell interference. It has been found convenient to use the reciprocal value of the path loss, referred to as

path gain, for the matrices. The path gain matrix for the MS $\leftrightarrow$ MS is a symmetric (L x L) block matrix given in equation (2-10):

$$\mathrm{M} = \begin{pmatrix} 0 & \mathrm{MM}_{c_1,c_2} & \ldots & \mathrm{MM}_{c_1,c_L} \\ \mathrm{MM}_{c_2c_1} & 0 & \ldots & \mathrm{MM}_{c_2,c_L} \\ \ldots & \ldots & \ldots & \ldots \\ \mathrm{MM}_{c_1,c_1} & \mathrm{MM}_{c_L,c_2} & \ldots & 0 \end{pmatrix} \tag{2.10}$$

where MM_{c_i,c_j} is a $|M_i| x |M_j|$ matrix that represents the path gain between all the MSs in cell c_i to all the MSs in cell c_j.

$$\mathrm{MM}_{c_i,c_j} = \begin{pmatrix} 1/a_{m_1,m_1} & \ldots & 1/a_{m_1,m_{|M_j|}} \\ \ldots & \ldots & \ldots \\ 1/a_{m_{|M_i|}m_1} & \ldots & 1/a_{m_{|M_i|},m_{|M_j|}} \end{pmatrix} \tag{2.11}$$

For example, a_{m_1,m_1} is the path loss between MS m_1 in cell c_i and MS m_1 in cell c_j. With equation (2.10), the path gain between any MS and all other MSs within the set C is described and used to calculate MS $\leftrightarrow$ MS interference.

The path gain matrix for the BS $\leftrightarrow$ BS case is an L x L matrix

$$\mathrm{BB} = \begin{pmatrix} 0 & 1/a_{b_1,b_2} & \ldots & 1/a_{b_1,b_L} \\ 1/a_{b_2,b_1} & 0 & \ldots & 1/a_{b_2,b_L} \\ \ldots & \ldots & \ldots & \ldots \\ 1/a_{b_L,b_1} & 1/a_{b_L,b_2} & \ldots & 0 \end{pmatrix} \tag{2.12}$$

The path gain matrix for the MS $\leftrightarrow$ BS case is a L x L symmetrical matrix:

$$\mathrm{MB} = \begin{pmatrix} 0 & \mathrm{MB}_{c_1,c_2} & \ldots & \mathrm{MB}_{c_1,c_L} \\ \mathrm{MB}_{c_2,c_1} & 0 & \ldots & \mathrm{MB}_{c_2,c_L} \\ \ldots & \ldots & \ldots & \ldots \\ \mathrm{MB}_{c_L,c_1} & \mathrm{MB}_{c_L,c_2} & \ldots & 0 \end{pmatrix} \tag{2.13}$$

where MB_{c_i,c_j} is a vector defined as path gain between all the MSs in cell c_i to the base station in cell c_j

$$\mathrm{MB}_{c_i,c_j} = \left(1/a_{m_1,b_j},...,1/a_{m_{|M_i|},b_j}\right)^T \tag{2.14}$$

where a_{m_1,b_j} is the path loss between m_1 in cell c_i and BS in cell c_j.

For the reciprocal case that the BS in cell *j* interferes with the MSs in cell *i*, the path gain matrix is,

$$\mathrm{BM} = \mathrm{MB}^T \tag{2.15}$$

The interference experienced by the MSs can be written as

$$\mathrm{Im} = (\mathrm{Pc}^u)\,(\alpha \Theta \mathrm{MM}) + (\mathrm{Pc}^d)(\bar{\alpha} \Theta \mathrm{BM}) \tag{2.16}$$

The interference experienced by the BSs

$$\mathrm{Ib} = (\mathrm{Pc}^d)(\alpha \Theta \mathrm{BB}) + (\mathrm{Pc}^u)\,(\bar{\alpha}\ \Theta \mathrm{MB}) \tag{2.17}$$

The first term in equations (2.16) and (2.17) refer to the same entity interference and the second term refers to the other entity interference. In equations (2.16) and (2.17), Θ refers to the Hadamard Product. The equations (2.16) and (2.17) show that the required uplink power of the MS is not only dependent on the transmitted power of the MSs in the other cells but also on the power transmitted by the BSs in the neighboring cells.

The vectors of transmission powers, Pc^u and Pc^d are calculated as follows. The carrier-to-interference ratio at BS *i* (γ_i^u) can be denoted as shown in equation (2.18).

$$\gamma_i^u = \frac{P_{u_i}^u}{\sum_{j;\, j\neq i}^{M} P_{u_j}^u + I_o^u + N} \tag{2.18}$$

where $P_{u_i}^u$ is the signal power of the desired user in the uplink, $P_{u_j}^u$ is the interference power from an MS using the same channel in the same cell, I_o^u is the interference power from other cells, N is the thermal noise power and M is the number of MSs per cell. Multiplying equation (2.18) by the denominator and also noting that

$$I_b = I_o^u + N \tag{2.18a}$$

$$\gamma_i^u \sum_{j;j\neq i}^{M} P_{u_j}^u + \gamma_i^u I_b = P_{u_i}^u \tag{2.18b}$$

$$P_{u_i}^u - \gamma_i^u \sum_{j;j\neq i}^{M} P_{u_j}^u = \gamma_i^u I_b \qquad i = 1,2,...,|M_i|$$

Equation (2.18b) can be expanded in matrix form as

$$\begin{pmatrix} 1 & -\gamma_1^u & \dots & -\gamma_1^u \\ -\gamma_2^u & 1 & \dots & -\gamma_2^u \\ \dots & \dots & \dots & \dots \\ -\gamma_{|M_i|}^u & -\gamma_{|M_i|}^u & \dots & 1 \end{pmatrix} \begin{pmatrix} P_{u_1}^u \\ P_{u_2}^u \\ \dots \\ P_{u_{|M_i|}}^u \end{pmatrix} = \begin{pmatrix} \gamma_1^u \\ \gamma_2^u \\ \dots \\ \gamma_{|M_i|}^u \end{pmatrix} Ib \tag{2.18c}$$

Equation (2.18c) describes the uplink of a single cell. This can be expanded to a multicell environment by applying the following:

$$\mathrm{Pu}_i^u = \mathrm{Pc}_i^u \Theta\ \mathrm{MB}\, c_i, c_i \qquad i=1, 2,\ldots,L \tag{2.18d}$$

The right hand side of equation (2.18c) can be written as,

$$(\mathbf{I} + \mathrm{diag}\,(\gamma^u) - \gamma^u \mathbf{J})\,(\mathrm{Pu}_i^u)^T \tag{2.18e}$$

where **I** is an identity matrix, diag (.) is a diagonal matrix representation, γ^u is the vector of the required carrier-to-interference ratios at the BS in cell $I = (\gamma_1^u,...,\gamma_{|M_i|}^u)$ and has the dimension: dim $(\gamma^u) = |M_i|$ and **J** is a vector of dimension: dim (J) = $|M_i|$ with each

element set to one. Substituting equations (2.18d) and (2.18e) into equation (2.18c), we obtain,

$$(\mathbf{I} + \text{diag}\,(\gamma^u) - \gamma^u\,\mathbf{J})\,(\text{Pc}_i^u)^T = (\gamma^u Ib_i)\Theta\,\bar{\text{MB}}_{c_i,c_i} \quad i = 1, \ldots, L \tag{2.19}$$

In equation (2.19), Ib_i is the accumulated interference from other cells and thermal noise at the BS in the cell c_i and $\bar{\text{MB}}_{c_i,c_i}$ is the path loss matrix between MSs in cell c_i to the BS in cell c_i

Substituting,

$$\mathbf{B} = \mathbf{I} + \text{diag}\,(\gamma^u) \tag{2.19a}$$

into equation (2.19),

$$(\mathbf{B} - \gamma^u\,\mathbf{J})\,(\text{Pc}_i^u)^T = (\gamma^u Ib_i)\Theta\,\bar{\text{MB}}_{c_i,c_i} \tag{2.20}$$

According to the Sherman-Morrison-Woodbury formula, which gives a simple expression for the inverse of $(A + UV^T)^{-1}$ where A is a n x n matrix, and U and V are n x k vectors,

$$(A + UV^T)^{-1} = A^{-1} - A^{-1}U(I + V^T A^{-1}U)^{-1}V^T A^{-1} \tag{2.20a}$$

In equation (2.20a) if we replace $A = \mathbf{B}$, $U = \gamma^u$, $V^T = \mathbf{J}$

$$(\mathbf{B} - \gamma^u\,\mathbf{J})^{-1} = \mathbf{B}^{-1} + \frac{\text{B}^{-1}\,\gamma^u\,\text{JB}^{-1}}{1 - \text{JB}^{-1}\,\gamma^u} \tag{2.21}$$

Substituting equation (2.21) into equation (2.20),

$$\text{Pc}_i^u = (\mathbf{B} - (\gamma^u)^T\,\mathbf{J})^{-1}\;((\gamma^u)^T Ib_i)\Theta\,\bar{\text{MB}}_{c_i,c_i}$$

$$\text{Pc}_i^u = (Ib_i\,\mathbf{B}^{-1}\,(\gamma^u)^T + \frac{Ib_i\text{B}^{-1}(\gamma^u)^T\,\text{JB}^{-1}(\gamma^u)^T}{1 - \text{JB}^{-1}(\gamma^u)^T})\;\Theta\;\bar{\text{MB}}_{c_i,c_i} \tag{2.22}$$

The denominator in equation (2.22) is a scalar. Equation (2.22) can be written as,

$$Pc_i^u = (\mathbf{B}^{-1}(\gamma^u)^T + \frac{B^{-1}(\gamma^u)^T JB^{-1}(\gamma^u)^T}{1 - JB^{-1}(\gamma^u)^T}) \Theta \bar{MB}_{c_i,c_i} Ib_i \quad (2.22a)$$

$$Pc_i^u = \left(\frac{B^{-1}(\gamma^u)^T - B^{-1}(\gamma^u)^T J B^{-1}(\gamma^u)^T + B^{-1}(\gamma^u)^T J B^{-1}(\gamma^u)^T}{1 - J B^{-1}(\gamma^u)^T} \right)$$

$$\Theta \bar{MB}_{c_i,c_i} Ib_i \quad (2.22b)$$

$$Pc_i^u = \left(\frac{B^{-1}(\gamma^u)^T}{1 - J B^{-1}(\gamma^u)^T} \right) \Theta \bar{MB}_{c_i,c_i} Ib_i \quad (2.22c)$$

Now, $\mathbf{B}^{-1}(\gamma^u)^T$ can be written in the following way:

We know that, $\mathbf{B} = \mathbf{I} + \text{diag}(\gamma^u)$ from equation (2.19a)

$$\mathbf{B}^{-1} = \text{diag}\left(\frac{1}{1+\gamma^T}\right) \quad (2.22d)$$

$$\mathbf{B}^{-1}(\gamma^u)^T = \left(\frac{\gamma_1^u}{1+\gamma_1^u}, ..., \frac{\gamma_{|M_i|}^T}{1+\gamma_{|M_i|}^T}\right) = \mathbf{V} \quad (2.22e)$$

Substituting equation (2.22e) into equation (2.22c)

$$Pc_i^u = \left(\frac{V}{1 - JV}\right) \Theta \bar{MB}_{c_i,c_i} Ib_i \quad (2.23)$$

where

$$\left(\frac{\gamma_1^u}{1+\gamma_1^u}, ..., \frac{\gamma_{|M_i|}^T}{1+\gamma_{|M_i|}^T}\right) = \mathbf{V} \quad (2.24)$$

In equation (2.23),

$$\mathbf{U}_{c_i} = \left(\frac{V}{1 - JV}\right) \Theta \bar{MB}_{c_i,c_i} \quad (2.24a)$$

$$\mathrm{Pc}_i^u = \mathbf{U}_{c_i} \Theta \bar{\mathrm{M}}\mathrm{B}_{c_i,c_i} \tag{2.24b}$$

From equation (2.23), the transmission powers of the mobiles are linearly dependent on the interference received at the associated BS. The interference power at BS i, Ib_i, is a function of the transmitted powers of the BSs and MSs in the other cells which is clear from equation (2.17). So, this leads to a system of mutual dependencies where any change of a transmission power, whether it is an MS or a BS, has an impact on the required transmission powers of all other entities.

Using the vector, $\mathrm{U} = (U_{c_1},...,U_{c_L})^T$, the general expression for Pc^u can be found as

$$\mathrm{Pc}^u = \mathrm{U} \Theta \mathrm{Ib}. \tag{2.25}$$

An equation similar to equation (2.25) can be obtained for the transmitted code powers in the downlink.

The main differences between uplink and downlink are:

- Synchronous transmission can be applied in the downlink while in the uplink asynchronous transmission must be assumed.
- Each BS may transmit user specific signals and a common pilot signal for coherent demodulation.

A consequence of the first difference is that if orthogonal codes are used to distinguish individual users, the orthogonality in the downlink can be maintained (no own-cell interference). So, an orthogonality factor τ is defined

$$\tau = 1\text{-}\ \frac{E_b}{I_0}\left(\frac{E_b}{N_0}\right)^{-1} = 1 - \frac{N_0}{I_0} \tag{2.26}$$

where $\frac{E_b}{I_0}$ is the bit energy to interference ratio when the orthogonality is not maintained and so the signal is corrupted by own-cell interference. The ratio $\frac{E_b}{N_0}$ is the bit-energy to interference ratio for the case that orthogonality is entirely maintained.

The definition in equation (2.26) assumes that $I_0 \approx I_{\text{int}ra}$, where $I_{\text{int}ra}$ is the intra-cell interference. It also holds that $I_0 \geq N_0$. From the definition of τ, it can be seen that the higher its value the more the signals are corrupted by multipath propagation. It has been seen that τ may vary between 0.3 and 0.8 with a greater value obtained in environments that are subject to severe multipath propagation.

When an additional pilot carrier is used, the total carrier power (downlink)

$$Pc^d = P_{pilot} + \sum_{i=1}^{M} \tilde{Pc}_i^d \tag{2.27}$$

where P_{pilot} is the pilot signal power, $\tilde{Pc}_i^d$ is the code power for the *i*th user. $P_{users} = \sum_{i=1}^{M} \tilde{Pc}_i^d$ can be substituted in equation (2.27). A factor ψ is used to model the user specific fraction of the total carrier power

$$\psi = \frac{P_{users}}{Pc^d}. \tag{2.28}$$

With the approximation of $\sum_{i-1}^{M-1} Pc_i^d = \sum_{i=1}^{M} Pc_i^d$, the carrier-to-interference ratio at the carrier *i*, γ_i^d, can be modeled as

$$\gamma_i^d = \frac{\frac{\tilde{Pc}_i^d}{a_i}}{\frac{\tau}{\psi a_i}(\sum_{i \neq j}^{M} Pc_j^d) + \tilde{I}_0^d + N} \tag{2.29}$$

where a_i is the path loss between the desired user *i* and the respective BS.

In a severe multipath environment, where τ =0.8, the advantages of synchronous transmission in the downlink may be cancelled due to a greater carrier power as a consequence of the pilot signal (ψ =0.8). In this case, where $\psi = \tau$, equation (2.29) becomes,

$$\gamma_i^d = \frac{\frac{\tilde{Pc}_i^d}{a_i}}{\frac{1}{a_i}(\sum_{i \neq j}^{M} \tilde{Pc}_j^d) + I_0^d + N}. \tag{2.30}$$

The above equation can be written in matrix notation as,

$$(\text{diag}((\gamma^d \oplus \text{MB}_{c_i,c_i})^T) + \text{diag}(\text{MB}_{c_i,c_i}) - (\gamma^d \oplus \text{MB}_{c_i,c_i})\text{J})(\text{Pc}_i^d)^T$$

$$= (\gamma^d \oplus \text{Im}_{c_i})^T \tag{2.31}$$

where Pc_i^d are the transmitted code powers at one TS in the *i*th cell, Im_{c_i} is the interference vector at the MSs in cell c_i, $\gamma = (\gamma_i^d, ..., \gamma_{|M_i|}^d)^T$ is the vector of the required carrier-to-interference ratios at the MSs in cell *i*.

Now, let $\text{B} = \text{diag}((\gamma^d \oplus \text{MB}_{c_i,c_i})^T) + \text{diag}(\text{MB}_{c_i,c_i})$ and $\text{e} = (\gamma^d \oplus \text{MB}_{c_i,c_i})$

$$(\text{B-eJ})\,(\text{Pc}_i^d)^T = (\gamma^d \oplus \text{Im}_{c_i})^T.$$

The inverse of (B-eJ) is

$$(\text{B} - \text{eJ})^{-1} = \text{B}^{-1} + \frac{\text{B}^{-1}\text{eJB}^{-1}}{1 - \text{JB}^{-1}e}. \tag{2.32}$$

Substituting equation (2.32) into equation (2.31), the required code powers at the BS in cell c_i is given as

$$(\mathrm{Pc}_i^{\mathrm{d}})^T = \frac{\mathrm{B}^{-1}(\gamma^d \oplus \mathrm{Im}_{c_i})^{\mathrm{T}} + \mathrm{B}^{-1}\mathrm{eJB}^{-1}(\gamma^{\mathrm{d}} \oplus \mathrm{Im}_{c_i})^{\mathrm{T}} - \mathrm{B}^{-1}(\gamma^{\mathrm{d}} \oplus \mathrm{Im}_{c_i})^{\mathrm{T}}\mathrm{JB}^{-1}\mathrm{e}}{1 - \mathrm{JB}^{-1}e}. \tag{2.33}$$

The slot powers for the cell c_i can be found from equation (2.33) as

$$\mathrm{Pc}_i^d = \mathrm{J}\,\mathrm{Pc}_i^{\mathrm{d}}. \tag{2.34}$$

Equation (2.34) gives the vector of transmitted slot powers as

$$\mathrm{Pc}^{\mathrm{d}} = (\mathrm{JPc}_1^{\mathrm{d}}, ..., \mathrm{JPc}_{\mathrm{L}}^{\mathrm{d}}). \tag{2.35}$$

Equation (2.35) shows that the slot power (BS transmission power) at each cell c_i is a function of the interference powers seen at the corresponding served MSs, Im_{c_i}. So, equation (2.35) can be more generally denoted as,

$$\mathrm{Pc}^{\mathrm{d}} = f(\mathrm{Im}). \tag{2.36}$$

Equation (2.25) gives the transmitted code powers for a user in a single cell and equation (2.36) gives the vector of transmitted slot powers. These two equations can be combined to rewrite the equations of (2.16) and (2.17) as shown in equation (2.37).

$$\begin{aligned} \mathrm{Im} &= \mathrm{U}\ \Theta\ \mathrm{Ib}\ (\alpha\ \Theta\ \mathrm{MM}) + \mathrm{Pc}^{\mathrm{d}}(\mathrm{Im})\ (\bar{\alpha}\ \Theta\ \mathrm{BM}) \\ \mathrm{Ib} &= \mathrm{Pc}^{\mathrm{d}}(\mathrm{Im})\ (\alpha\ \Theta\ \mathrm{MM}) + \mathrm{U}\ \Theta\ \mathrm{Ib}\ (\bar{\alpha}\ \Theta\ \mathrm{MB}) \end{aligned} \tag{2.37}$$

Equation (2.37) shows that a MS receives interference both from other MSs that are in uplink and also other BSs that are in downlink. Similarly, a BS receives interference from other BSs that are in downlink and other MSs that are in uplink. The process of a MS receiving interference from other MSs and a BS receiving interference from other BSs is

called self jamming and such a type of interference scenario is also present in a FDD system. But the process of a MS receiving interference from BSs and a BS receiving interference from other MSs is referred to as cross jamming and this effect is inherent to systems that employ TDD. The magnitude of self and cross jamming can be controlled by means of the synchronization matrix α and this idea is exploited by the TS-opposing algorithm presented next.

In UTRA-TDD, the multiple access mode consists of a hybrid TD-CDMA interface. One TDMA time slot (TS) can be divided into say a maximum of *Q* TSs and each TS can be used either in the uplink or downlink. This is used by the centralized TS-opposing algorithm to reduce interference. This algorithm is executed at the higher level in the radio network controller (RNC).

The TS-opposing algorithm is a DCA algorithm and it reduces interference at the BSs by either applying synchronous or asynchronous transmission with respect to the neighboring cell. The algorithm is executed for each BS of a cellular network. The algorithm begins at the point where the MS will go into outage. In other words, the execution of the algorithm starts when the MS in the reference cell is requested to transmit with more power than the maximum allowed transmission power. The algorithm assumes that each MS has at least two TSs for communication with the BS. It records the interference at all *n* TSs in all the neighboring cells. Assuming that the reference cell is in uplink, there can two different cases.

Case 1: The TS in the neighboring cell can be in uplink and in this case the interference is caused only by the MSs in the neighboring cell. This is a case where the neighboring cell is in synchronous transmission with the reference cell.

It can be assumed that the MSs in the neighboring can determine their path loss to the BS in the neighboring cell and this can be accomplished by means of a fixed transmission power on the pilot channel. The MSs in the neighboring cells report their transmission power and path loss to the BS which in turn makes it available to the RNC. Hence the vector of transmission powers of the mobile in cell *i*, $\mathrm{Pc}_{\mathrm{i}}^{\mathrm{u}}$, and the path gain matrix of mobiles in cell *i* to the BS in cell *j*, MB_{c_i,c_j} are assumed to be available to the TS-opposing algorithm.

Case 2: The TS in the neighboring cell can be in downlink and in this case the interference is caused only by the BSs in the neighboring cell to the BS in the reference cell. This is a case of asynchronous transmission with respect to the reference cell and the neighboring cell. The transmission power of the BSs can be easily reported to the RNC and also the path loss between the neighboring BS and the reference BS, BB_{c_i,c_j}.

The algorithm checks to see if there is one TS *n* in the neighboring cell, c_j, that would cause less interference than the present TS *k*. If so, and if both the TSs are in opposing directions of transmission (TS *n* is used for reception and TS *k* is used for transmission or TS *n* is used for transmission and TS *k* is used for reception), then the neighboring cell interchanges TS *n* with TS *k*. This results in TS-opposing time slots with respect to cell c_j.

The flowchart of the steps involved in the simulation is shown in figure 2-7.

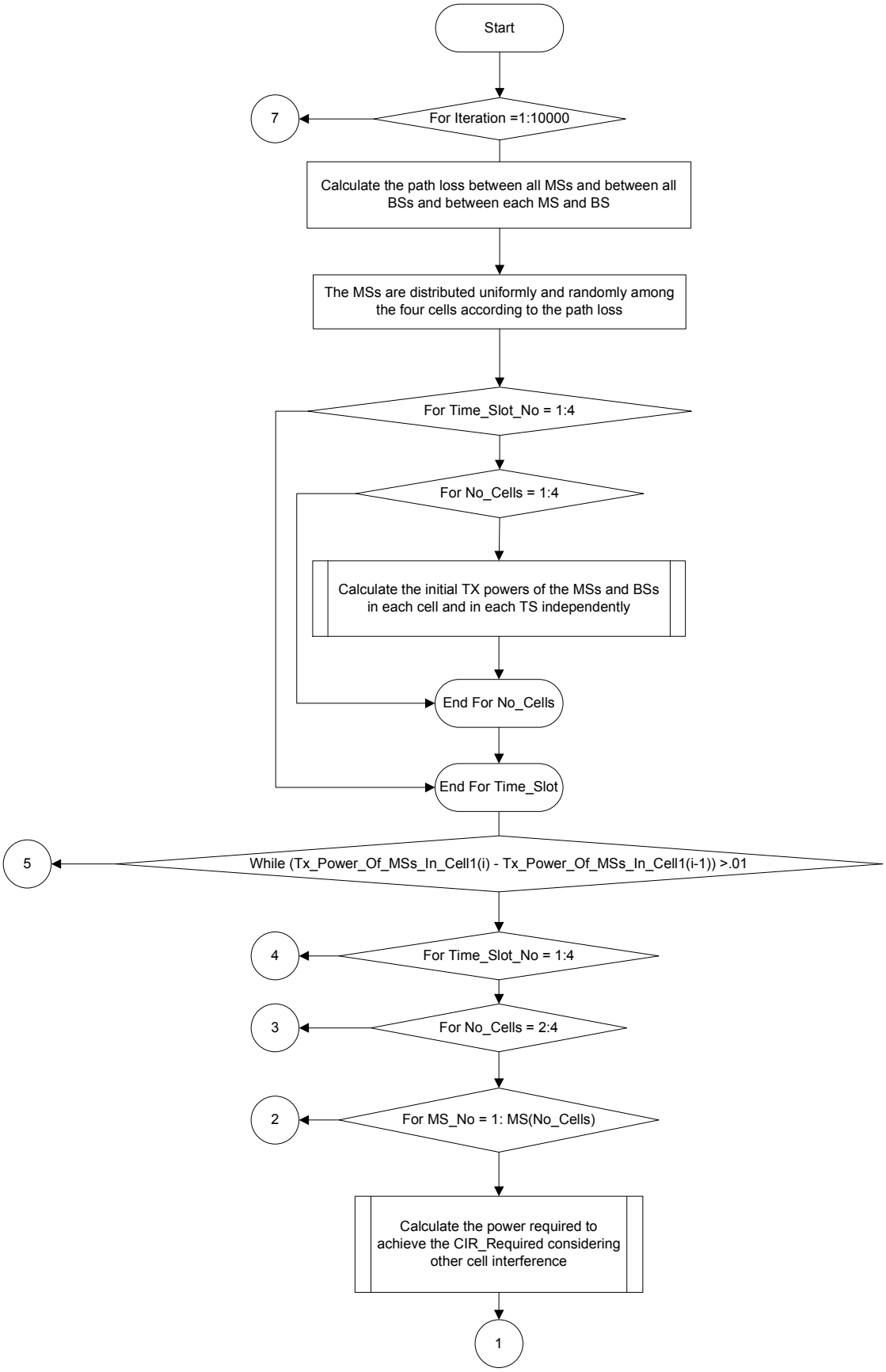
Start
For Iteration =1:10000
7
Calculate the path loss between all MSs and between all BSs and between each MS and BS
The MSs are distributed uniformly and randomly among the four cells according to the path loss
For Time_Slot_No = 1:4
For No_Cells = 1:4
Calculate the initial TX powers of the MSs and BSs in each cell and in each TS independently
End For No_Cells
End For Time_Slot
While (Tx_Power_Of_MSs_In_Cell1(i) - Tx_Power_Of_MSs_In_Cell1(i-1)) >.01
5
For Time_Slot_No = 1:4
4
For No_Cells = 2:4
3
For MS_No = 1: MS(No_Cells)
2
Calculate the power required to achieve the CIR_Required considering other cell interference
1

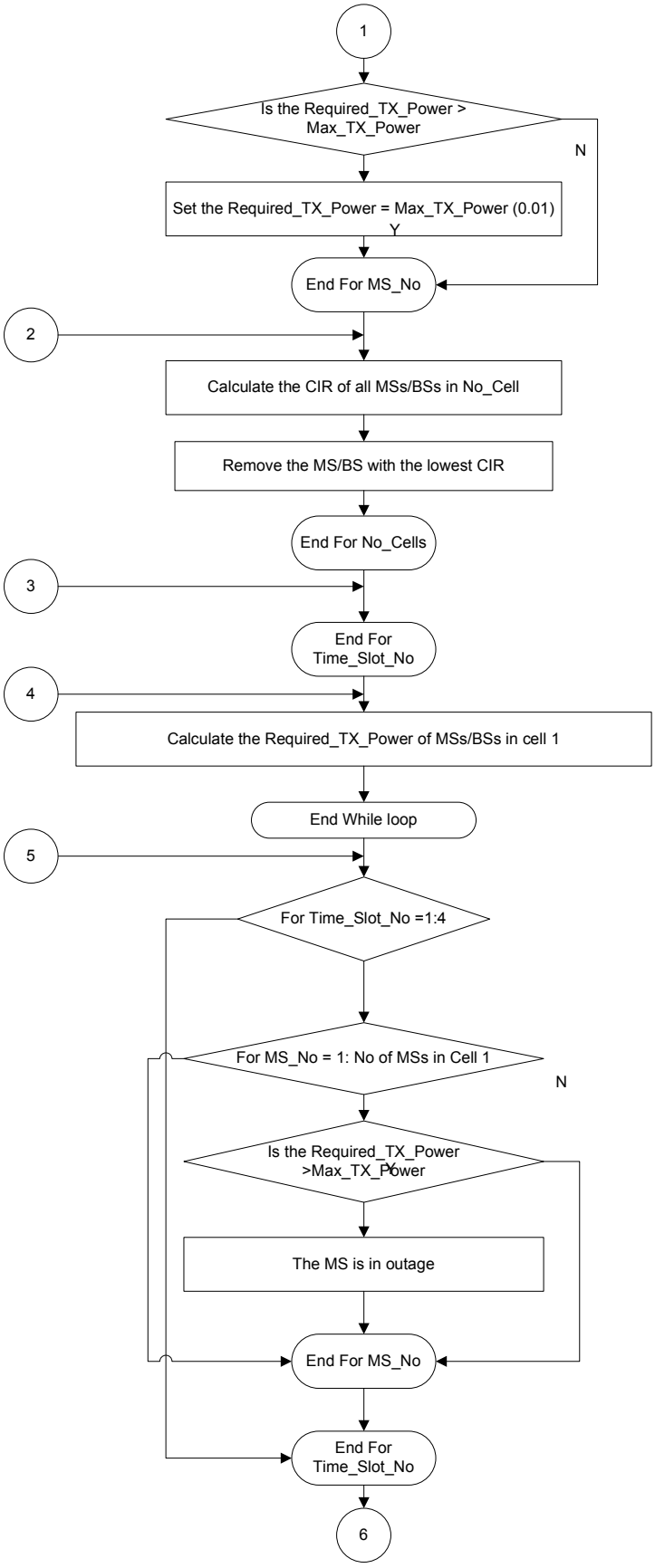
1
Is the Required_TX_Power > Max_TX_Power
N
Set the Required_TX_Power = Max_TX_Power (0.01)
Y
End For MS_No
2
Calculate the CIR of all MSs/BSs in No_Cell
Remove the MS/BS with the lowest CIR
End For No_Cells
3
End For Time_Slot_No
4
Calculate the Required_TX_Power of MSs/BSs in cell 1
End While loop
5
For Time_Slot_No =1:4
For MS_No = 1: No of MSs in Cell 1
N
Is the Required_TX_Power >Max_TX_Power
Y
The MS is in outage
End For MS_No
End For Time_Slot_No
6

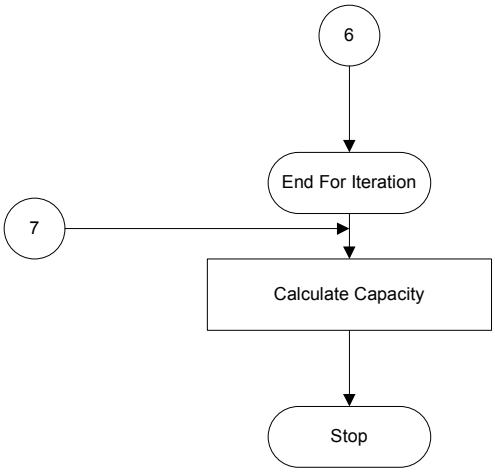

Figure 2-7: Flowchart depicting the steps invloved in the TS-opposing algorithm.

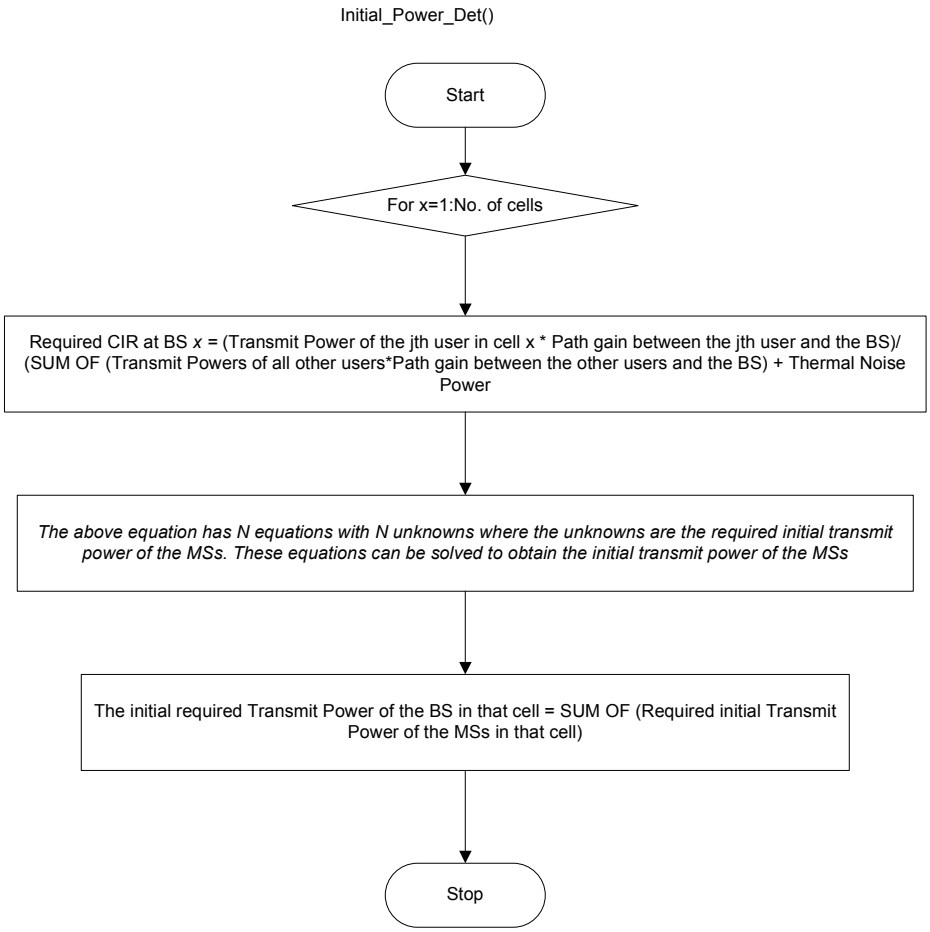

Figure 2-8: Flowchart depicting the calculation of initial power of MSs and BSs.

2.3.2 System Specification

The simulation platform consists of four square-shaped cells. Square-shaped cells are used as the cell wraparound technique is easy to apply and also the shape is a good approximation to an indoor environment. The wraparound technique ensures that each cell is surrounded by a symmetric pattern composed of three different cells. The MSs are assigned to the BS offering the lowest path cell with a handover margin of 5dB. The path loss formula used is given in equation (2.38).

$$a = 37 + 30\log_{10}(d) + 18.3p^{(((p+2)/(p+1))-0.46)} + \xi \quad \text{in dB} \tag{2.38}$$

where, d is the distance between the transmitter and receiver in meters, p is the number of floors in the path and ξ is the lognormal variable modeling shadow fading.

In the simulation environment 4 consecutive TSs are considered. Also, each user or MS in cell 1 occupies four consecutive TSs and each user in cells 2, 3, and 4 occupies 2 consecutive TSs. The deployment scenario is shown in figures 2-9 and 2-10.

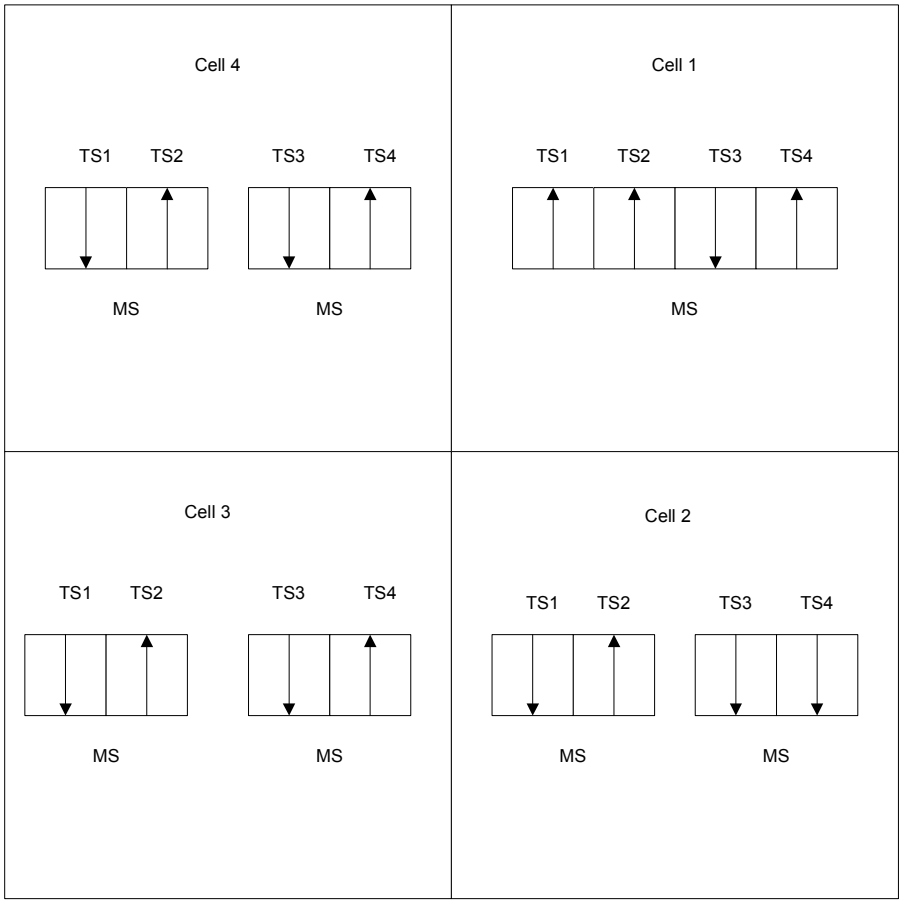

Figure 2-9: Diagram showing the Transmit and Receive Directions of the MSs in Cells 1, 2, 3, and 4.

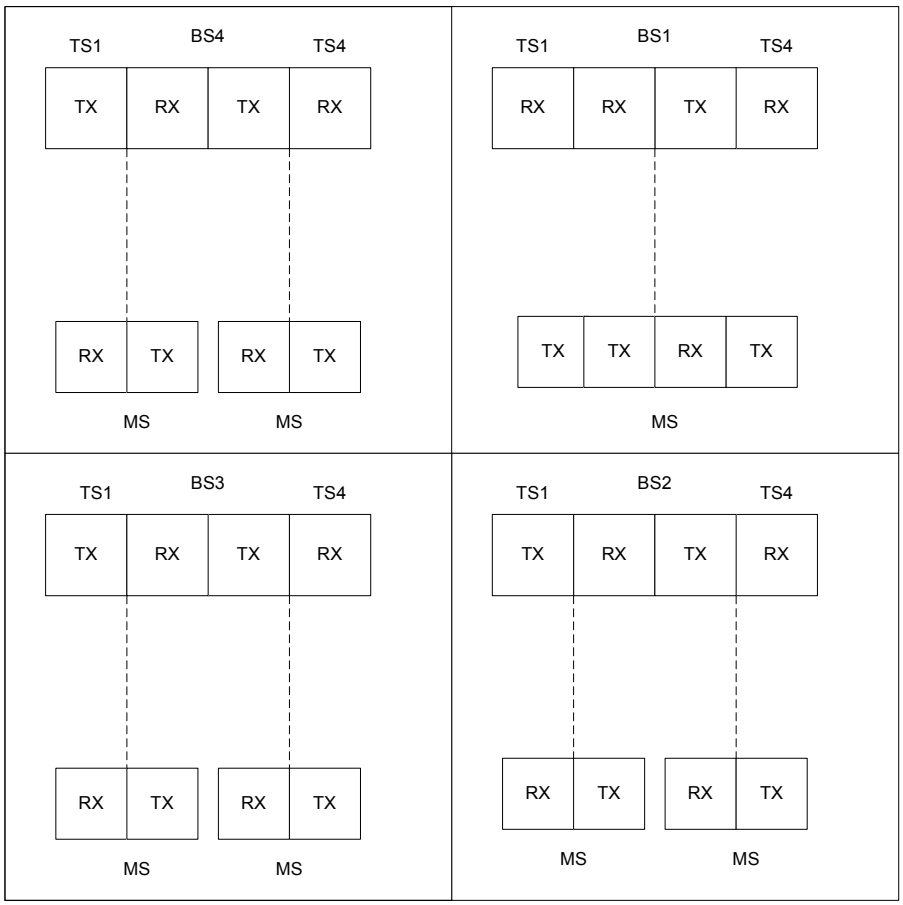

Figure 2-10: Deployment scenario of the BS and MS configurations in Cells 1, 2, 3, and 4.

As a user in cell 1 uses 4 TSs, an asymmetric communication channel can be created in cell 1 with respect to the uplink and downlink transmissions. Channel asymmetry in cell 1 leads to asynchronous TS overlaps with respect to at least one of the neighboring cells. A predefined number of users are randomly and uniformly distributed throughout the network that is composed of the four square-shaped cells. Then the power control loops in the uplink (equation (2.25)) and downlink (equation (2.33)) are initiated. When a MS is required to transmit with power greater than the maximum allowable transmission

power, the TS-opposing algorithm would try to reduce the interference at the BS to which the MS is connected, so that it could transmit with lesser power to maintain the required carrier-to-interference ratio at the corresponding BS. If the algorithm fails, then the particular MS is in outage. This algorithm is repeated for all the MSs in the cell if needed and then the capacity for a cell c_i is calculated using the following equation:

$$\overline{C}_{c_i} = 1/4(E[M_{tot_i}] - E[M_{out_i}])W_i \qquad i = 1,\ldots, L \text{ [kbps/TS]} \qquad (2.39)$$

where $E[M_{tot_i}]$ is the average number of MSs that are distributed in cell c_i, $E[M_{out_i}]$ is the average number of MSs that experience outage in cell c_i, W_i is the data rate of the user in cell c_i. As 4 TSs are assumed an averaging factor of 4 is used. The capacity per cell and per TS can be found using equation (2.40).

$$\overline{C} = 1/4\sum_{i=1}^{4}\overline{C}_{c_i} \qquad \text{[kbps/cell/TS]} \qquad (2.40)$$

The experiments are carried out using Monte-Carlo simulation and the following two channel assignment strategies are used and compared:

Channel Assignment 1: The transmission and reception directions are chosen so that the number of asynchronous overlaps is minimum and then the MSs are allocated randomly and uniformly. So, this assignment resembles a FCA strategy as the direction of transmission for each TS is fixed.

Channel Assignment 2: The new TS-Opposing algorithm is applied that dynamically adjusts the direction of transmission for each TS.

The following parameters are used in the simulation:

Table 2-1: Parameters used for the simulation of Centralized DCA Algorithm.

Parameter	Value
Cell Radius	50 m
Bit rate	16 Kbps
Chip rate	3.84 Mcps
Shadowing	10 dB
Thermal noise density	169 dBm
Max. MS TX power	10 dBm
Max. BS TX power	24 dBm
Min. bit-energy to interference ratio	3.5 dB
Path loss	Indoor test environment (2.38)
Handover Margin	5 dB

2.3.3 Numerical Results

The result of the capacity in terms of [Kbps/TS] obtained for cell 1, cell 2, cell 3 and cell 4 is given in this section.

Simulations were conducted for four different scenarios. The results for Scenario 1 are given in figure 2-11. In this scenario, a MS in cell 1 uses TS 1, 2, and 4 for UL communication and TS 3 for DL communication while MSs in cells 2, 3, and 4 use TS 1 for DL communication and TS 2 for UL communication.

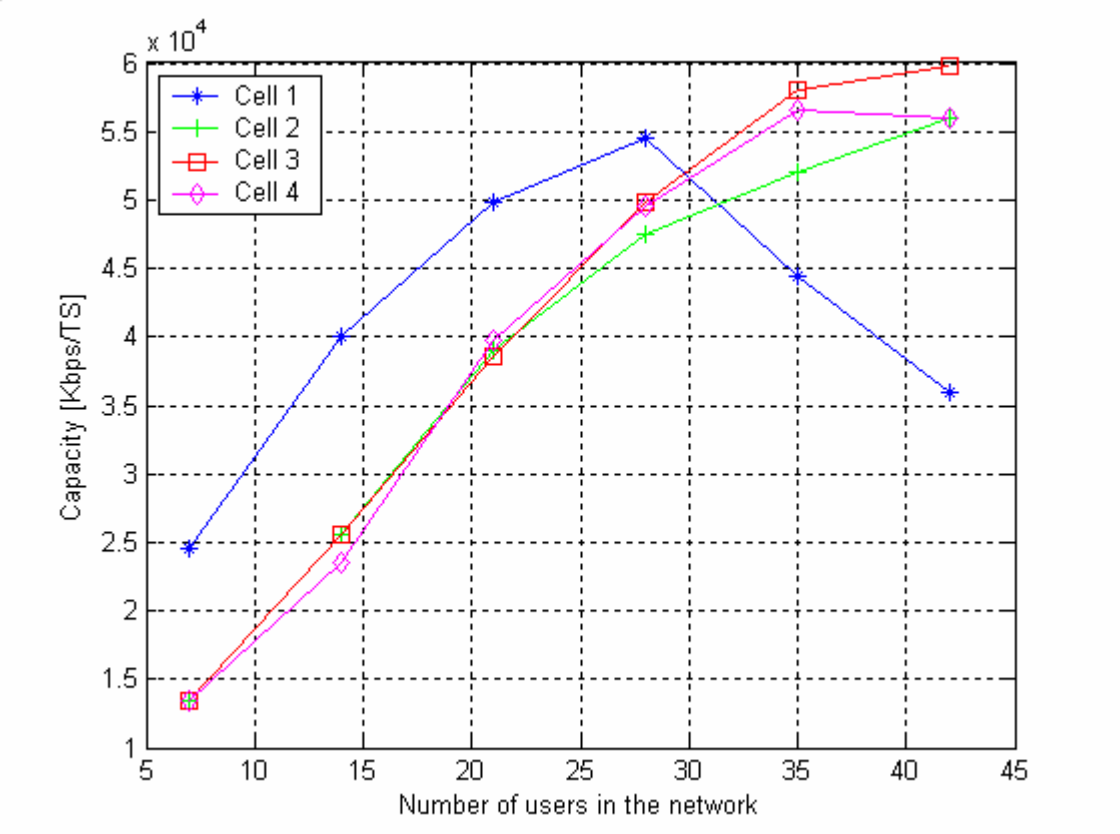

Figure 2-11: FCA Average Capacity in Kbps/TS for Cell 1, Cell2, Cell 3, and Cell 4 in scenario 1.

The plots in figure 2-11 show that the capacity of cells 2, 3 and 4 are about the same due to symmetry as the MSs use the same of time Slots (TSs) to communicate with the BSs. The capacity of Cell 1 is initially higher than the other cells and this can be explained as follows: each user in cell 1 uses four TSs while the users in other cells use only two TSs. Also, the capacity of the cell is maximum for about 28-32 users. This is because the pole capacity of the cell is reached when eight MSs are active simultaneously and every user beyond the eight is in outage. But the MSs in cells 2, 3, and 4 use only two TSs and so can accommodate twice the number of users. The increase in the number of users in these cells leads to more interference power in cell 1 and so a reduction in capacity.

The result obtained for the total capacity in the network is shown in figure 2-12.

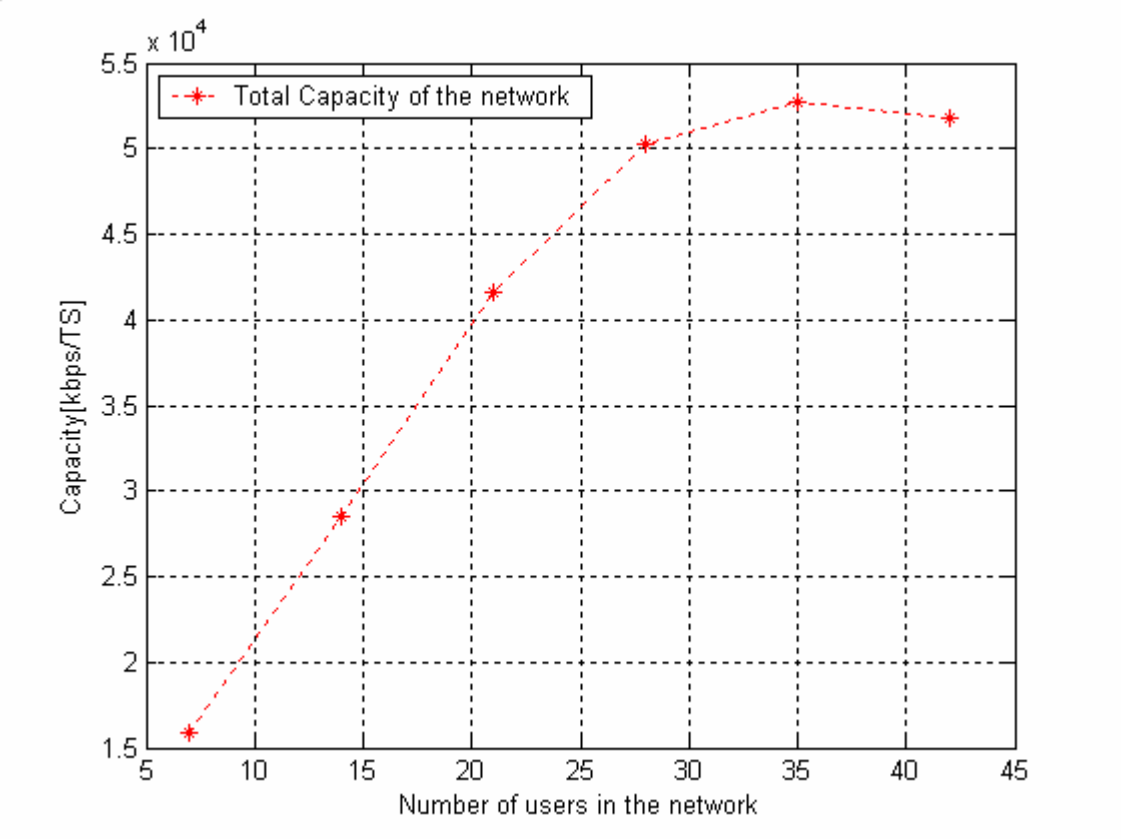

Figure 2-12: Accumulated Average Capacity over All Cells in Kbps/Cell/TS.

The results for Scenario 2 are given in figure 2-13. In this scenario, a MS in cell 1 and 2 uses TS 1, 2, and 4 for UL communication and TS 3 for DL communication while MSs in cells 3, and 4 use TS 1 for DL communication and TS 2 for UL communication.

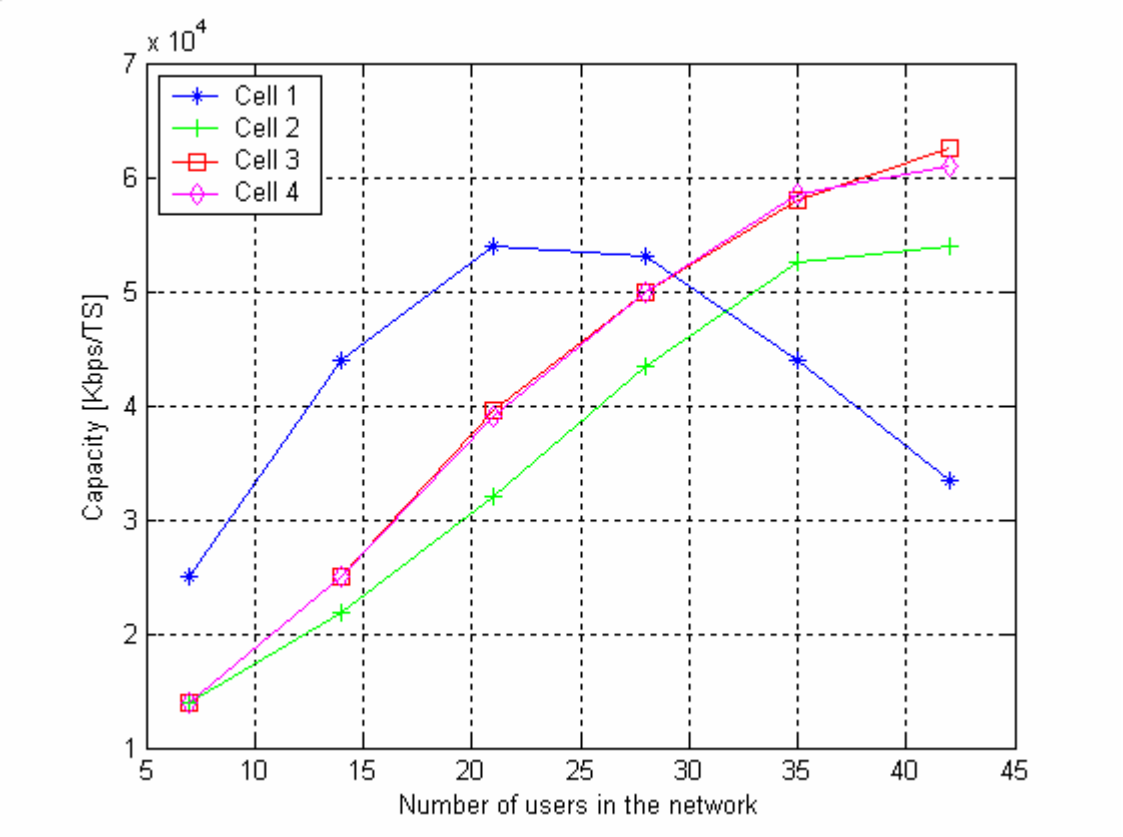

Figure 2-13: FCA Average Capacity in Kbps/TS for Cell 1, Cell2, Cell 3, and Cell 4 in scenario 2.

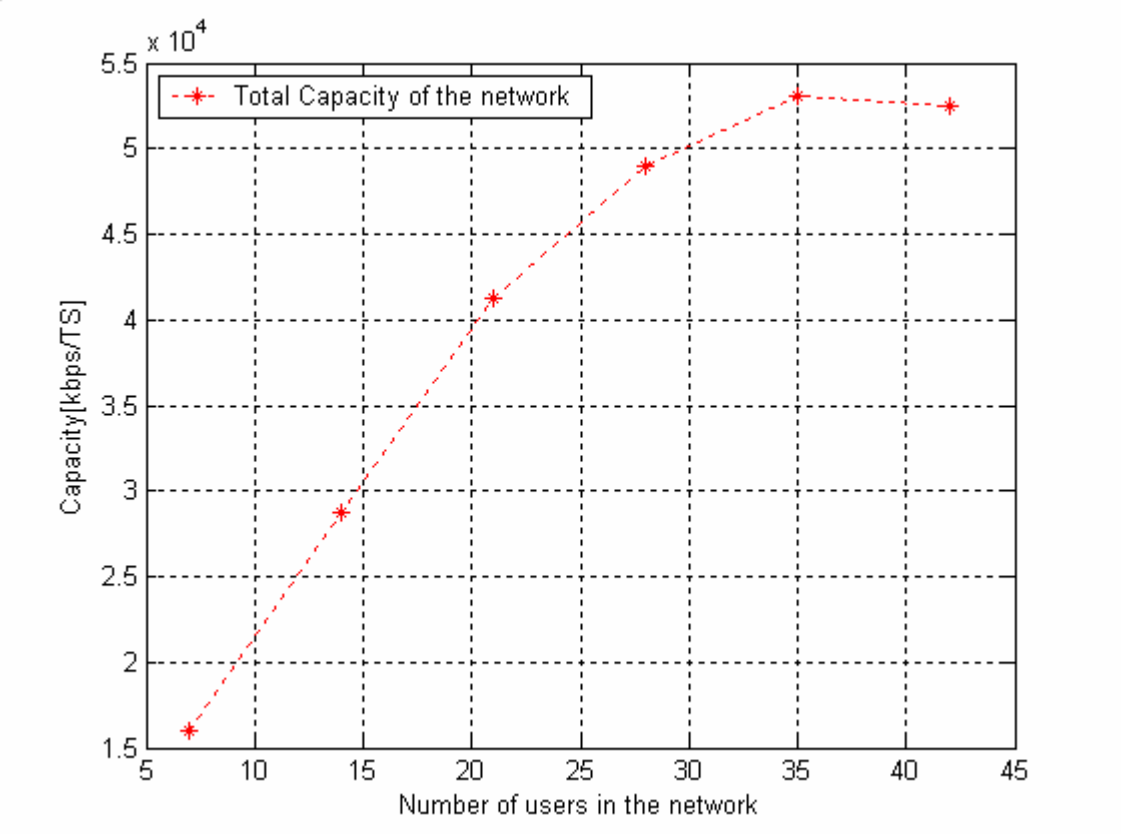

Figure 2-14: Accumulated Average Capacity over All Cells in Kbps/Cell/TS.

In this scenario, the capacity of cell 1 is greater than in scenario 1 as it faces only opposing transmission from two neighboring cells (cells 3 and 4 and not cell 2). But, as cell 2 faces asynchronous overlap (from cells 3 and 4), the capacity of cell 2 is reduced compared to scenario 1. The capacity of cells 3 and 4 remains the same due to symmetry.

The results for Scenario 3 are given in figure 2-15. This is a symmetric scenario where MS in cell 1 uses TS 1 and 3 for DL communication and TS 2 and 4 for UL communication while MSs in cells 2, 3, and 4 use TS 1 for DL communication and TS 2 for UL communication

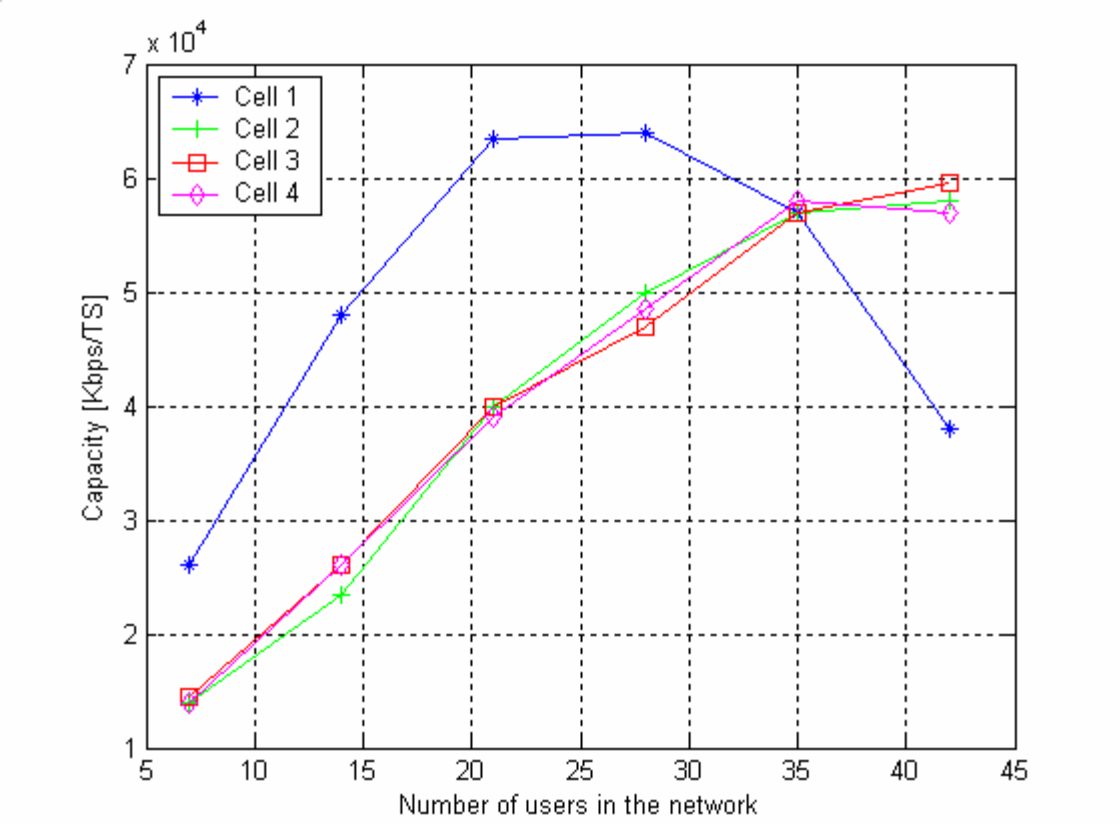

Figure 2-15: FCA Average Capacity in Kbps/TS for Cell 1, Cell2, Cell 3, and Cell 4 in scenario 3.

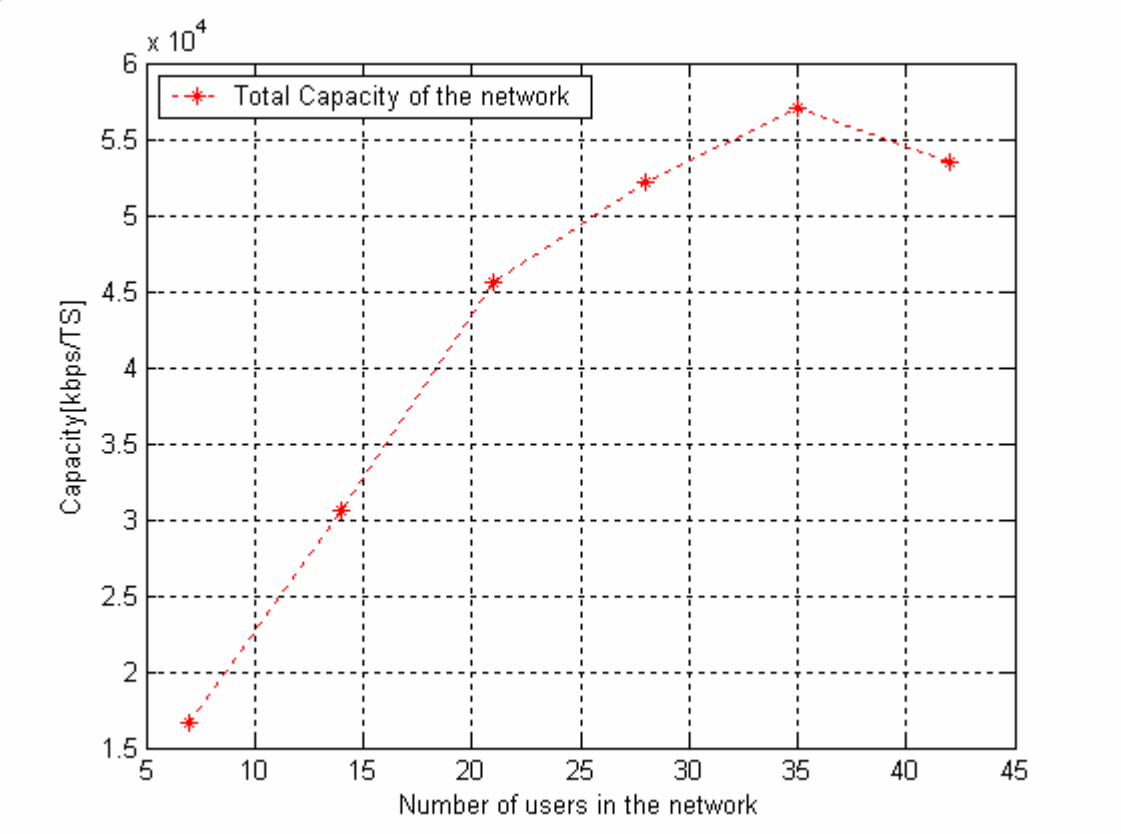

Figure 2-16: Accumulated Average Capacity over All Cells in Kbps/Cell/TS.

The results obtained when the TS-opposing algorithm is applied to scenario 1 are shown in figures 2-17 and 2-18.

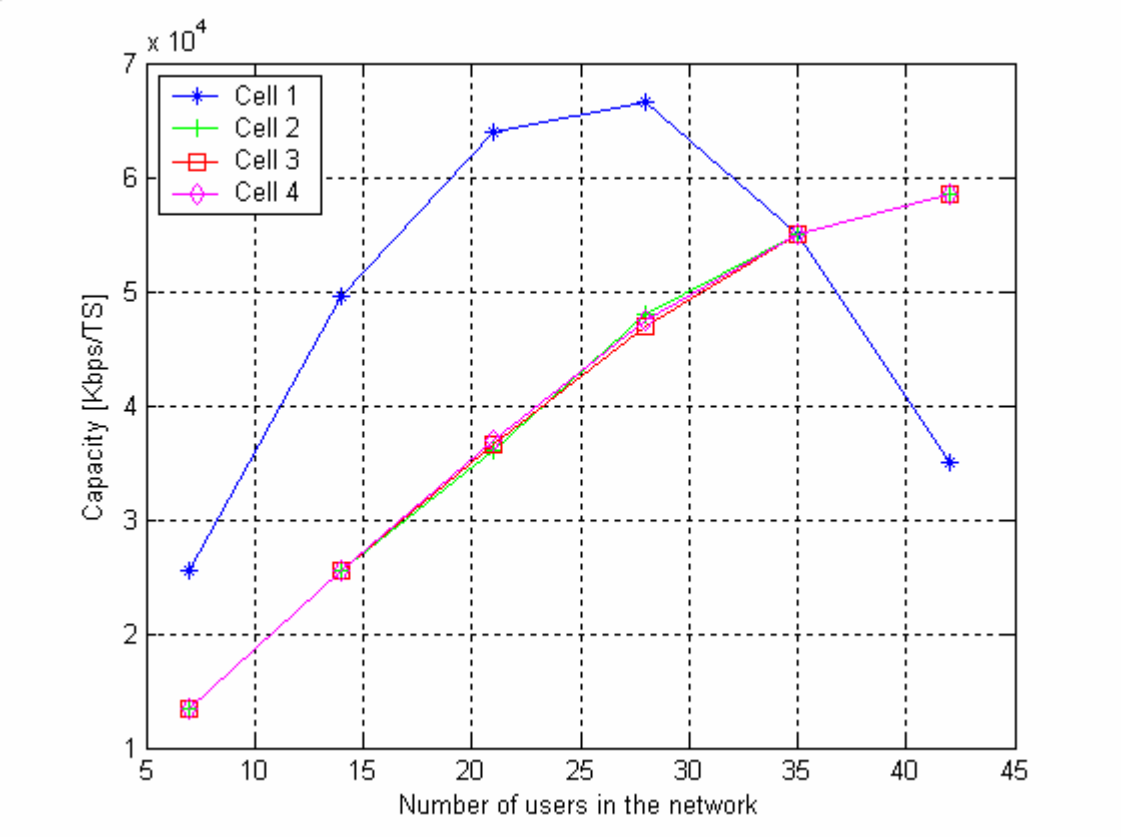

Figure 2-17: DCA Average Capacity in Kbps/TS for Cell 1, Cell2, Cell 3, and Cell 4 in scenario 1.

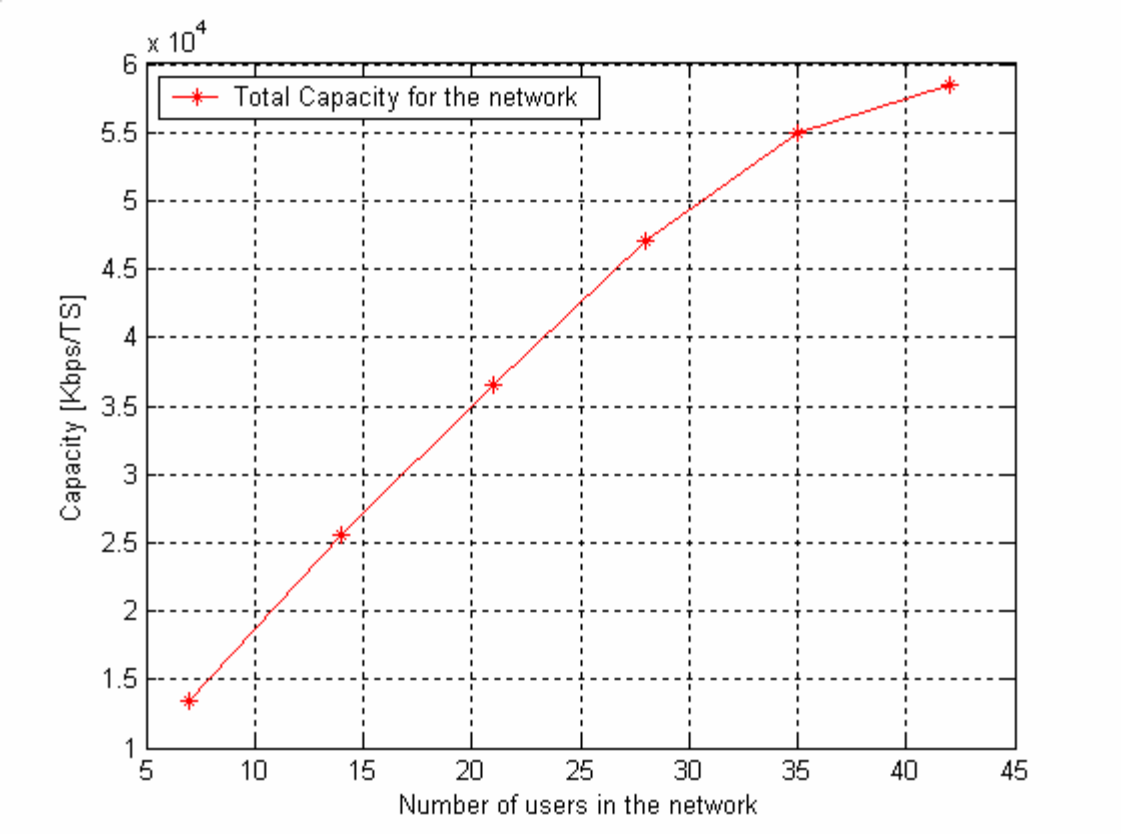

Figure 2-18: Accumulated Average Capacity over All Cells in Kbps/Cell/TS.

Comparing figures 2-11 and 2-17, it can be seen that the TS-opposing algorithm improves the capacity in cell 1 by about 20% - 30% when the number of distributed users is between 14 and 35. The increase in capacity in the other cells is negligible. Thus it can be concluded that the TS-opposing algorithm increases the capacity in Cell 1 without affecting the capacity in Cells 2, 3, and 4.

2.4 D-TDD in TDMA systems

The poor performance of TDMA/D-TDD cellular systems when omni-directional antennas were used at the base stations was shown in [3]. Smart antenna concepts were applied to alleviate the serious BS-BS interference problem. When there is co-channel interference from other base stations in downlink, smart antenna adaptively forms a reception beam pattern to place nulls in the direction of the strong interfering signals. In

[3], smart antennas with *m* elements (*m* = 8, 16, 26) were used at the base station. The SIR was found to increase as the number of sensor elements was increased from 8 to 16 and to 26. As an example, at an outage of 1%, the SIR obtained using omni-directional antennas was 5dB which increased to 17dB when an 8-element smart antenna was used. The corresponding SIR using 16 and 26 element smart antenna was 22dB and 25dB respectively.

Time slot allocation (TSA) methods were combined with sectored antennas to improve the outage performance in uplink performance in [5]. The TSA techniques avoid the co-channel interference by exploiting the spatial distributions of the location of MSs within a cell and the time orthogonal nature of the TDMA frames. Two algorithms, namely, *Max* {SIR} and *Max Min* {SIR} were introduced to achieve the same. According to these algorithms, the BS can schedule a MS transmission request for the uplink time slots so that the best sector is active for that time slot. The outage probability showed significant improvements in performance when the TSA techniques were employed. As an example, the outage probability at 1% increased by about 14 dB when TSA was used compared to no usage of TSA.

The TSA techniques developed in [5] were used to analyze the spectral efficiency of TDMA/D-TDD systems in [51]. The spectral efficiency was found to increase by nine times when TSA techniques are used compared to no usage of TSA technique. Moreover, the spectral efficiency increased by a factor of 26 when adaptive modulation was used in these systems.

In [3], the analysis of the performance of a fixed cellular D-TDD system that use omni-directional antennas at the base station was carried out. In this analysis, square

shaped cellular architecture having a radius of 4000 m was considered for simplicity. The separation between co-channels was provided through frequency reuse and TDD was used in each carrier to provide for two way communication, that is, communication in the uplink and downlink. Each TDD frame was assumed to have 48 time slots (TSs) and these time slots can be used for either uplink or downlink transmission. The TSs are shared by many subscribers that are uniformly and randomly distributed over each cell. Each subscriber can use a different number of TSs and the requirement for each subscriber is decided by the service requirement of each subscriber. It is also assumed that the system is fully loaded, that is, the primary TSs are always occupied by active subscribers. Omni-directional or sectored antennas are used at the base station to provide uniform coverage. Also, the antenna is located at a much higher height at the base station and so the attenuation between two base station antennas is less compared to the attenuation between two subscriber antennas or between a base station antenna and a subscriber antenna. It is also assumed that the cellular system is perfectly synchronized and so all the base stations simultaneously start a new TDD frame. Only the signal to interference ratio is analyzed to measure the system performance. Also, only log-normal fading is assumed to model the shadowing effects. The transmission power from the subscribers and the base station is assumed to be of the same level. Practically, these are of different levels, but this difference is taken care of by using different propagation exponent factors. The subscriber-to-subscriber interference in the downlink is less severe than the expected base-to-subscriber interference and so the downlink performance will be improved and will not be a limiting factor.

There are 12 subscribers served in each TDD frame and so there are at-least 12 TSs for uplink traffic, one TS for each user. Thus, the maximum number of downlink TSs is 36. The maximum number of extra uplink time slots is chosen as a variable, denoted as *DyBD*. The specific number of extra uplink TSs for each individual cell is drawn from (1, *DyBD*) as a discrete uniformly distributed random variable.

The received desired signal power for the first 12 UL TSs at the *m*-th TS is given by,

$$S_m = \frac{P}{R_m^n} \times 10^{\frac{\xi_m}{10}} \tag{2.41}$$

where, P is the power transmitted by the subscriber in the *m*-th TS,

R_m is the distance between the *m*-th subscriber and the base station,

ξ_m is a Gaussian random variable with zero-mean and a standard deviation of 6 dB to 8 dB.

The subscriber to base power attenuation factor used in (2.41) is n=4.

The interference power coming from the subscribers in the first and second tier of cells is similar to the equation (2.41). In the first 12 TSs, all the users in all the cells are in uplink transmission and so the interference power obtained at the desired base station is given by,

$$I_{S-B}^m(k) = \frac{P}{R_{mk}^n} \times 10^{\frac{\xi_{mk}}{10}} \tag{2.42}$$

where, P is the power transmitted by the *m*-th subscriber in the *k*-th co-channel cell,

R_{mk} is the distance between the *m*-th subscriber in the *k*-th co-channel cell and the desired base station,

ξ_m is a Gaussian random variable with zero-mean and a standard deviation of 6 dB to 8 dB.

The subscriber to base power attenuation factor used in (2.42) is n=4.

The signal-to-interference ratio in the first 12 TSs is therefore given by,

$$\frac{S_m}{I} = \frac{S_m}{\sum_{k=1}^{K} I_{S-B}^{m}(k)} \tag{2.43}$$

where K is the number of co-channel cells and K=8 if only the first tier of co-channel cells is considered and K=24 is both the first and second tier of co-channel cells are considered.

In the analysis, the maximum number of extra uplink TSs (*DyBD*) is chosen from {3, 6, and 12}. In each cell, the exact number of extra uplink TSs, N_{extra}^{M}, is chosen as a uniformly distributed discrete random variable that can take values in the range (1, *DyBD*). Thus, the total number of uplink TSs in the M-th cell is given by,

$$N_{up}^{M} = 12 + N_{extra}^{M}. \tag{2.44}$$

During, the extra TSs, the interference at the desired base station maybe the uplink signal power from other subscribers located in the co-channel cells or the downlink signal power from the other co-channel base stations. The interference power from the subscribers in the co-channel cells is given by equation (2.42) and is repeated again.

$$I_{S-B}^{m}(k) = \frac{P}{R_{mk}^{4}} \times 10^{\frac{\xi_{mk}}{10}}.$$

The interference power from the co-channel base stations is given by,

$$I_{B-B}^{m}(k) = \frac{P}{R_{Bk}^{3}} \times 10^{\frac{\xi_{Bk}}{10}} \tag{2.45}$$

where, P is the power transmitted by base station in the k-th co-channel cell,

R_{Bk} is the distance between the base station in the k-th co-channel cell and the desired base station,

ξ_{Bk} is a Gaussian random variable with zero-mean and a standard deviation of 4 dB to 6 dB.

The base station to base station power attenuation factor used in (2.45) is 3.

Now, the signal-to-interference ratio during the extra uplink time slots is given by,

$$\frac{S_m}{I} = \frac{S_m}{\sum_{k=1}^{K} [Q_k \times I_{S-B}^{m}(k) + (1 - Q_k) \times I_{B-B}(k)]} \tag{2.46}$$

where Q_k is a Bernoulli random variable. If the number of extra uplink TSs in the desired cell is N_{extra}^{0} and the number of extra uplink TSs in the k-th co-channel cell is N_{extra}^{k}, the probability distribution of Q_k is given by,

$$\text{Prob}(Q_k) = \begin{cases} \text{Prob}(N_{extra}^{k} < N_{extra}^{0}), Q_k = 0 \\ \text{Prob}(N_{extra}^{k} \geq N_{extra}^{0}), Q_k = 1 \end{cases}. \tag{2.47}$$

Initially, omni-directional antennas are used both at the subscriber site and base station site. The simulations are performed for the following four cases: when there are no extra uplink slots; when the maximum number of extra uplink TSs in a cell is 3; when the maximum number of extra uplink TSs in a cell is 6; and when the maximum number of extra uplink TSs in a cell is 12. The probability of SIR outage is compared for the four cases. The various parameters used in the simulation are summarized in table 2-2. The results of the simulation are shown in figure 2-19.

Table 2-2: Simulation parameters when omni-directional antennas are used at the subscriber and base station site.

Parameter	*Value*
Cell size	4000 m
Frequency reuse	25
Number of Co-channel cells	24 (First and second tier)
Number of users per cell	12
Path loss exponent – MS to BS	4
Path loss exponent – BS to BS	3
Lognormal shadowing – MS to BS	6 dB
Lognormal shadowing – BS to BS	4 dB
Number of iterations	10000

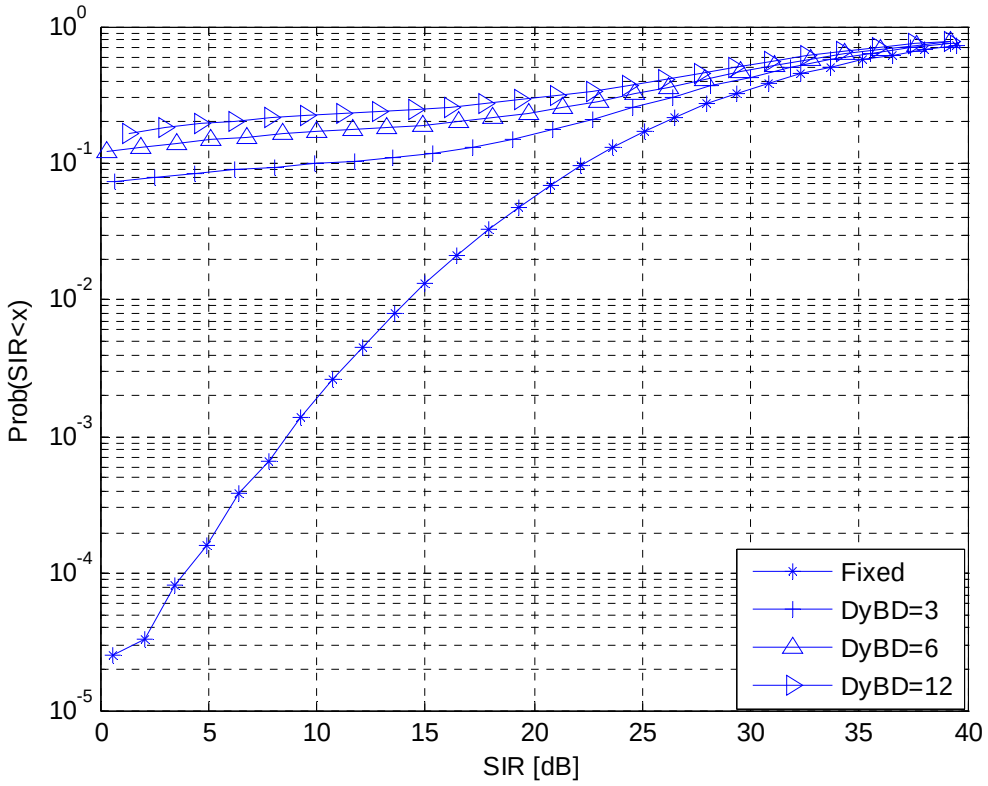

Figure 2-19: SIR outage using omni-directional antennas.

It can be seen that the performance of the system degrades when the boundary between the uplink and downlink transmission is made dynamic. When the boundary is fixed, at an SIR outage of 1%, the achievable SIR is 15 dB but the SIR curve saturates at a rapid rate when the maximum number of extra uplink TSs is chosen to be three. This proves that the base station-to-base station interference in the extra uplink time slots reduces the throughput of the system and this is a disadvantage of dynamic TDD systems unless a countermeasure is developed.

Next, sectored antennas can be considered to suppress the co-channel interference. *S*-sectored antennas are deployed at the site of the base station and in the present analysis *S*=4. A square aperture antenna is deployed at each sector. The far-field antenna pattern under uniform illumination over the azimuth plane is proportional to [52]

$$E(\phi) \propto \frac{1+\cos(\phi)}{2} \times \frac{\sin(\frac{ka}{2}\sin\phi)}{\frac{ka}{2}\sin(\phi)} \tag{2.48}$$

where, a is the lateral size of the aperture in meters,

ϕ is the azimuth angle,

f is the frequency of operation that equals 1.9 GHz, and

k is the wave number where

$$k = w\sqrt{\mu_0 \varepsilon}_0 \tag{2.49}$$

with $\varepsilon_o = 8.85 * (10^{-12})$ F/m and $\mu_0 = 4 * \pi * (10^{-7})$ H/m.

Now, the power gain pattern is given as,

$$G(\phi) \propto 20\log_{10}(|E(\phi)|) \tag{2.50}$$

S-square-aperture antennas are mounted so that the half power beam width (HPBW) points of antennas overlap and so the normalized antenna beam pattern is characterized by the number of sectors. Thus, if the number of sectors is eight, the HPBW of each sector is 45^0. Also, square-aperture antennas with a HPBW of 20^0 are deployed at the subscriber site to suppress the co-channel interference between subscribers. The various parameters used in the simulation are summarized in table 2-3.

Table 2-3: Simulation parameters when four-sectored antennas are used at the base station site.

Parameter	*Value*
Cell size	4000 m
Frequency reuse	25
Number of Co-channel cells	24 (First and second tier)
Number of users per cell	12
Path loss exponent – MS to BS	4
Path loss exponent – BS to BS	3
Lognormal shadowing – MS to BS	6 dB
Lognormal shadowing – BS to BS	4 dB
HPBW at BS	90 degrees
HPBW at MS	20 degrees
Frequency	1.9 GHz
Antenna aperture size – BS	0.0739 m
Antenna aperture size – MS	0.385 m
Number of iterations	10000

Again, the simulations are performed for the following four cases: when there are no extra uplink slots; when the maximum number of extra uplink TSs in a cell is 3; when the maximum number of extra uplink TSs in a cell is 6; and when the maximum number of extra uplink TSs in a cell is 12. The probability of SIR outage is compared for the four cases. The results obtained from the simulation are shown in figure 2-20.

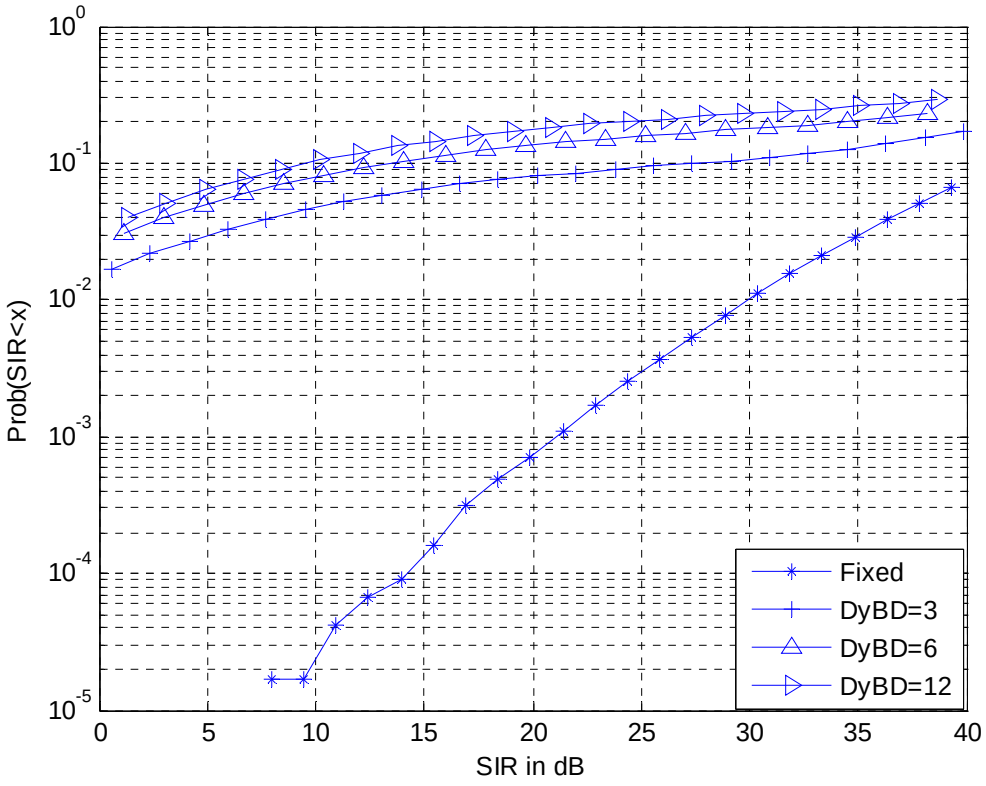

Figure 2-20: SIR outage using four-sectored antennas.

When there are no extra uplink TSs, the SIR at an outage of 1% is 30 dB which is twice the SIR value achieved when omni-directional antennas are used but the performance of the system when the dynamic boundary between uplink and downlink transmission is introduced do not show much improvement over the omni-directional antenna system. So, the number of sectors used at the base station site needs to be increased beyond 4, say $S \in \{8,12,15,25,40,75,100\}$.

The sectored antenna scheme suppresses the co-channel interference by increasing the spatial resolution given the configuration of the co-channel interferers. The SIR over the extra uplink TSs can also be increased by scheduling the subscriber transmission request over these extra TSs by exploiting the spatially distributed

subscribers so that the expectation of SIR over the extra uplink TS region is increased. In this method, by employing a simple spatial-filtering scheme like sectored antennas, a BS can estimate the aggregate co-channel interference due to the co-channel base stations for each sector. Also, the spatially distributed subscribers provide an additional degree of freedom for the BS to choose a sector in reference to the position of the subscriber so that minimum co-channel interference is introduced. This method is referred to as interference avoidance where the co-channel interference is avoided by exploiting the spatial distribution of subscriber locations within a cell. This technique is referred to as time slot allocation (TSA) strategy where the TSA fall under the category of dynamic channel allocation (DCA) Algorithms. .

One of the TSA techniques presented in [5] is known as the *Max* {SIR} algorithm. Let us assume that there are *L* subscribers in each cell and there is at least one uplink TS for each subscriber. Also, the number of extra uplink TSs is denoted by *N'*. At the *m*th extra uplink time slot, there are *k* co-channel cells in downlink transmission, whose direction of arrival is assumed to be known to the reference BS. The BS estimates the co-channel interference levels due to these *k* co-channel cells. Then, the BS estimates the SIR values for all the subscribers served for the frame based on the estimated co-channel interference levels due to *k* co-channel cells. As there are (*L +N'*) uplink time slots for *L* subscribers, some of the subscribers are allowed to transmit over multiple time slots. The (*L + N'*) subscriber's uplink transmission requests are denoted as subscriber resource table (**L**). From the estimated SIR values, the BS selects the subscriber from **L**, for which the estimated value of SIR is maximum for the *m*th uplink TS and then the

table **L** is updated. So, in the *Max* {SIR} algorithm, the *l*th subscriber is assigned to the *m*th TS if it satisfies the following condition

$$\text{Max } \{g\ (m,\ l)\}$$

where $g\ (m,\ l)$ is the estimated SIR value for the *l*th subscriber at the *m*th TS. The expected number of downlink co-channel interferers increases as the time slot index *m* increases and so it is expected that the SIR is lowest at the *N* 'th extra uplink time slot. So, the algorithm searches for the subscriber from the *N* 'th extra uplink time slot. The subscriber is assigned and this procedure is repeated until the first extra uplink time slot is assigned. The flowchart of this algorithm is illustrated in figure 2-21.

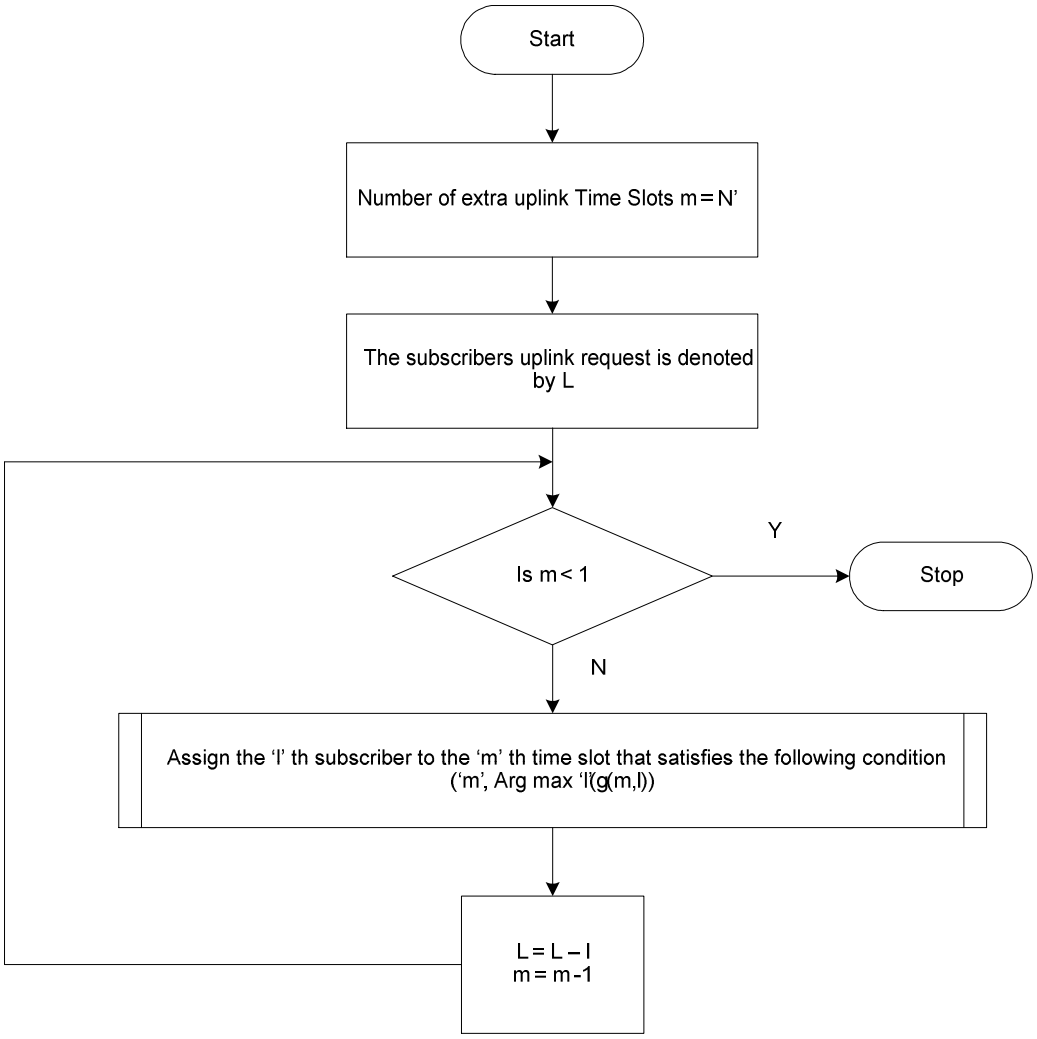

Figure 2-21: Flowchart depicting the steps involved in the *Max* {SIR} algorithm.

The various parameters used in the simulation of the *Max* {SIR} algorithm are summarized in table 2-4.

Table 2-4: Simulation parameters when four-sectored antennas are used at the base station site and the *Max* {SIR} algorithm is executed.

Parameter	*Value*
Cell size	4000 m
Frequency reuse	25
Number of Co-channel cells	24 (First and second tier)
Number of users per cell	12
Path loss exponent – MS to BS	4
Path loss exponent – BS to BS	3
Lognormal shadowing – MS to BS	6 dB
Lognormal shadowing – BS to BS	4 dB
HPBW at BS	90 degrees
HPBW at MS	20 degrees
Frequency	1.9 GHz
Antenna aperture size – BS	0.0739 m
Antenna aperture size – MS	0.385 m
Number of iterations	10000

Again, the simulations are performed for the following four cases: when there are no extra uplink slots; when the maximum number of extra uplink TSs in a cell is 3; when the maximum number of extra uplink TSs in a cell is 6; and when the maximum number of extra uplink TSs in a cell is 12. The probability of SIR outage is compared for the four cases. The results obtained from the simulation are shown in figure 2-22.

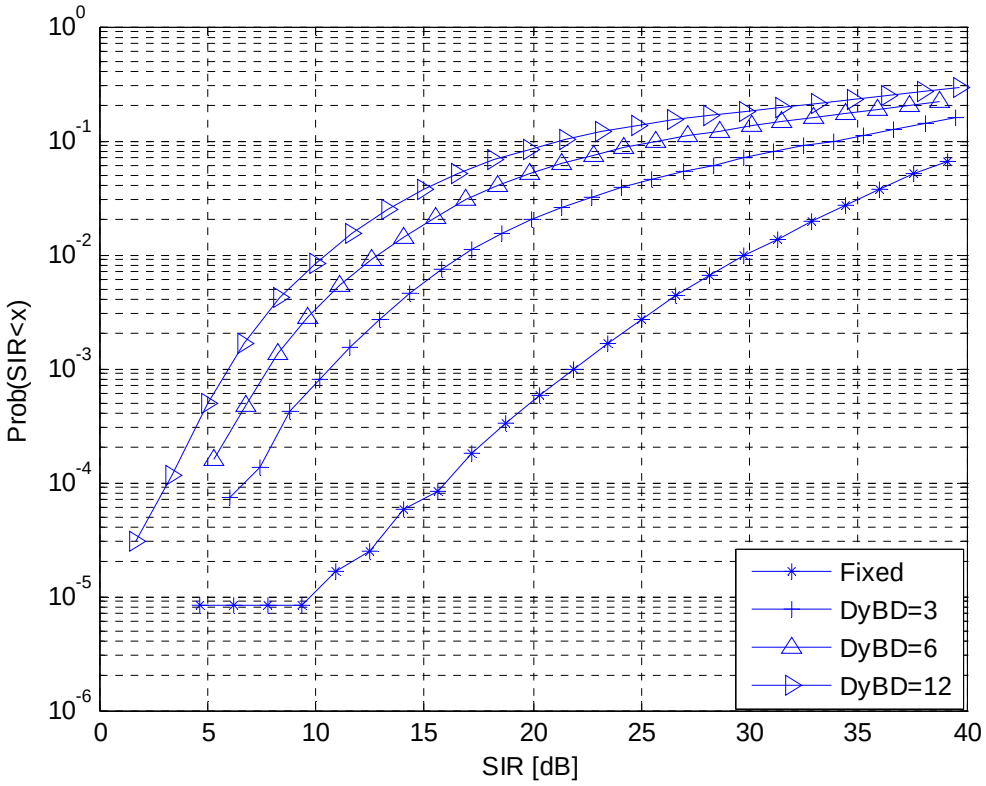

Figure 2-22: SIR outage using four-sectored antennas and the *Max* {SIR} algorithm.

As expected, the performance of the system when there are no extra uplink time slots remains the same regardless of the application of the *Max* {SIR} algorithm. But, the performance of the system when extra uplink time slots are used shows considerable improvement. For example, the SIR value for an outage of 1% when the maximum number of extra uplink TSs can be six is 13 dB. Comparing this with the case when the TSA algorithm was not executed, the SIR outage curve was seen to saturate quickly. The combination of the TSA algorithm and sectored antennas gives us considerable improvement in the performance of the system. The combination of TSA algorithm and sectored antennas provides significant improvement in the SIR outage probability when the number of sectored antennas used is S=15.

The simulations are conducted for fifteen-sectored antennas used at the BSs. Initially the *Max* (SIR) algorithm is not employed and the results are obtained. The simulations are repeated by employing the *Max* (SIR) algorithm and a comparison is made between the results obtained from both the cases. Table 2-5 shows the simulation parameters used for both cases.

Table 2-5: Simulation parameters when fifteen-sectored antennas are used at the base station site.

Parameter	*Value*
Cell size	4000 m
Frequency reuse	25
Number of Co-channel cells	24 (First and second tier)
Number of users per cell	12
Path loss exponent – MS to BS	4
Path loss exponent – BS to BS	3
Lognormal shadowing – MS to BS	6 dB
Lognormal shadowing – BS to BS	4 dB
HPBW at BS	24 degrees
HPBW at MS	20 degrees
Frequency	1.9 GHz
Antenna aperture size – BS	0.3302 m
Antenna aperture size – MS	0.385 m
Number of iterations	10000

Again, the simulations are performed for the following four cases: when there are no extra uplink slots; when the maximum number of extra uplink TSs in a cell is 3; when the maximum number of extra uplink TSs in a cell is 6; and when the maximum number of extra uplink TSs in a cell is 12. The probability of SIR outage is compared for the four

cases. The results obtained from the simulation when the *Max* {SIR} algorithm is not employed are shown in figure 2-23.

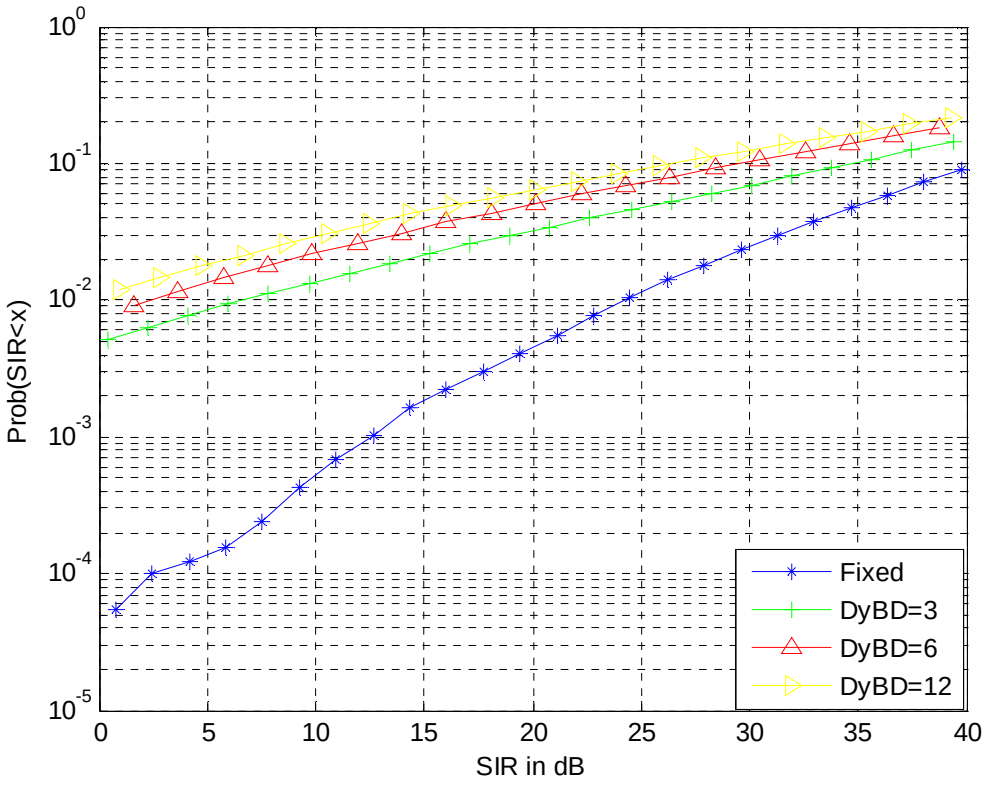

Figure 2-23: SIR outage using fifteen-sectored antennas.

The results obtained when the *Max* {SIR} algorithm is employed are shown in figure 2-24.

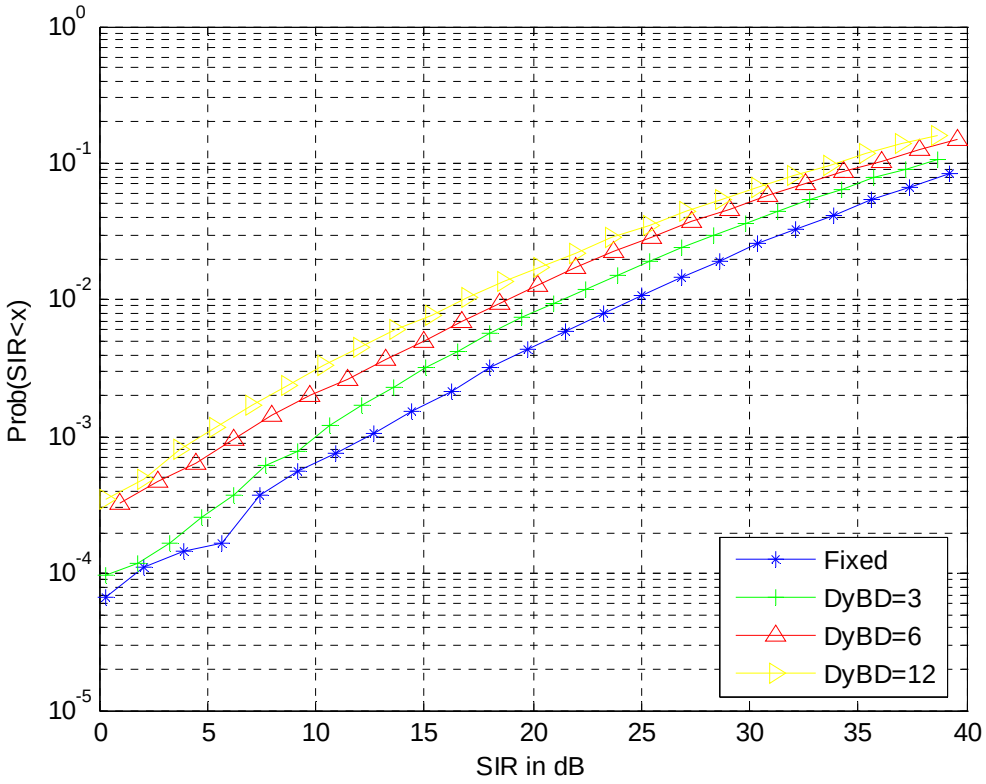

Figure 2-24: SIR outage using fifteen-sectored antennas and the Max {SIR} algorithm.

Comparing figures 2-23 and 2-24, there is a noticeable improvement in the SIR outage for the cases of fifteen-sectored antennas and when fifteen-sectored antennas are combined with *Max* {SIR} algorithm. For example, at an outage of 1%, the achievable SIR when just fifteen-sectored antennas are employed at the BS for a dynamic boundary Value of 6 is about 2.5 dB and this increases to about 18 dB when the fifteen-sectored antennas are combined with the *Max* {SIR} algorithm.

2.5 Analytical model of SIR in D-TDD systems

This section gives an analytical model of SIR in D-TDD systems. This analysis is based on the derivation of the probability of co-channel interference in Rayleigh and

lognormal fading when an omni-directional antenna is used at the BS in [55] and a spatial filter is used at the BS in [56].

The normalized antenna gain is 0 dBi for all values of the azimuth angle for an omni-directional antenna layout. The desired signal power is then given as,

$$P_S = \mu_s + \varsigma_{SB} \tag{2-51}$$

In equation (2-51), $\mu_S = -10\eta_{SB}\log_{10} R_d$.

The Probability Density Function (PDF) of the desired signal power is a Gaussian random variable given in equation (2-52).

$$f_{PS}(\gamma) = N(\mu_S, \sigma_{SB}^2) \tag{2-52}$$

In equation (2-52), μ_s is the mean and σ_{SB} is the standard deviation of the random variable P_S in equation (2-51).

The co-channel interference over the time slots is mutually exclusive due to the orthogonality of a TDMA system. The PDF of the aggregate co-channel interference is then given as,

$$f_{P_I}(\gamma) = \sum_{N'=0}^{N} f_{P_{I|N'}}(\gamma) \times \Pr(\text{Number of extra Time Slots at the Reference cell} = N') \tag{2-53}$$

In equation (2-53), $f_{P_{I|N'}}$ is the conditional PDF of aggregate co-channel interference when the number of extra uplink time slots is N'. This conditional PDF can be expressed as the sum of PDF's over two regions, Π_{Fix} and Π_{Ext}. Π_{Fix} refers to the fixed uplink time slots and Π_{Ext} refers to the extra uplink time slots of the frame. The PDF of aggregate co-channel interference is analyzed separately over these two regions.

The co-channel cells are in the same cycle as the reference cell during Π_{Fix}. The interfering signals from co-channels cells are homogeneous. When the frames are fully loaded, the number of co-channel interferers is the same for all the time slots. Thus, the distribution of co-channel interference is the same for all time slots in the fixed time slot region. The distribution of co-channel interference over this region is the same for D-TDD and S-TDD systems. The co-channel interference over Π_{Fix} is expressed as

$$10\log_{10} p_i = \mu_{SB} + \varsigma_{SB}. \tag{2-54}$$

In equation (2-54), ς_{SB} is a Gaussian random variable with $N(0, \sigma_{SB}^2)$ where σ_{SB} is the standard deviation in dB due to the propagation between the MS and BS. The local mean power, μ_{SB}, is given by,

$$\mu_S = P_t + G_t(\varphi) + G_r(\phi) - 10n_{SB}\log_{10} D_i. \tag{2-55}$$

In equation (2-55), D_i is the distance between the BS in the reference cell and the *i*-th co-channel interferer and n_{SB} is the propagation exponent for MS-to-BS environment. D_i is determined by the geographical location of the co-channel interferer.

The aggregate co-channel interference in Π_{Fix} is given by,

$$P_{I|Fix} = 10\log_{10}(\sum_{i=1}^{\alpha} p_i). \tag{2-56}$$

In equation (2-56), α is the number of co-channel interferers. It is assumed that the frame is fully loaded and so the number of co-channel interferers is fixed in the analysis. It is also assumed that the interfering signals from co-channel cells are statistically independent. It has been known from [57] and [58] that the sum of independent lognormal random variables can be approximated by another lognormal random variable.

Using Schwartz and Yeh's method [58], the mean and standard deviation of the sum of lognormal variables can be obtained. In reference to this $f_{P_{I|Fix}}$ can now be expressed as,

$$f_{P_{I|Fix}}(\gamma) = N(\mu_{P_{I|Fix}}, \sigma^2_{P_{I|Fix}}) = \chi^{\alpha}_{SC}(\gamma). \tag{2-57}$$

In equation (2-57), $\mu_{P_{I|Fix}}$ and $\sigma_{P_{I|Fix}}$ are the mean and standard deviation of the random variable $P_{I|Fix}$ in equation (2-56). $\chi^{\alpha}_{SC}(\gamma)$ denotes the PDF of the sum of *u* co-channel interference originated from the SC sites.

Over the uplink time slots in Π_{Ext}, the number of co-channel cells allocated for downlink transmission is a random variable. So, the aggregate co-channel interference over time slots in Π_{Ext} is a function of *k* and *m*, where *k* is the number of co-channel cells in the downlink cycle and *m* is the time slot index in the reference cell in Π_{Ext}.

At the *m*-th extra time slot, $f_{P_{I|Ext}}$ is expressed as,

$$f_{P_{I|Ext}} = \sum_{k=1}^{\alpha} W(k,m).\chi_{Ext}(\gamma,k) = W(m).\chi_{Ext}(\gamma). \tag{2-58}$$

In equation (2-58), $W(k,m)$ is the probability that *k* co-channel cells are in downlink and $\alpha - k$ co-channel cells are in uplink at the *m*-th extra uplink time slot.

$$W(k,m) = c_m^k d_m^{\alpha-k}. \tag{2-59}$$

In equation (2-59), c_m is the probability that the number of uplink time slots at a co-channel cell is less than *m*.

$$c_m = \sum_{i=o}^{m-1} \frac{1}{N+1} = \frac{m}{N+1}. \tag{2-60}$$

Also in equation (2-59), $d_m = 1 - c_m$.

It is assumed that the number of extra uplink time slots is determined independently for different BSs.

$$\mathrm{W}(m) = [W(0,m) \;\; W(1,m) \;\; W(2,m) \;\; .....W(\alpha,m)] \tag{2-61}$$

and

$$\chi_{Ext}(\gamma) = [\chi_{Ext}(\gamma,0) \;\; \chi_{Ext}(\gamma,1) \;\; \chi_{Ext}(\gamma,2).....\chi_{Ext}(\gamma,\alpha)]^T \tag{2-62}$$

$\chi_{Ext}(\gamma,k)$ is the PDF of sum of co-channel interference that k co-channels are in downlink and $\alpha - k$ co-channel cells are in uplink cycle and can be expressed as:

$$\chi_{Ext}(\gamma,k) = \sum_i \Psi[\chi^k_{BB,i}(\gamma) + \chi^k_{SC,i}(\gamma)] \tag{2-63}$$

The co-channel interference depends on the configuration of the co-channel interferer. In equation (2-63), subscript i denotes the different configurations of co-channel interferers, given the values for k and α. The constant Ψ is used to satisfy $\int_\gamma \chi_{Ext}(\gamma,k)d\gamma = 1$.

If the total number of extra uplink time slots at the reference cell is $N^{'}$, the PDF of co-channel interference is given by,

$$f_{P|N^{'}}(\gamma) = \frac{L}{L+N^{'}} f_{P_{I|Fix}}(\gamma) + \frac{1}{L+N^{'}} \sum_{m=1}^{N^{'}} f_{P_{I|Ext}}(\gamma,m) \tag{2-64}$$

The PDF of co-channel interference can be expressed as,

$$f_{P_I}(\gamma) = \sum_{N^{'}=0}^{N} f_{P_{I|N^{'}}}(\gamma) \times = \text{Prob(Number of Extra Time Slots at the Reference cell} = N^{'})$$

$$= \sum_{N^{'}=0}^{N} f_{P_{I|N^{'}}}(\gamma) \times \frac{1}{N+1} \tag{2-65}$$

Substituting equations (2-64) and (2-57) into equation (2-65),

$$f_{P_I}(\gamma) = \frac{\chi_{SC}^{\alpha}(\gamma)}{N+1}\sum_{N'=0}^{N}\frac{L}{L+N'} + \frac{1}{N+1}.\sum_{N'=1}^{N}\frac{1}{L+N'}\sum_{m=1}^{N'} f_{P_{I|Ext}}(\gamma, m) \qquad (2\text{-}66)$$

In equation (2-66), the term corresponding to $N' = 0$ is excluded from the summation in the second term as it is zero. Thus,

$$f_{P_I}(\gamma) = \frac{C(0)\times L\times \chi_{SC}^{\alpha}(\gamma)}{N+1} + \frac{1}{N+1}\times\sum_{N'=1}^{N}\frac{1}{L+N'}\sum_{m=1}^{N'} f_{P_{I|Ext}}(\gamma, m) \qquad (2\text{-}67)$$

In equation (2-67), $C(m) = \sum_{i=m}^{N}\frac{1}{L+i}$.

The summation in the second term of equation (2-67) can be written as,

$$\begin{aligned}\sum_{N'=1}^{N}\sum_{m=1}^{N'}\frac{f_{P_{I|Ext}}(\gamma)}{L+N'} &= \left(\frac{1}{L+1}+\frac{1}{L+2}+...+\frac{1}{L+N}\right)\times f_{P_{I|Ext}}(\gamma,1)+\left(\frac{1}{L+2}+\frac{1}{L+3}+...+\frac{1}{L+N}\right)\\ &\times f_{P_{I|Ext}}(\gamma,2)+....+\left(\frac{1}{L+i}+\frac{1}{L+i+1}+...+\frac{1}{L+N}\right)\times f_{P_{I|Ext}}(\gamma,i)+\frac{1}{L+N}\\ &\times f_{P_{I|Ext}}(\gamma,N)\\ &= \sum_{m=1}^{N} f_{P_{I|Ext}}(\gamma,m)\sum_{j=m}^{N}\frac{1}{L+j} = \sum_{m=1}^{N} C(m)\times f_{P_{I|Ext}}(\gamma,m) \qquad (2-68)\end{aligned}$$

By substituting equation (2-68) into equation (2-67), the PDF of co-channel interference can be expressed in matrix form as shown in equation (2-69).

$$f_{P_I}(\gamma) = \frac{1}{N+1}[LC(0)\chi_{SC}^{\alpha}(\gamma) + C..W.\chi_{Ext}(\gamma) \qquad (2\text{-}69)$$

In equation (2-69), C =$[C(1)\ \ C(2)....C(N)]$, and W = $[\mathrm{W}(1)\ \ \mathrm{W}(2)....\mathrm{W}(N)]^T$.

SIR outage probability is next analyzed. Outage is declared when the SIR is lower than a threshold value τ, that is,

$$\text{Prob }\{\text{Outage}\} = \text{Prob }\{\text{SIR} < \tau\} = \int_{-\infty}^{\varsigma} f_{SIR}(\gamma)d\gamma = 1 - \int_{\varsigma}^{\infty} f_{SIR}(\gamma)d\gamma \qquad (2\text{-}70)$$

In equation (2-70), f_{SIR} is the PDF of SIR. The desired signal and aggregate co-channel interference are assumed to be statistically independent. The desired signal and aggregate co-channel interference are Gaussian random variables and the PDF of SIR can be written as the convolution of the PDF of desired signal and the PDF of aggregate co-channel interference.

$$f_{SIR}(\gamma) = f_{P_S}(\gamma) \otimes f_{P_I}(\gamma) \tag{2-71}$$

In equation (2-71), f_{P_S} is the PDF of the desired signal power and f_{P_I} is the PDF of the aggregate co-channel interference.

2.6 Conclusion

This chapter started with a comparison between the conventional duplex schemes of TDD and FDD and listed out the advantages as well as disadvantages of D-TDD. Co-channel interference reduction was needed to increase capacity in multi-user access systems and the different techniques for doing so were studied. The role of D-TDD in achieving this reduction in TDMA systems was discussed. Next, an example of a DCA algorithm which reduces interference and thereby increases capacity in TD-CDMA/TDD systems was shown.

The performance of TMDA/D-TDD systems was then analyzed. An analytical model of SIR outage probability ratio in D-TDD systems was presented. The performance analysis was done when the cellular system employed omni-directional antennas, sectored antennas and finally a combination of sectored antennas and time slot allocation algorithms. The combination of sectored antennas with time slot allocation

algorithms helped in reducing the co-channel interference in dynamic TDD systems and gave the best performance in terms of SIR probability outage ratio.

3 FUNDAMENTAL TRAFFIC ANANLYSIS

In this chapter, the definition and properties of self similarity are presented. Objects are self-similar if they roughly look the same on any scale. [19] The techniques and methods for modeling self-similar traffic and estimating the Hurst parameter [*H*] are described next. These methods are then used on two sets of data and the analysis of whether the data is self-similar or not are carried out. The truncated Gaussian traffic model is applied to model the static TDD and dynamic TDD traffic and also the expressions for the spectral efficiency of the static TDD and dynamic TDD systems under truncated Gaussian traffic model assumptions are studied.

We model the dataset from [34] using ON-OFF traffic modeling and apply the modeling to a TDMA/D-TDD system employing the *Max* {SIR} algorithm. The results obtained are compared with the results obtained from chapter 2 where the number of extra uplink time slots in each cell was based on a uniform density function. It was concluded that the results obtained using the ON-OFF traffic modeling matched the results obtained using the uniform density function.

3.1 Self-Similarity

The authors of [16] shattered the illusion that queuing analysis using the Poisson traffic assumption is adequate to model all network traffic. They reported the results of a detailed, high-resolution collection of Ethernet traffic measurements conducted between

1989 and 1992. The data were collected from various Ethernet Local Area Networks (LANs) at Bellcore.

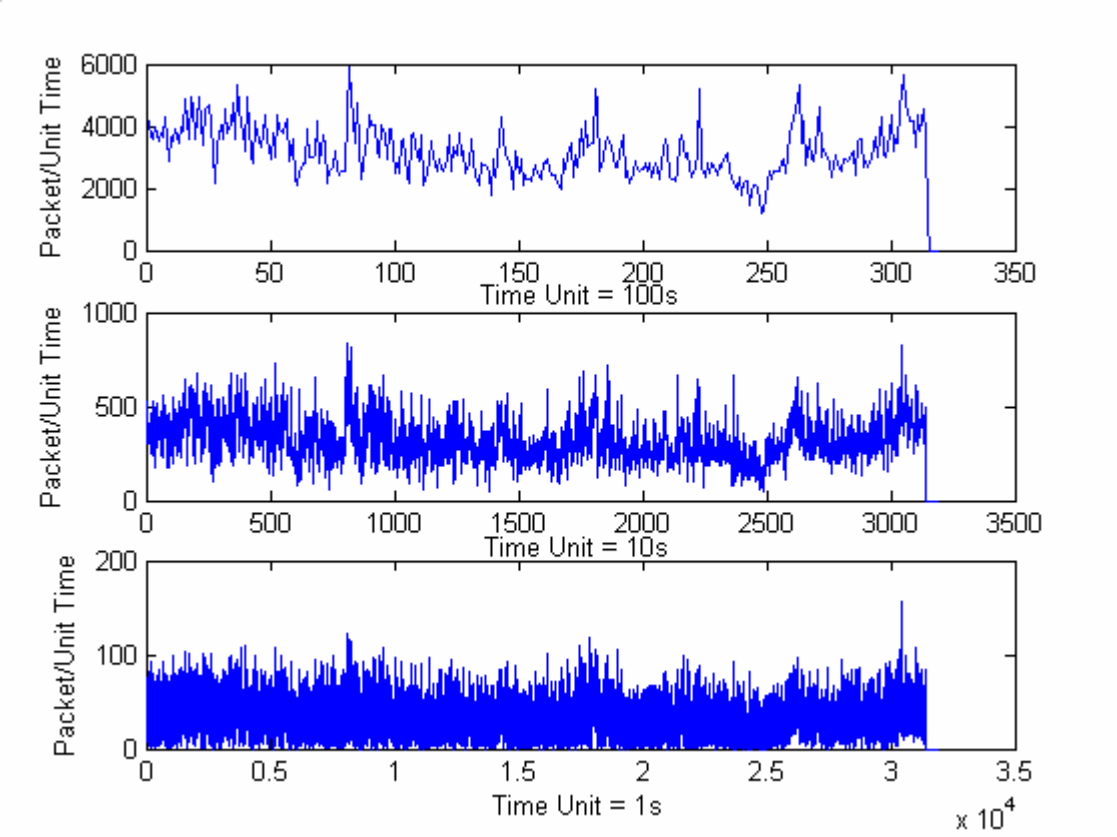

Figure 3-1: Traffic trace of Ethernet traffic showing the self-similar nature.

Figure 3-1 shows plots of the number of packets per unit time for a measurement set from 1989 which consisted of about an hour of continuous monitoring of Ethernet traffic. The first plot shows the entire one-hour run using a time unit of 100 seconds. Each subsequent plot is obtained by reducing the time resolution by a factor of 10. For example, the second plot covers the entire one-hour run using a time unit of 10 seconds. We can see that all of the plots look similar to one another in a distributional sense and all the plots involve a fair amount of burstiness. So, Ethernet traffic tends to look the same at large scales and at small scales. Also, there is no natural length to bursts. At every time

scale, bursts consist of bursty subperiods separated by less bursty subperiods. This self-similar character is drastically different from stochastic models traditionally used in data network analysis and design.

If the plot in figure 3-1 was to be compared with a plot generated using a Poisson model comparable to the real data in terms of average packet size and arrival rate the results would be different. It has been noted that for Poisson modeling, at high resolution, traffic is bursty but as the data are aggregated over increasingly long time scales, the traffic pattern smoothes out. The resulting difference shows that the Ethernet traffic is self-similar.

3.1.1 Properties

A phenomenon that is self-similar looks the same or behaves the same when viewed at different degrees of magnification or different scales on a dimension. The dimension can be space, length, width or time [20]. Let

$$X = X_t \qquad t = 0,1,2... \tag{3-1}$$

be a covariance stationary stochastic process with mean μ, variance σ^2 and autocorrelation $r(k), k \geq 0$. X has an autocorrelation function given by,

$$r(k) \sim k^{-\beta} L(t), k \to \infty \tag{3-2}$$

where $0 < \beta < 1$ and L is slowly varying at infinity. For each m=1, 2, 3 … let

$$X^{(m)} = X_k^{(m)} \quad k=1, 2, 3 \ldots \tag{3-3}$$

denote the new covariance stationary time series, with autocorrelation function $r^{(m)}$, obtained by averaging the original series over non-overlapping blocks of size m.

$$X^{(m)} = X_k^{(m)} = \frac{X_{km-m+1} + \ldots + X_{km}}{m}, k \geq 1 \tag{3-4}$$

The process X is called exactly second-order self similar with self-similarity parameter

$$H = 1 - \beta / 2 \tag{3-5}$$

If for all m = 1, 2 …

$$\text{var}(X^{(m)}) = \sigma^2 m^{-\beta} \tag{3-6a}$$

and

$$r^{(m)}(k) = r(k), k \geq 0 \tag{3-6b}$$

X is called asymptotically second-order self similar with parameter

$$H = 1 - \beta / 2$$

if for all k large enough,

$$r^{(m)}(k) \to r(k), m \to \infty \tag{3-7}$$

That is, X is exactly or asymptotically second-order self-similar if the corresponding aggregated processes $X^{(m)}$ are the same as X or become indistinguishable from X at least with respect to their autocorrelation functions.

Self-similarity manifests in the following ways, mathematically,

1) The variance of the sample mean decreases more slowly than the reciprocal of the sample size

$\text{var}(X^{(m)}) \sim z_2 m^{-\beta}$, $.m \to \infty, 0 < \beta < 1$, z_2-constant

2) The autocorrelations decay hyperbolically rather than exponentially fast implying a non-summable autocorrelation function.

3) The spectral density obeys a power-law near the origin

$f(\lambda) \sim z_3 \lambda^{-\gamma} \lambda \to 0, 0 < \gamma < 1, \gamma = 1 - \beta$, z_3-constant

The most striking feature of second-order self-similar processes is that their aggregated processes possess a nondegenerate correlation structure as $m \to \infty$.

Self-similar processes help in the determination of the Hurst parameter (*H)*. A stochastic process is statistically self-similar with parameter $H(0.5 \le H \le 1)$ if for any real $a>0$, the process $a^{-H} x(at)$ has the same statistical properties as x*(t)*. This can be explained by the following conditions:

1) Mean E[x(*t*)] = E[x(*at*)]/ a^H

2) Variance Var[x(*t*)] = Var[x(*at*)]/ a^{2H}

3) $R_x(t,s) = R_x(at,as) / a^{2H}$

The Hurst parameter is the key measure of self-similarity. It is the measure of the persistence of a statistical phenomenon and the length of the long-range dependence of a stochastic process. A value of *H*=0.5 indicates the absence of long-range independence and a value of *H*=1 indicates the presence of long-range independence. Some of the processes that satisfy the definition of self-similarity are Brownian motion process, and fractional Brownian motion process.

3.2 Modeling of self-similar traffic

Many different approaches have been proposed to determine whether a given time series of data is self-similar and if so to estimate the Hurst parameter *H*. Some of the methods used are Aggregate Variance-Time plot, Rescaled Adjusted Range-Statistics plot, Wavelet method and Whittle's estimator.

3.2.1 Aggregate Variance-Time Plot

For the aggregated time series $X^{(m)}$ of a self-similar process, the variance obeys

$$\mathrm{Var}(X^{(m)}) \sim \mathrm{Var}(X)/m^{\beta} \tag{3-8}$$

with $H = 1-\beta/2$. Rewriting (3-8),

$$\log[\mathrm{Var}(X^{(m)})] \sim \log[\mathrm{Var}(X)] - \beta \log(m) \tag{3-9}$$

As log [Var(X)] is a constant independent of m, if log [Var(X)] is plotted against log [m], the result must be a straight line with a slope of $-\beta$. The plot can be generated from a data series $X(t)$ by generating the aggregate process at different levels of aggregation m and then computing the variance and then by fitting a simple least squares line through the resulting points in the plane. Slope values between -1 and 0 suggest self-similarity.

3.2.2 Rescaled Adjusted Range-Statistics (R/S) plot

For a given set of observations, $X_k : k = 1,2,...,n$, with sample mean $\overline{X}(n)$ and sample variance $S^2(n)$, the R/S statistic is given by,

$$R(n)/S(n) = 1/S(n)[\max(0, W_1, W_2, ...W_n) - \min(0, W_1, W_{2,} ...W_n)] \tag{3-10}$$

with

$$W_k = (X_1 + X_2 + ... + X_k) - k\,\overline{X}(n) \; (k \geq 1) \tag{3-11}$$

The numerator in equation (3.10) is a measure of the ratio of the range of the process and the denominator is the sample standard deviation. For a self-similar process, the range has the following characteristic for large n

$$\mathrm{E}[R(n)/S(n)] \sim z_4 n^H$$

where z_4 is a constant with H about 0.7.

3.2.3 Wavelet analysis

A wavelet is a waveform of effectively limited duration that has an average value of zero. Wavelets are irregular and asymmetric. Wavelet analysis is the breaking up of a signal into shifted and scaled versions of the original wavelet. In this method, the Hurst parameter is estimated by the ratio of the energies between two adjacent resolutions. [21].

The power spectrum *P(w)* of a fractal signal is represented by

$$P(w) = \alpha w^{-2H-1} \tag{3-12}$$

In equation (3-12), α is a constant.

The power spectrum $P_2(w)$ of a fractal signal filtered by the high pass filter is expressed as

$$P_2(w) = P(w)|\Psi(2^{-j}w)|^2 \tag{3-13}$$

where $\Psi_{2^j}(w) = \Psi(2^{-j}w)$ denotes the wavelet function at resolution 2^j.

The power spectrum $P_{2^j}^d(w)$ of a discrete signal sampled by a factor of 2^j, is written as

$$P_{2^j}^d(w) = 2^j \sum_{m=-\infty}^{\infty} P_{2^j}(w + 2^j 2m\pi) \tag{3-14}$$

Let,

$$\sigma_{2^j}^2 = \frac{2^{-j}}{2\pi} \int_{-2/\pi}^{+2^j\rho} P_{2^j}^d(w)dw \tag{3-15}$$

From equations (3-13), (3-14) and (3-15),

$$\sigma^2{}_{2^j} = 2^{2H} \sigma_{2^{j+1}}^2 \tag{3-16}$$

Then the Hurst parameter is computed as

$$H = \frac{1}{2} \log_2 \frac{\sigma_{2^j}^2}{\sigma_{2^{j+1}}^2} \tag{3-17}$$

Another method in which the time series is converted into discrete wavelet can also be used to compute the Hurst parameter. The Hurst exponent for a set of data can be calculated from the wavelet spectral density as follows:

$$P_j = \frac{1}{2^j} \sum_{i=1}^{2^j} c_i^2 \tag{3-18}$$

where c_i represents the wavelet coefficients. A graph of $\log_2(P)$ is plotted against $\log_2(2^j)$ and the slope of the curve obtained can be used to find the value of β and then the value of *H*.

3.3 Simulation algorithms

The aggregate variance, R/S-statistic and wavelet algorithms are developed and tested on the two test data. The steps used in the simulation are given below. These steps are used with respect to the video trace data set of Star IV with high-quality level obtained from [22].

3.3.1 Aggregate Variance

Step 1: The given data set of length *N* is divided into blocks of size *m* giving a total of int (*N/m*) blocks.

Step 2: The mean of the values in each block is calculated giving a total of (*N/m)* mean values.

Step 3: The variance of the mean values from step 2 is calculated.

Step 4: The above steps (steps 1-3) are repeated for different values of *m*.

Step 5: A graph of log(*m*) versus log(variance) is plotted.

Step 6: Least squares method is used to give a best fit for the graph obtained in step 5.

Step 7: The slope of the fit obtained in step 6 gives the value of β.

Step 8: Hurst parameter H is calculated from H=1-(β /2).

3.3.2 Rescaled Adjusted Range-Statistics (R/S) plot

Step 1: The given data set of length N is divided into blocks of size m giving a total of int (N/m) blocks.

Step 2: The standard deviation of the values in each block is calculated.

Step 3: The mean of the values in each block is calculated.

Step 4: A loop with an index n, a starting value of one and an ending value of block size m is started.

Step 5: The partial sum until n is calculated yielding a total of n partial sum terms.

Step 6: The W values are calculated by subtracting the n values times the mean from the partial sum for the index value n.

Step 7: The loop started in Step 4 is ended here.

Step 8: The maximum of the W values obtained above is calculated and if the maximum is less than one the maximum value is set to zero.

Step 9: The minimum of the W values obtained above is calculated and if the minimum is greater than one the minimum value is set to zero

Step 10: The value R is obtained by the difference of the maximum W and minimum W.

Step 11: The ratio of R/S is calculated.

Step 12: The above steps (steps 1-11) are repeated for each of the blocks yielding a total of int (N/m) R/S values.

Step 13: The mean of all the R/S values is calculated.

Step 14: The above steps (steps 1-13) are repeated for different values of m.

Step 15: A graph of log(m) versus log(mean(R/S)) is plotted.

Step 16: Least squares method is used to give a best fit for the graph obtained in step 15.

Step 17: The slope of the fit obtained in step 6 gives the value of H.

3.3.3 Wavelet analysis

Step 1: The power spectrum is computed by averaging the squares of the coefficients of the transform $P(j)$.

Step 2: A graph of $\log_2(P)$ is plotted against $\log_2(2^j)$.

Step 3: Least squares method is used to give a best fit for the graph obtained in step 2.

Step 4: The slope of the fit obtained in step 3 gives the value of β.

Step 5: Hurst parameter H is calculated from $H=1-(\beta/2)$.

For the Ethernet data set (BC-pAug89) from [34] one additional step is performed (for each of the three methods) where the random time instants arrival of the data is converted into a form of deterministic time instants.

3.4 Flowcharts

3.4.1 Aggregate Variance

The steps involved in the simulation using the aggregate variance method are shown in figure 3-2

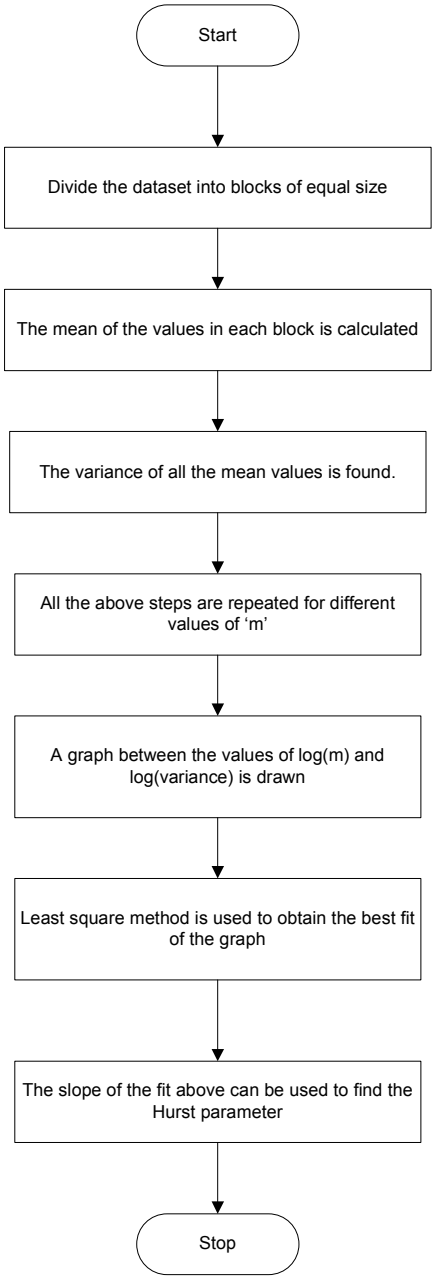

Figure 3-2: Flowchart depicting the aggregate variance method.

3.4.2 Rescaled Adjusted Range-Statistics (R/S) plot

The steps involved in the simulation using the R/S method are shown in figure 3-3

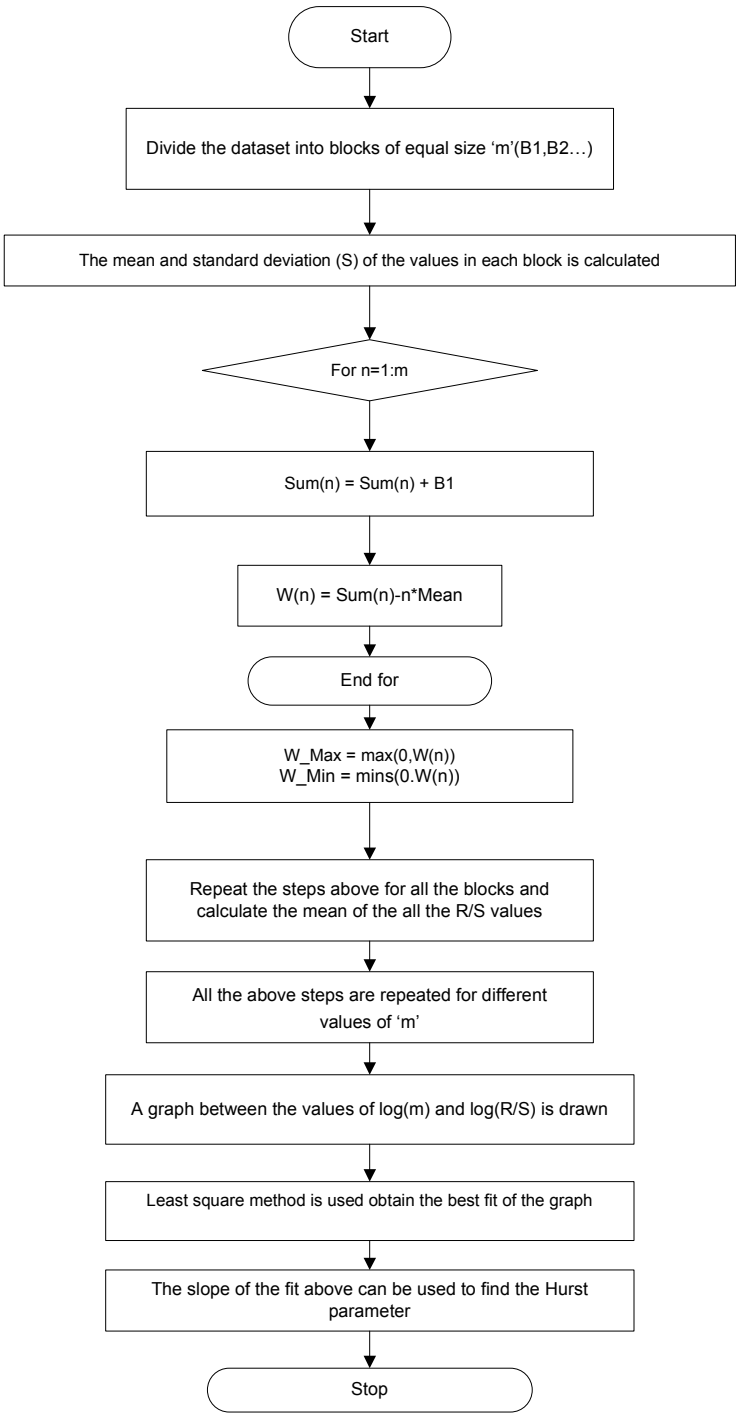

Figure 3-3: Flowchart depicting the R/S method.

3.4.3 Wavelet method

The steps involved in the simulation using the wavelet method are shown in figure 3-4

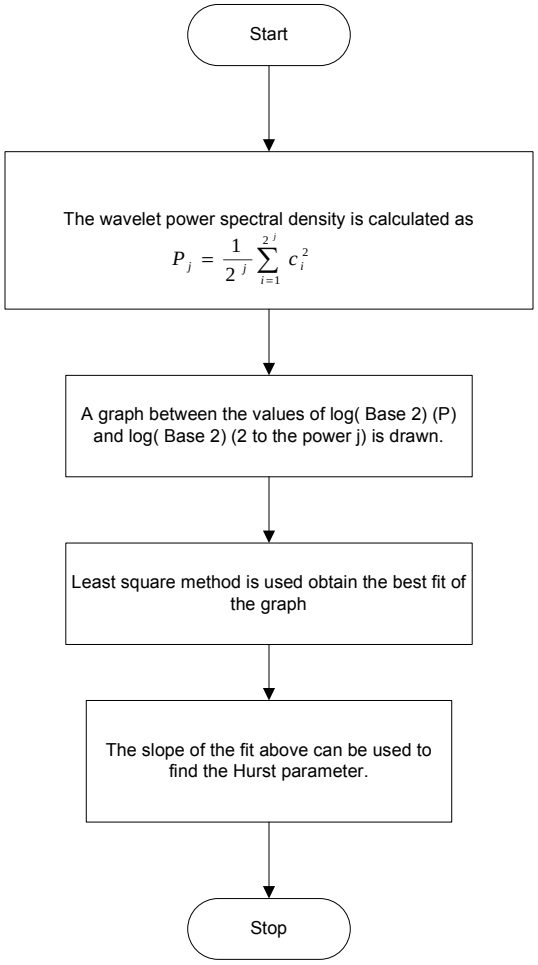

Figure 3-4: Flowchart depicting the wavelet method.

3.5 Simulation results

The simulation was performed on the following two data sets.

1. BC-pAug89 from [34]. These contain a million packet arrivals at the Bellcore Morristown Research and Engineering faculty.
2. Star Wars-High Quality from [35].

The Hurst parameter for the above two data sets is calculated using the three methods – Aggregate variance, Rescaled Adjusted Range Statistics and Wavelet. The plot obtained is approximated using the least squares method and the slope of the resulting approximation is used to calculate the Hurst parameter as shown in the sections below.

3.5.1 Aggregate Variance method for Star-Wars High Quality

The aggregate variance method is used on the trace obtained from [35] and the resulting plot obtained is shown in figure 3-5. The plot is approximated using the least squares method and the slope of the approximation can be used to calculate Hurst parameter as shown.

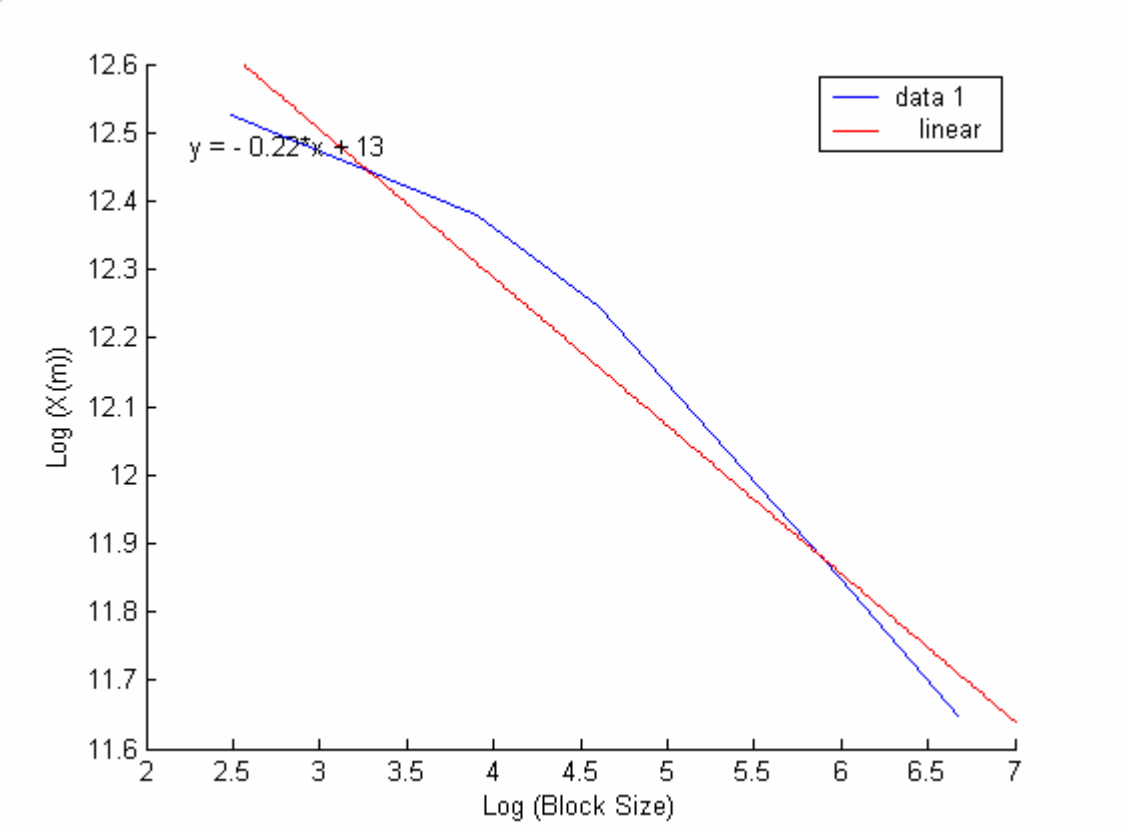

Figure 3-5: Plot of Log(Block Size) vs Log (X(m)) for Star Wars-High Quality using aggregate variance.

In figure 3-5, the slope of the line $\beta = -0.22$. So, the Hurst parameter, H = 1-(0.22/2) = 0.89.

3.5.2 Aggregate variance for BC-pAug99

The aggregate variance method is used on the data set obtained from [34] and the resulting plot obtained is shown in figure 3-6. The plot is approximated using the least squares method and the slope of the approximation can be used to calculate Hurst parameter as shown.

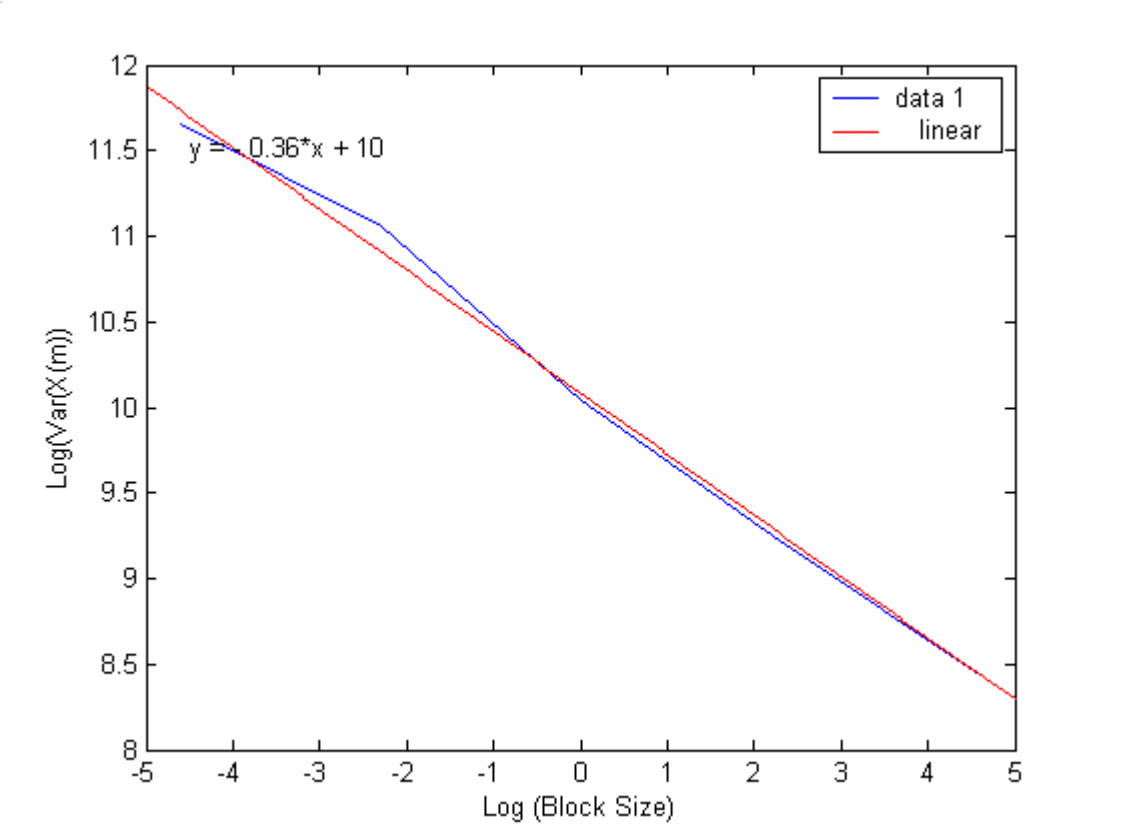

Figure 3-6: Plot of Log(Block Size) vs Log (X(m)) for BCpAug89 using aggregate variance.

In figure 3-6, the slope of the line $\beta = -0.36$. So, the Hurst parameter, H = 1-(0.36/2) = 0.82.

3.5.3 R/S method for Star-Wars High Quality

The rescaled adjusted range statistics method is used on the trace obtained from [35] and the resulting plot obtained is shown in figure 3-7. The plot is approximated using the least squares method and the slope of the approximation can be used to calculate Hurst parameter as shown.

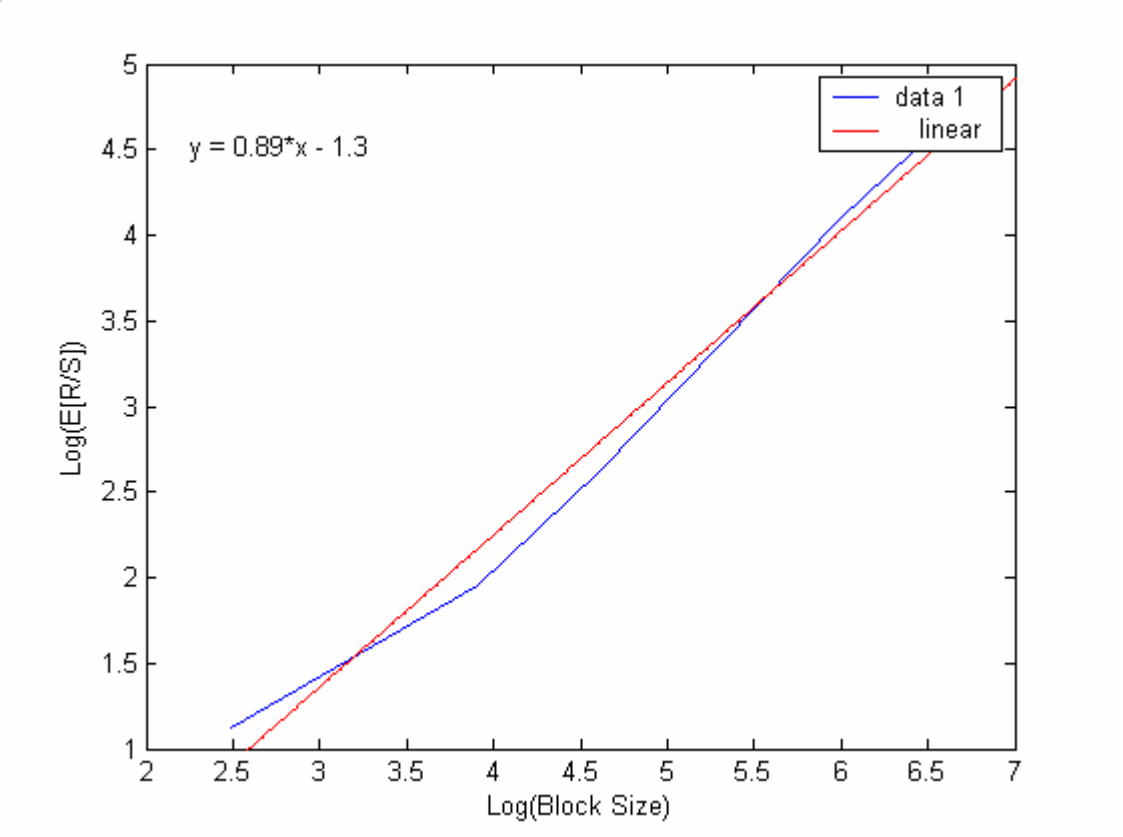

Figure 3-7: Plot of Log(Block Size) vs Log (E[R/S]) for Star Wars-High Quality using R/S method.

In figure 3-7, the slope of the line gives the value of the Hurst parameter and here Hurst parameter, H = 0.89.

3.5.4 R/S method for BC-pAug99

The rescaled adjusted range statistics method is used on the data set obtained from [34] and the resulting plot obtained is shown in figure 3-8. The plot is approximated using the least squares method and the slope of the approximation can be used to calculate Hurst parameter as shown.

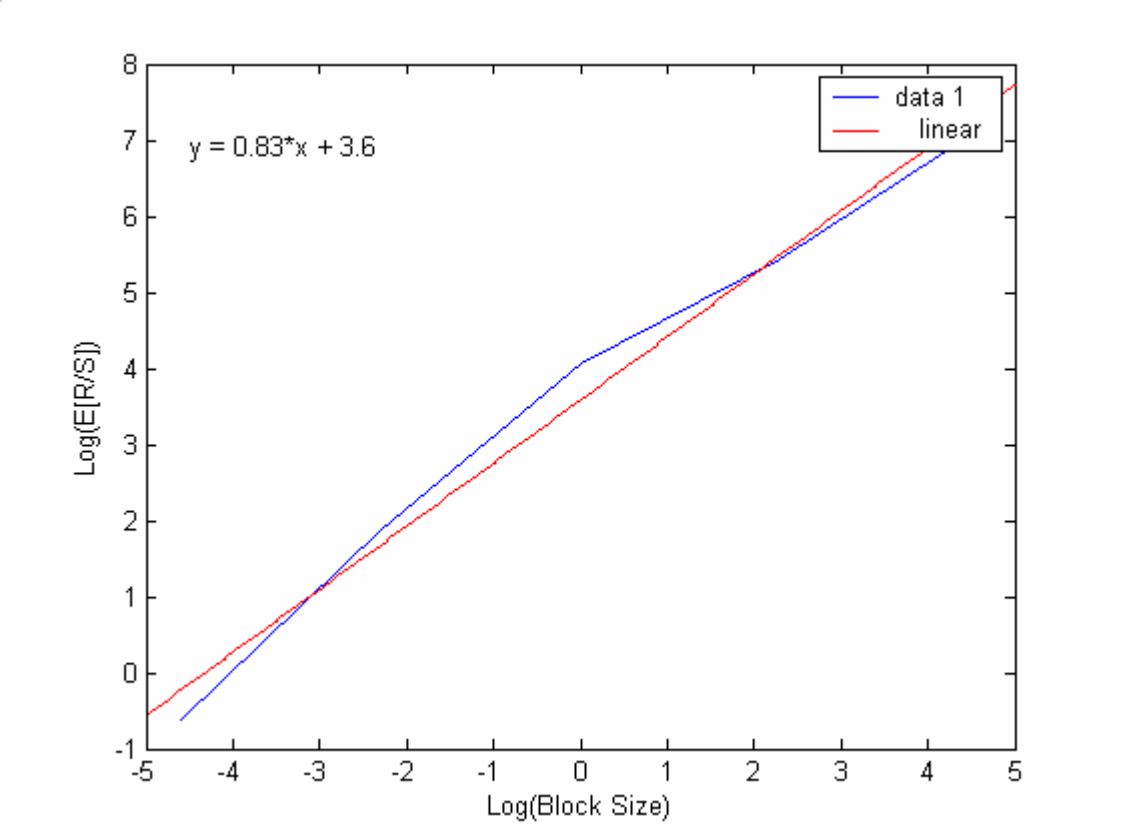

Figure 3-8: Plot of Log(Block Size) vs Log (E[R/S]) for BCpAug89using R/S method.

In figure 3-8, the slope of the line gives the value of the Hurst parameter and here Hurst parameter, $H = 0.83$.

3.5.5 Wavelet method for Star-Wars High Quality

The wavelet method is used on the trace obtained from [35] and the resulting plot obtained is shown below in figure 3-9. The plot is approximated using the least squares

method and the slope of the approximation can be used to calculate Hurst parameter as shown.

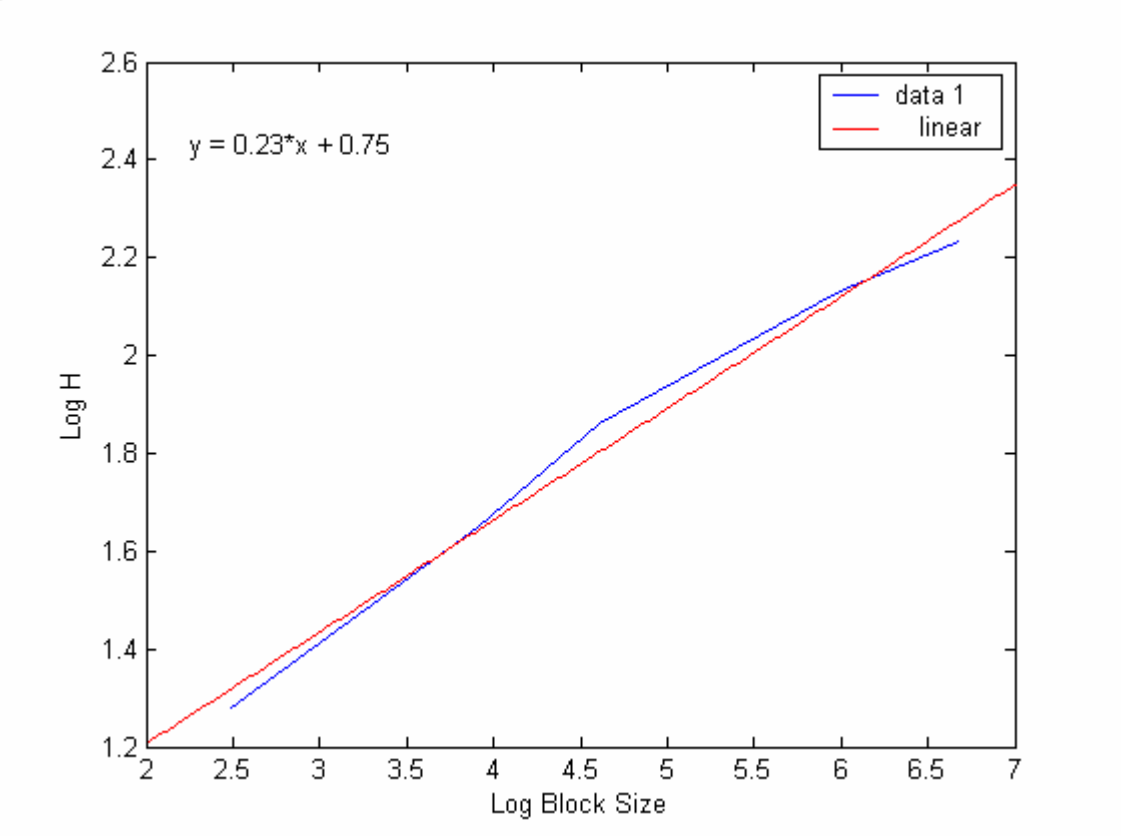

Figure 3-9: Plot of Log(Block Size) vs Log (H) for Star Wars-High Quality using wavelet method.

In figure 3-9, the slope of the line is $\beta = 0.23$. So the Hurst parameter, H = 1-(0.23/2) = 0.885.

3.5.6 Wavelet method for BC-pAug99

The wavelet method is used on the data set obtained from [34] and the resulting plot obtained is shown below in figure 3-10. The plot is approximated using the least squares method and the slope of the approximation can be used to calculate Hurst parameter as shown.

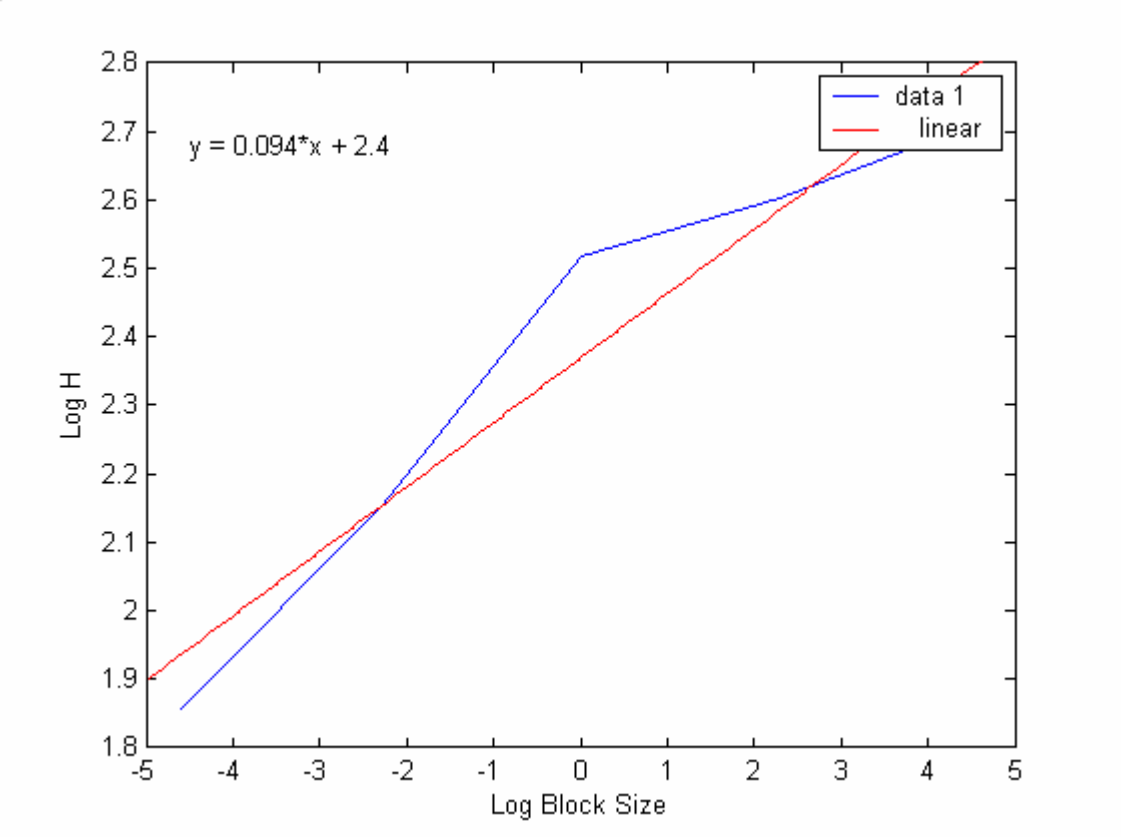

Figure 3-10: Plot of Log(Block Size) vs Log (H) for BCpAug89 using wavelet method.

In figure 3-10, the slope of the line is $\beta = 0.094$. So the Hurst parameter, H = 1-(0.094/2) = 0.953.

3.6 Truncated Guassian traffic model in TDMA/TDD systems

In this section, the truncated Guassian traffic model that can be applied to TDMA/TDD systems is given.

As seen earlier, TDD operates in two modes – static-TDD and dynamic-TDD. The boundary between uplink and downlink traffic is adjustable in D-TDD but is fixed in S-TDD systems.

Let us assume that there are L subscribers supported by both types of system and also each of the L subscribers can request more than one time slot for transmission either

in the UL or DL direction. The first L time slots and the last L time slots are allotted to uplink transmission and downlink reception respectively. These are called the fixed time slots. The rest of the time slots can be assigned either to uplink transmission or downlink reception depending on the traffic load in the system. The time slots can also remain idle. The region from the (L+1)-th time slot to the last uplink time slot is called the extra uplink time slot region.

Let us assume that the offered traffic for uplink transmission in a D-TDD system λ_{UP} follows a truncated Gaussian distribution given as

$$\lambda_{UP} \sim N(\mu_{UP}, \sigma_{UP} \mid n_{UP}^{\min} \le \lceil \lambda_{UP} \rceil \le n_{UP}^{\max}) \tag{3-19}$$

where, μ_{UP} is the mean number of uplink time slots,

σ_{UP} is the standard deviation of uplink time slots,

$n_{UP}^{\min}$ is the minimum number of uplink time slots which equals L, and

$n_{UP}^{\max}$ is the maximum number of uplink time slots.

The number of uplink time slots in a D-TDD frame can be obtained as,

$$n_{UP}^{D} = \lceil \lambda_{UP} \rceil \tag{3-20}$$

where $\lceil x \rceil$ selects the smallest integer that is greater than the argument x.

The probability of the number of uplink time slots can be obtained as:

$$P(n_{UP} = k \mid n_{UP}^{\min} \le n_{UP} \le n_{UP}^{\max}) = \frac{\Pr((n_{UP} = k) \bigcap (n_{UP}^{\min} \le n_{UP} \le n_{UP}^{\max}))}{\Pr(n_{UP}^{\min} \le n_{UP} \le n_{UP}^{\max})}$$

$$= \frac{\Pr(n_{UP} = k)}{\Pr(n_{UP}^{\min} \le n_{UP} \le n_{UP}^{\max})} = \frac{\Pr(k-1 < n_{UP} \le k)}{\Pr(n_{UP}^{\min} \le n_{UP} \le n_{UP}^{\max})}$$

$$= \frac{\Pr(k) - \Pr(k-1)}{\Pr(n_{UP}^{\max}) - \Pr(n_{UP}^{\min})} \Pr$$

$$= \frac{(1-Q(\frac{k-\mu_{UP}}{\sigma_{UP}}))-(1-Q(\frac{k-1-\mu_{UP}}{\sigma_{UP}}))}{(1-Q(\frac{n_{UP}^{\max}-\mu_{UP}}{\sigma_{UP}}))-(1-Q(\frac{n_{UP}^{\min}-1-\mu_{UP}}{\sigma_{UP}}))}$$

$$= \frac{Q(\frac{k-1-\mu_{UP}}{\sigma_{UP}})-Q(\frac{k-\mu_{UP}}{\sigma_{UP}})}{Q(\frac{n_{UP}^{\min}-1-\mu_{UP}}{\sigma_{UP}})-Q(\frac{n_{UP}^{\max}-\mu_{UP}}{\sigma_{UP}})} \quad (3\text{-}21)$$

where, n_{UP} is the number of uplink time slots,

$p_{n_{UP}}(k \mid n_{UP}^{\min} \le n_{UP} \le n_{UP}^{\max}) = \Pr(n_{UP} = k \mid n_{UP}^{\min} \le n_{UP} \le n_{UP}^{\max})$ is the Probability Mass function and

$Q(x) = \int_{x}^{\infty} \frac{1}{\sqrt{2\pi}} e^{-t^2/2} dt$ is the Q-function.

The S-TDD systems cannot make use of the bandwidth efficiently as the D-TDD systems as the dynamic boundary is fixed in S-TDD systems. This means, the transmission bandwidth in one direction cannot be allotted for the other direction even if there is available bandwidth. Generally, the bandwidth ratio of uplink to downlink traffic bandwidth is asymmetric and dynamic especially for multimedia applications. So, the dynamic boundary in S-TDD systems has to be chosen carefully. In [53], it is assumed that the number of time slots in the S-TDD frame is equal to the average number of uplink time slots in a fully loaded D-TDD frame.

$$n_{UP}^{s} = \lceil \mu_{UP} \rceil \quad (3\text{-}22)$$

3.6.1 Spectral Efficiency of S-TDD and D-TDD systems

In [54], the spectral efficiency was expressed as the average bit rate per unit bandwidth per unit area supported by a cell's base station.

$$A_e = \frac{\sum_{k=1}^{N_s} C_k}{W\pi(\varepsilon/2)^2} \quad \text{bits/s/Hz/m}^2 \tag{3-23}$$

where N_s is the total number of active serviced channels per cell

W is the total allocated bandwidth per cell in Hz

ε is the frequency reuse distance in meter.

The channel capacity of the *k*-th SC is given by the well known Shannon's equation as

$$C_k = W_k \log_2(1+\gamma_k) \tag{3-24}$$

where γ_k is the SIR of the *k*-th SC. As SIR is a random variable even when the SC is stationary, the average channel capacity is used to obtain spectral efficiency. The average channel capacity of the *k*-th SC is given as,

$$C_k = W_k \int_0^\infty \log_2(1+\gamma_k)\, f_\gamma(\gamma_k) d\gamma_k \tag{3-25}$$

where $f_\gamma(\gamma_k)$ is the PDF of the SIR of the *k*-th SC.

In [53], the focus is on the spectral efficiency of TDD systems for dynamic traffic and so a cellular system with typical configuration is considered where the cellular system parameters like cell size, frequency reuse are assumed to be fixed. Hence, the denominator of (3-23) is fixed for all spectral efficiency representations.

In TDMA system, the whole bandwidth is allocated to one user as there is only one user that is served per time slot. So, $N_s = 1$ and $W_k = W$. If the channel is ergodic, the distribution of SIR is identical in a fully loaded S-TDD/TDMA system. Thus, the spectral efficiency (η) of the cellular system is given as,

$$\eta = \frac{\sum_{k=1}^{N_s} C_k}{W} = \int_0^{\infty} \log_2(1+\gamma) f_\gamma(\gamma) d\gamma \quad \text{bits/s/Hz.} \tag{3-26}$$

But, in D-TDD systems, each time slot experiences different statistics of SIR over the extra time slot region and hence the spectral efficiency of a certain time slot cannot represent the average spectral efficiency of the D-TDD system as shown in equation (3-26). The average spectral efficiency of the *i*-th time slot can be expressed as

$$\eta_i = (1 - \frac{T_G}{T_S}) \int_0^{\infty} \log_2(1+\gamma_i) f_\gamma(\gamma_i) d\gamma_i$$

$$i = 1, 2 \ldots, n_{UP}^{\max} \qquad \text{bits/s/Hz} \tag{3-27}$$

where γ_i is the SIR value for the *i*-th time slot,

$f_\gamma(\gamma_i)$ is the PDF of SIR at the *i*-th time slot,

T_s is time slot interval and

T_G is the guard time.

The average spectral efficiency, $\bar{\eta}$, can be obtained as the expectation of equation (3-27) for all active time slots.

$$\bar{\eta} = (1 - \frac{T_G}{T_S}) \sum_{i=1}^{n_{UP}} \frac{\eta_i}{n_{UP}}$$

$$= (1 - \frac{T_G}{T_S}) \frac{\sum_{i=1}^{n_{UP}} \int_0^{\infty} \log_2(1+\gamma_i) f_\gamma(\gamma_i) d\gamma_i}{n_{UP}} \tag{3-28}$$

The uplink spectral efficiency of D-TDD systems can be given as,

$$\eta_{D-TDD} = E\left[\frac{(1-\frac{T_G}{T_S})\sum_{i=1}^{n_{UP}^D}\bar{C}_i}{n_{UP}^D}\right]$$

$$= (1-\frac{T_G}{T_S})\sum_{j=L}^{n_{UP}^{\max}}\left(\frac{\sum_{i=1}^{j}\bar{C}_i}{j}\right)\times p_{n_{UP}}(j \mid n_{UP}^{\min} \le n_{UP} \le n_{UP}^{\max}) \quad \text{bits/s/Hz} \qquad (3\text{-}29)$$

where $p_{n_{UP}}(j \mid n_{UP}^{\min} \le n_{UP} \le n_{UP}^{\max})$ is the PMF.

The S-TDD may not be fully loaded even if the D-TDD frame is loaded due to the dynamic nature of multimedia traffic. So, the spectral efficiency of S-TDD/TDMA systems can be expressed as

$$\bar{\eta} = E\left[\left(1-\frac{T_G}{T_S}\right)\frac{\sum_{j=1}^{n_{UP}^{'}}\bar{C}_j}{n_{UP}^S}\right] = \left(\frac{1-\frac{T_G}{T_S}}{n_{UP}^s}\right)\sum_{j=L}^{n_{UP}^{'}}\left(\sum_{i=1}^{j}\bar{C}_i\right)\hat{p}_{n_{UP}}(j) \qquad \text{bits/s/Hz} \qquad (3\text{-}30)$$

where $n_{UP}^{'} = \min(n_{UP}^S, n_{UP}^D)$

$$\hat{p}_{n_{UP}}(x) = \begin{pmatrix} p(x \mid n_{UP}^{\min} \le n_{UP} \le n_{UP}^{\max}), x < n_{UP}^S \\ \sum_{x=n_{UP}^S}^{n_{UP}^{\max}} p(x \mid n_{UP}^{\min} \le n_{uP} \le n_{UP}^{\max}, x = n_{UP}^S \end{pmatrix}$$

For S-TDD systems, the boundary between the uplink and downlink direction is fixed and so there can be idle time slots. This underutilized bandwidth is represented by the equation (3-30).

3.7 ON-OFF traffic model in TDMA/D-TDD systems

In this section, we model the traffic in a TDMA/D-TDD system using the ON-OFF traffic modeling. The ON-OFF source is the prototype of a bursty source [59]. In an ON-OFF source, information is sent in a succession of active (ON) periods separated by silent (OFF) periods. ON-OFF sources can also be distinguished by the way information is sent during the ON period [59]. It can be strictly periodic ("deterministic") emission of traffic or the Bernoulli process. They can also be distinguished according to the statistical properties of the ON and OFF periods. The source may switch from the ON state to the OFF state according to a Continuous Time Markov Chain (CTMC) with two states.

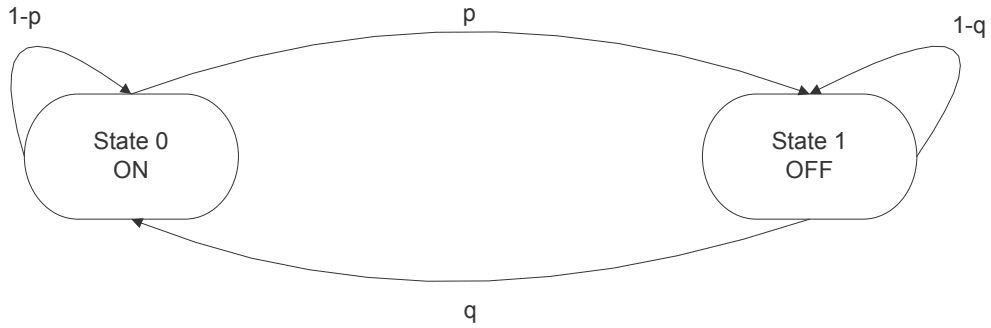

Figure 3-11: ON-OFF Traffic model.

A Discrete Time Markov Chain (DTMC) is a process making transitions from one state to another at well defined instants of time t_n. The DTMC is fully determined when the one-step transition probabilities Prob$[X_{n+1} = j \mid X_n = i]$ are known. The transition probabilities are independent of time when the system is homogeneous. The one-step transition probabilities are then just numbers P_{ij} that can be arranged into the one-step transition matrix or simply the transition probability matrix P = (P_{ij}). It follows that,

$$\sum_{k=0}^{\infty} P_{jk} = 1 \tag{3-31}$$

P is called the stochastic matrix. If the initial state vector $(p_0^{(0)}, p_1^{(0)},..., p_n^{(0)})$ is known, the state vector at time instant t_1 can be calculated by applying the one-step transition matrix P once.

$$[p_0^{(1)}, p_1^{(1)},..., p_n^{(1)}] = [p_0^{(0)}, p_1^{(0)},..., p_n^{(0)}].\mathrm{P} \tag{3-32}$$

The equilibrium distribution is represented as

$$\pi = (\pi_0, \pi_1,..., \pi_n)$$

with $\sum_i \pi_i = 1$.

As the equilibrium distribution is invariant under the one-step transition matrix,

$$\pi\mathrm{P} = \pi \tag{3-33}$$

Let the transition matrix T be

$$T = \begin{pmatrix} 1-p & p \\ q & 1-q \end{pmatrix} \tag{3-34}$$

The entries in the transition matrix correspond to figure 3-11. The equilibrium distribution is given by,

$$\text{Prob [State is ON]} = \pi_0 = \frac{q}{p+q}$$

$$\text{Prob [State is OFF]} = \pi_1 = \frac{p}{p+q} \tag{3-35}$$

Equation (3-35) is valid for $p+q \neq 0$. From figure 3-11, there are two "once in never out" states without interesting applications [59]. The value $\pi_0(\pi_1)$ gives the probability that the chain observed at an arbitrary instant is in state 0 (1). The probability can be calculated in the following way. Let the average length of the ON (OFF) period

be $\bar{T}_{\text{ON}}(\bar{T}_{\text{OFF}})$. The probability that an ON state has length *n*, p_n, is needed to calculate $\bar{T}_{\text{ON}}$. So, the chain being in the ON state should be in the ON state for another (*n*-1) time steps and then switch to the OFF state. This probability can be given as in equation (3-36) from figure 3-11.

$$p_n = (1-p)^{n-1} p \tag{3-36}$$

The average ON period is then given by,

$$\bar{T}_{\text{ON}} = \sum_{n=1}^{\infty} n p_n = \frac{1}{p} \tag{3-37}$$

Similarly for the OFF period,

$$\bar{T}_{OFF} = \frac{1}{q} \tag{3-38}$$

The time axis is covered by a succession of ON and OFF periods and the probability of finding the chain in the ON state equals,

$$\text{Prob[chain is ON]} = \frac{\bar{T}_{\text{ON}}}{\bar{T}_{\text{OFF}} + \bar{T}_{\text{ON}}} = \pi_0$$

If the average interarrival time in the ON period is *D* (cell periods), the average load in the ON period equals,

$$\lambda_0 = \frac{1}{D} \tag{3-39}$$

The overall average load ρ produced by such a source is then,

$$\rho = \frac{\bar{T}_{\text{ON}}}{\bar{T}_{\text{ON}} + \bar{T}_{\text{OFF}}} \lambda_0 = \frac{q}{p+q} \lambda_0 \tag{3-40}$$

Calculation of the correlation properties of the ON-OFF source is straight forward and a closed form expression for the autocorrelation of the arrival process can be found.

$$T^k = \begin{pmatrix} 1-p & p \\ q & 1-q \end{pmatrix}^k = \begin{pmatrix} \pi_0 + \pi_1\alpha^k & \pi_1 - \pi_1\alpha^k \\ \pi_0 - \pi_0\alpha^k & \pi_1 + \pi_0\alpha^k \end{pmatrix} \tag{3-41}$$

In equation (3-41),

$$\alpha = 1 - p - q$$

and π_0 and π_1 are defined in equation (3-35).

The autocorrelation of the arrival process of the ON-OFF process can be written as,

$$R(k) = (\pi_0\lambda_0, 0)\begin{pmatrix} \pi_0 + \pi_1\alpha^k & \pi_1 - \pi_1\alpha^k \\ \pi_0 - \pi_0\alpha^k & \pi_1 + \pi_0\alpha^k \end{pmatrix}\begin{pmatrix} \lambda_0 \\ 0 \end{pmatrix} \tag{3-42}$$

We model the traffic in the DTMA/D-TDD system using an ON-OFF two state model. The ON period consists of a sequence of document transmission requests from an individual subscriber. The ON and OFF periods are modeled as heavy-tailed Weibull and Pareto distributions respectively. The inter-arrival time of requests within the ON periods is modeled using another Weibull distribution. An ON-OFF process is used to model the several requests during the active or ON period followed by an inactive or OFF period, whose duration is significantly longer than the interarrival times during the ON period.

The model was created for the physical process of the World Wide Web (WWW) document arrivals.

3.7.1 WWW Request Arrival Model

When a WWW user clicks on a hypertext link, several Uniform Resource Locator (URL) requests may follow. The first request transmits the user's direct request to the server. When the user's request is being executed, other requests may be generated automatically by the client program. As an example, each in-line image will require a separate request be sent automatically by the client program when a page is being downloaded. Each of these new requests opens a new Transfer Control Protocol (TCP) connection. After the completion of the user's request and the associated requests, the user will take time absorbing the information just received before initiating the next request. So, the traffic can be modeled with an OFF period, following an ON period consisting of a series of requests. The model can be described by the distributions of the following three random variables.

- *r*: The inter-arrival time of requests during the ON period.
- *s*: The duration of an OFF period.
- *n*: The duration of an ON period.

3.7.1.1 ON period distribution

The exact boundaries of the ON and OFF periods are dependent on the choice of the threshold. A method from [60] is adapted where a specific value of the threshold is chosen and then the insensitivity of the distribution to the chosen value is tested within a large range. A threshold value of 60 seconds is used in the modeling. A sequence of requests with interarrival times of less than 60 seconds is considered to form an ON period while the occurrence of a request more than 60 seconds after the previous request indicates an OFF period.

A Weibull distribution is given by

$$p(x) = \frac{k}{\theta}\left(\frac{x}{\theta}\right)^{k-1} e^{-(x/\theta)^k} \tag{3-43}$$

The probability distribution function is given by

$$F(x) = \Pr ob(t \le x) = 1 - e^{-\left(\frac{x}{\theta}\right)^k} \tag{3-44}$$

The parameter k represents the shape of the distribution. The distribution function is positively skewed when $k > 3.6$ and negatively slewed when $k \le 3.6$. Also, the distribution is light tailed when $k > 1$ and heavy tailed when $k \le 1$.

The dataset from [34] is tested for the Weibull distribution. The test can be performed by fitting a straight line on a probability plot of $y = \ln(x)$ versus $z = \ln(-\ln(l - F(x))$ [61]. The value of $k = \frac{1}{b}$ and $\theta = \exp(a)$ is obtained from a straight line fit of $z = \frac{(y-a)}{b}$. The Weibull probability plotting for ON period duration with a threshold value of 60 seconds is shown in figure 3-12. The figure clearly suggests a Weibull distribution with $k = \frac{1}{1.3} = 0.77$ and $\theta = \exp(4.6) = 99.5$.

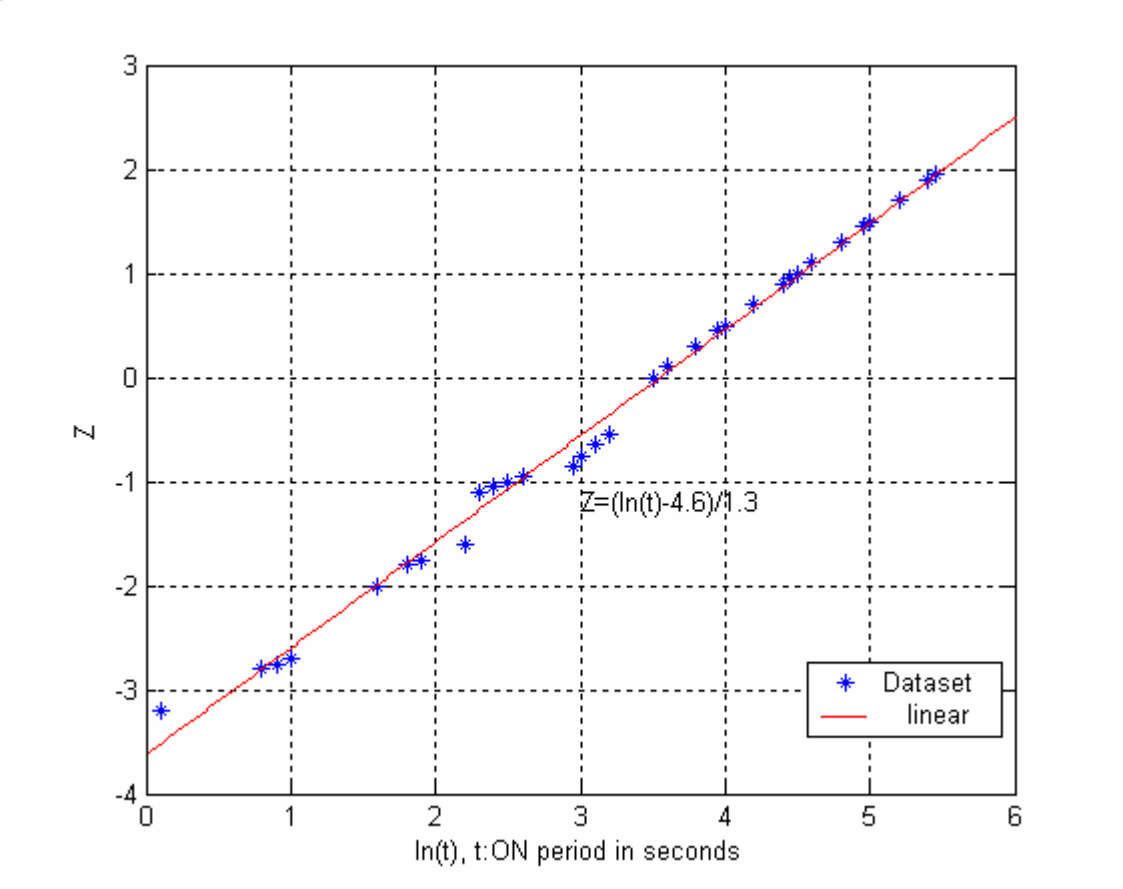

Figure 3-12: Weibull plot of ON period distribution.

The empirical model for the ON period probability density can be devised as:

$$p(x) = \frac{0.022}{x^{0.23}} e^{-\left(\frac{x}{99.5}\right)^{0.77}} \tag{3-45}$$

3.7.1.2 OFF period distribution

The OFF period indicates the presence of significant pause in the communication. A Pareto distribution is given by,

$$p(x) = \alpha k^{\alpha} / x^{\alpha+1} \tag{3-46}$$

for $x \geq k$. $\alpha \geq 1$.

The probability distribution function is given by,

$$F(x) = \Pr ob(t \le x) = 1 - \left(\frac{k}{x}\right)^{\alpha} \tag{3-47}$$

A Pareto distribution has infinite mean if $\alpha \le 1$ and infinite variance if $\alpha \le 2$.

The dataset from [34] is tested for Pareto distribution. An α value of 0.5 was obtained for the date set and this shows that the distribution has infinite mean and variance. The probability density function of an empirical model for the OFF period distribution is given by,

$$p(x) = \frac{\sqrt{60}}{2x\sqrt{x}} \tag{3-48}$$

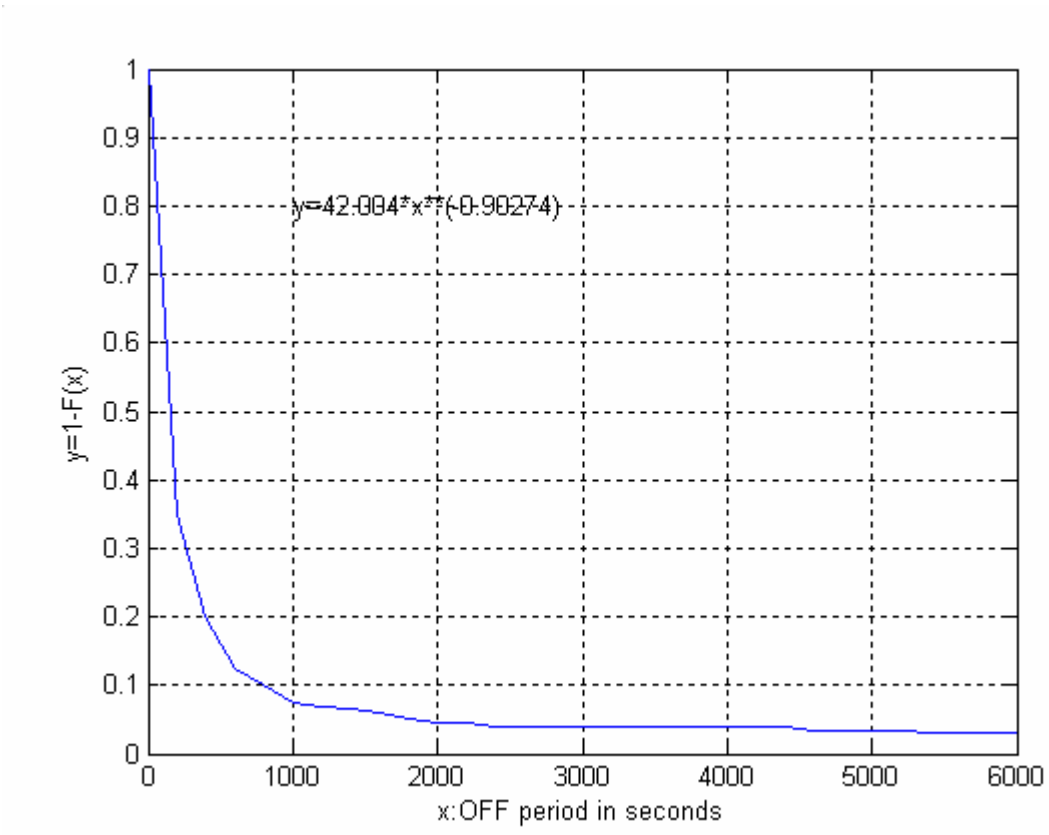

Figure 3-13: Pareto distribution plot of OFF period.

3.7.1.3 Interarrival distribution during ON period

The Weibull distribution of the interarrival times of the dataset from [34] is obtained. The plot is shown in figure 3-14. From figure 3-14, the value of k can be determined to be 0.5 and the value of θ to be 1.5. The probability density function for the Weibull distribution is given as

$$p(t) = \frac{e^{\sqrt{\frac{t}{e^{1.5}}}}}{2\sqrt{e^{1.5}t}} \tag{3-49}$$

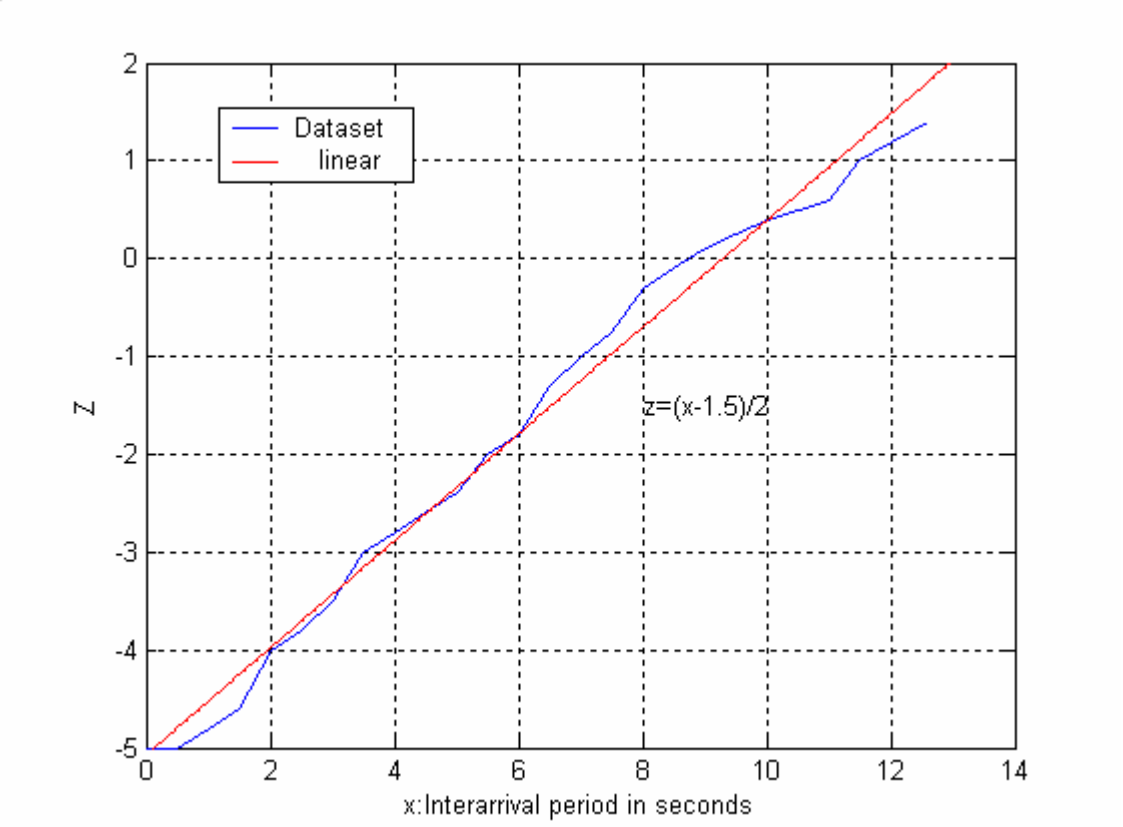

Figure 3-14: Weibull plot of interarrival distribution during the ON period.

3.7.2 Numerical results

The ON-OFF traffic modeling is applied to a TDMA/D-TDD system. The number of extra UL TSs for each user is based on the ON-OFF density function. The probability

density function for the ON and OFF period is given in equation (3-45) and (3-48) respectively. The results obtained from simulation are given in figure 3-15.

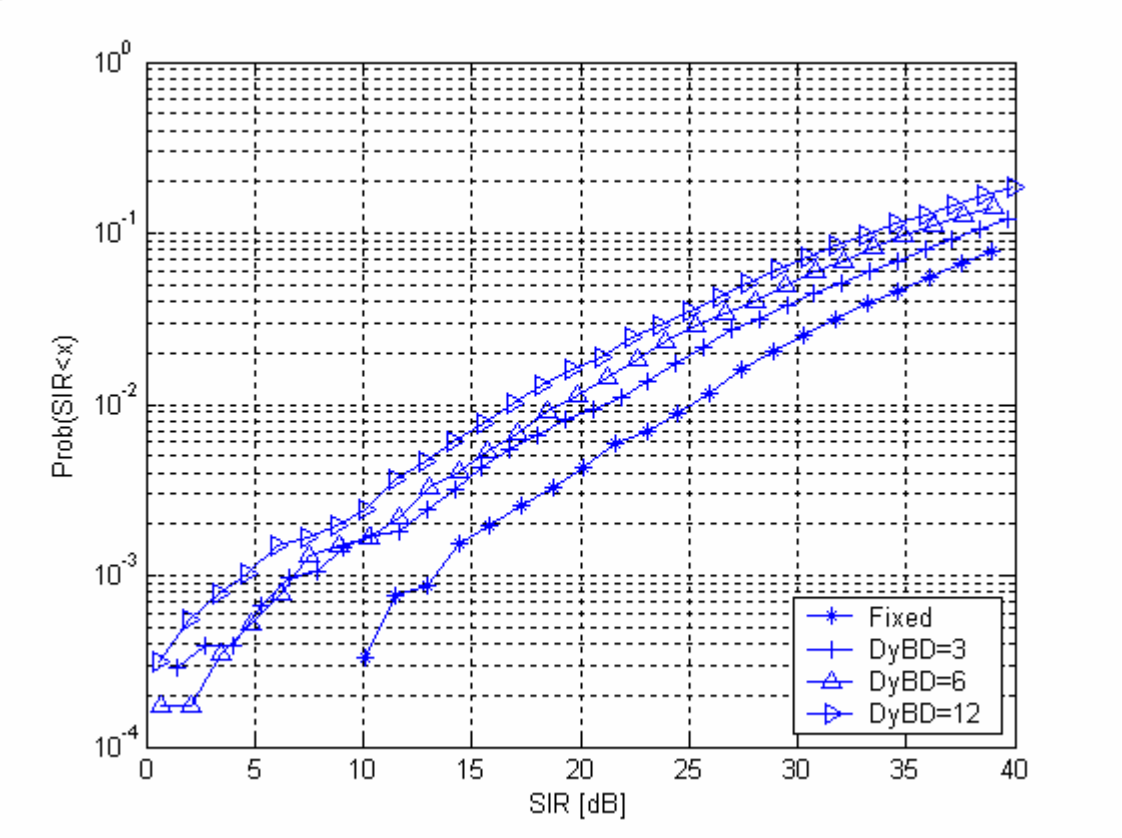

Figure 3-15: SIR outage using fifteen-sectored antennas with the *Max* {SIR} algorithm and ON-OFF traffic model.

The result in figure 3-15 matches the result obtained in figure 2-22 where the number of extra UL TSs for each user was based on a uniform density function. As a comparison, at an outage of 1% , the achievable SIR when the number of extra UL TSs is six is 19 dB from figure 2-22 and the corresponding value from figure 3-15 is 18 dB.

3.8 Conclusion

This chapter began with the definition and properties of self similarity. The techniques and methods for modeling self-similar traffic and estimating the Hurst

parameter [*H*] were described. Two sets of Internet data traffic were introduced and the self similar nature of these data sets was proven. The truncated Gaussian traffic model is applied to model the static TDD and dynamic TDD traffic and also the expressions for the spectral efficiency of the static TDD and dynamic TDD systems under truncated Gaussian traffic model assumptions were studied.

We then modeled the dataset from [34] using ON-OFF traffic modeling. Simulations were carried out for D-TDD systems where the traffic was modeled based on the ON-OFF traffic model and results obtained matched with the results obtained when traffic was modeled using a uniform density function.

4 MULTI-CELL COORDINATED D-TDD RESOURCE ALLOCATION FOR MULTI-CELL ENVIRONMENTS

In this chapter, the *Max* {SIR} algorithm is extended to a multi-cell environment. We call this algorithm the multi-cell D-TDD allocation algorithm. This algorithm was found to improve the SIR outage probability ratio when the interference power and signal power from multiple cells are well coordinated to reduce the co-channel interference.

The *Max* {SIR} algorithm is also applied to TDMA/D-TDD systems with priority. All the subscribers are grouped into priority groups and the performance of TDMA/D-TDD systems with and without the allocation of the *Max* {SIR} algorithm is compared.

The rest of the chapter is organized as follows. The multi-cell D-TDD allocation algorithm is explained in detail and the results obtained from simulation are summarized. The *Max* {SIR} algorithm with priority is then explained and the conclusions for the chapter are drawn.

4.1 Multi-cell D-TDD allocation algorithm

The multi-cell D-TDD allocation algorithm is explained in this section.

The execution of the algorithm starts from the last extra uplink time slot in the reference cell. The algorithm is executed only for the co-channels that are in DL cycle in the TS corresponding to the extra UL time slot in the reference cell. The algorithm is not executed for the co-channels that are in UL cycle in the TS corresponding to the extra UL

time slot in the reference cell. This is because the BS-BS co-channel interference is the main source of co-channel interference in D-TDD systems as explained in chapter 2 and the multi-cell D-TDD allocation algorithm intends to reduce this BS-BS co-channel interference. The algorithm does an exhaustive search among the MSs that are in DL reception in the co-channel cells in which the algorithm will be executed. From this search, it places the MS that will introduce the least co-channel interference to the BS in the reference cell in the TS corresponding to last extra UL time slot in the reference cell. If there is more than one TS occupied by this MS in DL reception, they are placed in the second last extra UL time slot corresponding to the reference cell and so on. If there is only one TS occupied by this MS in the DL reception, then the MS that causes the second least co-channel interference to the BS in the reference cell is placed in the time slot corresponding to the second last extra UL time slot in the reference cell. The execution of the algorithm is terminated when there no more extra UL time slots in the reference cell. The algorithm is explained in detail with the help of figures 4-1 and 4-2.

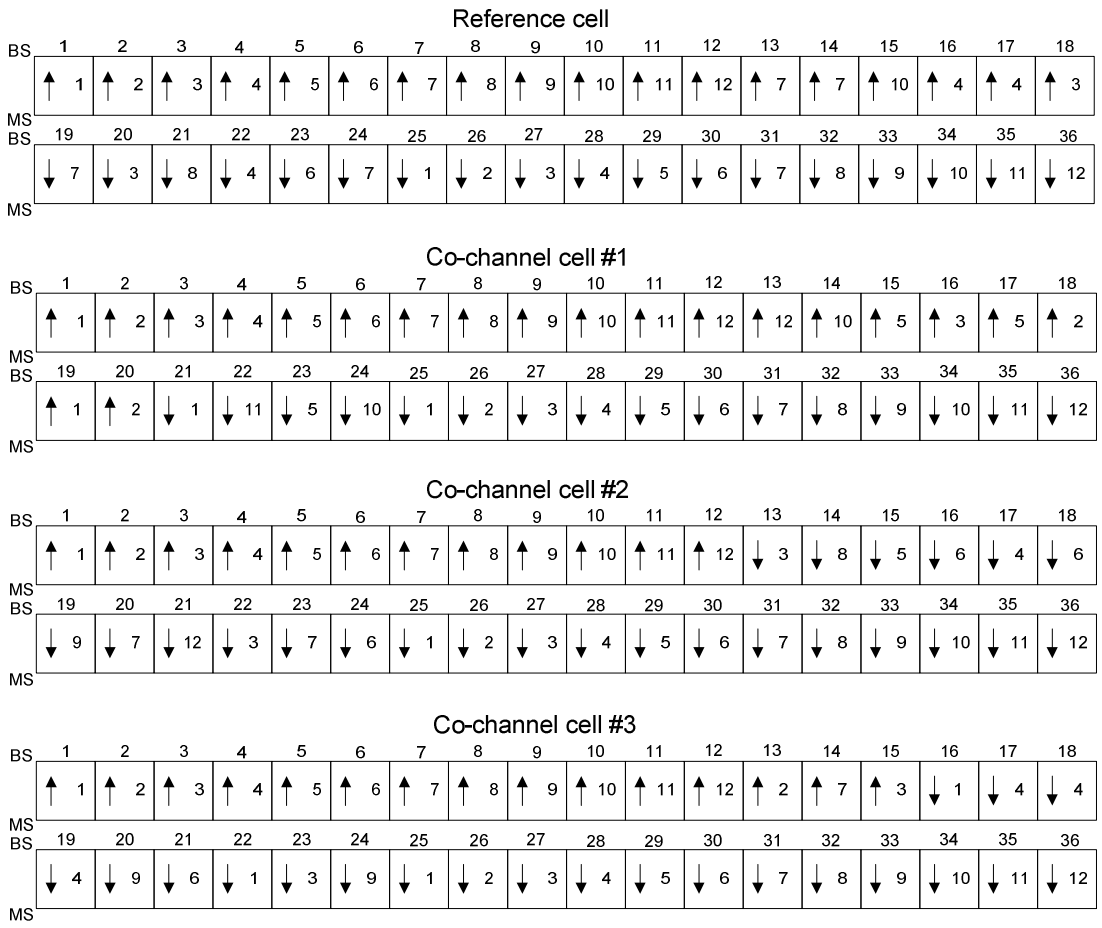

Figure 4-1: D-TDD frame with 36 time slots in the reference cell and three co-channel cells.

Figure 4-1 shows a D-TDD frame with 36 times slots in the reference cell, and three co-channel cells, co-channel cell #1, #2, and #3. The time slots are numbered on the top of each frame as shown. There are assumed to be 12 MSs in each cell, numbered from 1 to 12. Also, the first 12 time slots, TSs 1 -12, are used for UL transmission and the last 12 time slots, TSs 25 – 36, are used for DL reception in all the cells. The remaining 12 TSs, TS 13 – 24 can be used for either UL or DL in each cell. The extra UL and DL time slots fall into TSs 13 – 24. The number of extra UL TSs are allocated to the users in a random and uniform manner. The number of extra UL time slots in the reference cell is

six, from TSs 13 – 18. The number of extra UL time slots in the co-channel cells 1, 2, and 3 are 8, 0, and 3 respectively. Thus, the number of extra DL time slots in the reference cell, co-channel cells 1, 2, and 3 are 6, 4, 12, and 9 respectively.

The execution of the multi-cell D-TDD allocation algorithm starts at the last extra UL time slot in the reference cell. From figure 4-1, TS 18 is the last extra UL time slot in the reference cell. During TS 18, co-channel cells #2 and #3 are in DL and hence the algorithm is executed in these cells. The algorithm is executed in co-channel cell #2 initially. Let us assume that the MSs that cause the least interference to the BS in the reference cell is found to be as follows from the execution of the algorithm, in descending order.

MS co-channel interference order = [12, 3, 2, 1, 10, 7, 11, 6, 9, 4, 8, 5]

MS 12 in DL reception causes the least interference to the BS in reference cell and MS 5 causes the most interference, respectively, from co-channel cell #2. The MSs in TS 13 – 24 in co-channel cell # 2 can be rearranged so that the MSs causing the least co-channel interference occupy the TSs corresponding to TSs 13 – 18, the extra UL TSs in the reference cell. The MSs occupying the TSs 13 – 36 in co-channel cell #2 are given as {1, 2, 3, 3, 3, 4, 4, 5, 5, 6, 6, 6, 6, 7, 7, 7, 8, 8, 9, 9, 10, 11, 12, 12}. As MS 12 causes the least interference, it is exchanged with the MS in TS 18, the TS corresponding to the last extra UL TS in the reference cell. MS 6 that was originally present in TS 18 is placed in the TS occupied by MS 12, which is TS 21 from figure 4-1. The second occurrence of MS 12 is exchanged with the MS in TS 17, the second last extra UL TS in the reference cell. After MS 12, MS 3 introduces the least interference to the reference cell BS. Thus, the three occurrences of MS 3 are placed into TSs 16, 15, and 14. TS 13 is occupied by MS

2. The execution of the algorithm stops at TS 13 corresponding to the first extra UL TS in the reference cell.

The algorithm is again repeated for co-channel cell #3. The MSs causing the least interference are placed in TSs 18, 17, and 16 as only these three TSs are in DL reception when the reference cell is in UL transmission. Let us assume that from the execution of the multi-cell D-TDD allocation algorithm, the MS co-channel interference order is as follows.

MS co-channel interference order = {8, 5, 11, 1, 9, 4, 7, 10, 3, 6, 12, 2}

The MS 8 from TS 32 is exchanged with MS 4 from TS 18. Next, MS 5 from TS 27 is exchanged with MS 4 from TS 17 and finally MS 11 from TS 35 is exchanged with MS 1 from 16. The execution of the algorithm stops now and the final D-TDD frame arrangement is given as shown in figure 4-2.

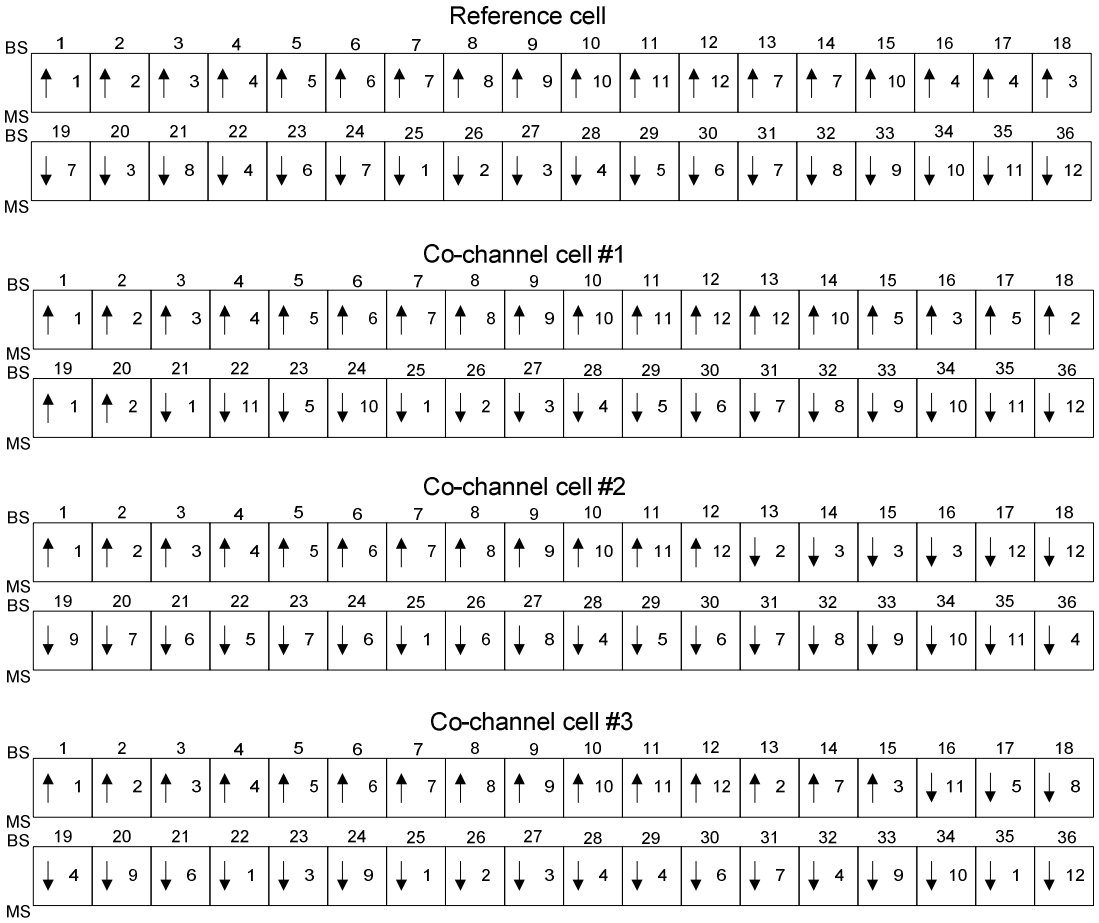

Figure 4-2: D-TDD frame from Figure 4-1 after execution of the multi-cell D-TDD allocation algorithm.

The flowchart of the multi-cell D-TDD allocation algorithm is given in figure 4-3.

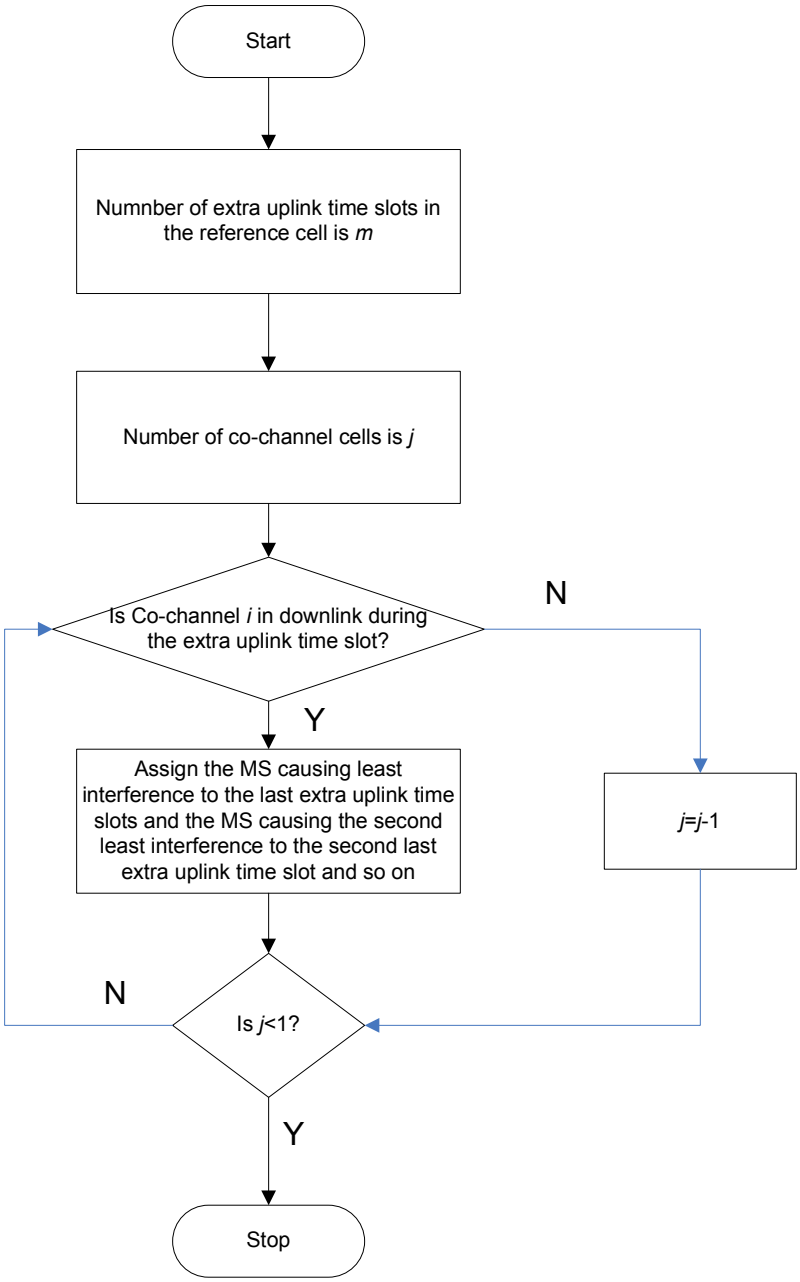

Figure 4-3: Flowchart of the multi-cell D-TDD allocation algorithm.

The results obtained from the simulation are summarized below. The results are compared with the results of the *Max* {SIR} algorithm from [5]. Initially four-sectored antennas are used at the BS. The different parameters used in the simulation are given in table 4-1.

Table 4-1: Simulation parameters when four-sectored antennas are used at the base station site.

Parameter	*Value*
Cell size	4000 m
Frequency reuse	25
Number of Co-channel cells	24 (First and second tier)
Number of users per cell	12
Path loss exponent – MS to BS	4
Path loss exponent – BS to BS	3
Lognormal shadowing – MS to BS	6 dB
Lognormal shadowing – BS to BS	4 dB
HPBW at BS	90 degrees
HPBW at MS	20 degrees
Frequency	1.9 GHz
Antenna aperture size – BS	0.0739 m
Antenna aperture size – MS	0.385 m
Number of iterations	10000

The results obtained from the *Max* {SIR} algorithm are shown in figure 4-4.

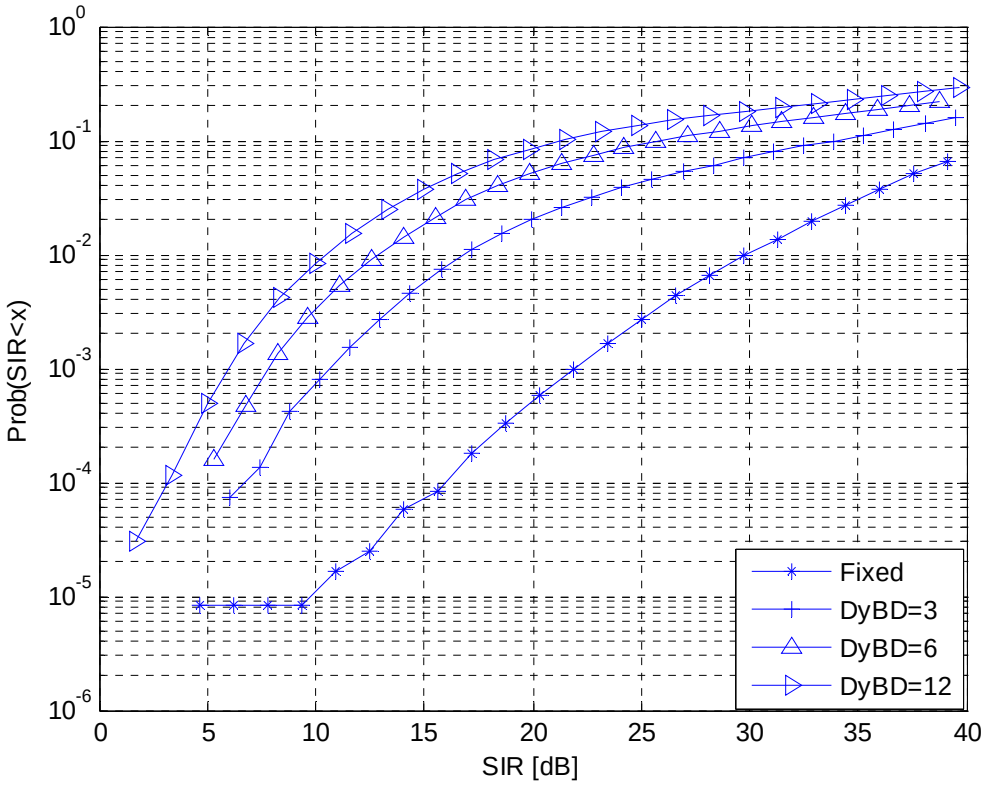

Figure 4-4: SIR outage using four-sectored antennas and the Max {SIR} algorithm.

The results obtained when the multi-cell D-TDD allocation algorithm is used are shown in figure 4-5.

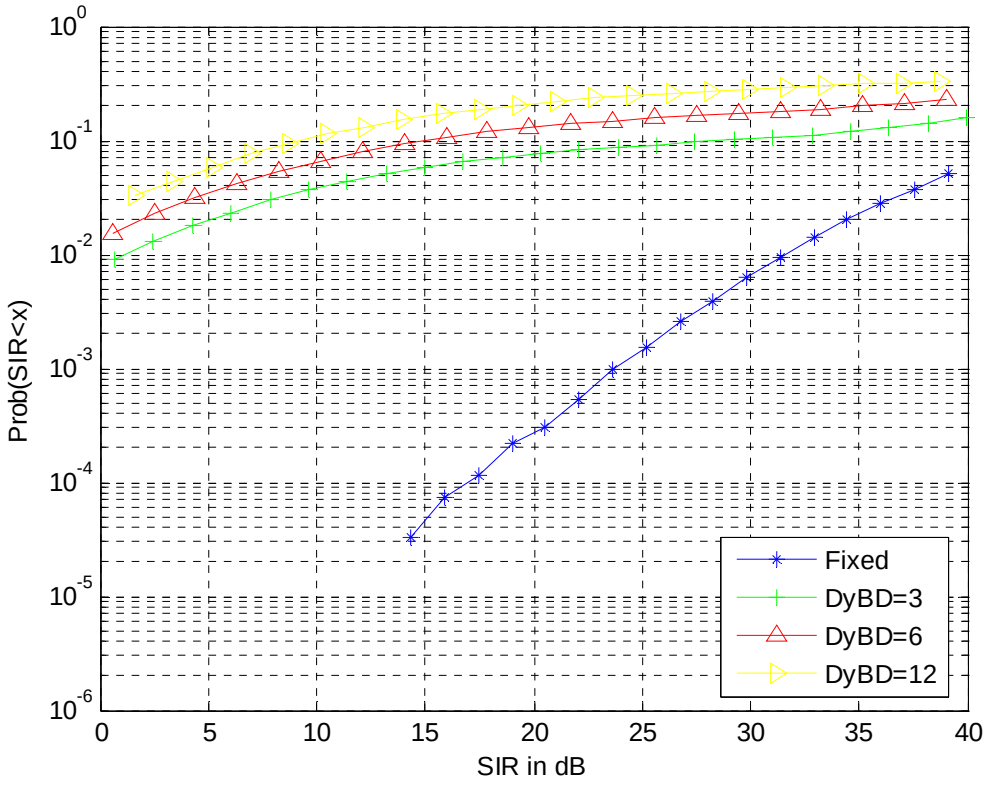

Figure 4-5: SIR outage using four-sectored antennas and the multi-cell D-TDD allocation algorithm.

From figures 4-4 and 4-5, there is not much difference in the SIR outage for the cases of the Max {SIR} algorithm and the multi-cell D-TDD allocation algorithm. It can be seen that the SIR curve saturates at a rapid rate when the dynamic boundary is introduced for both the cases. The results are next compared when fifteen-sectored antennas are deployed at the BS. The various parameters used in the simulation are given in table 4-2.

Table 4-2: Simulation parameters when fifteen-sectored antennas are used at the base station site.

Parameter	*Value*
Cell size	4000 m
Frequency reuse	25
Number of Co-channel cells	24 (First and second tier)
Number of users per cell	12
Path loss exponent – MS to BS	4
Path loss exponent – BS to BS	3
Lognormal shadowing – MS to BS	6 dB
Lognormal shadowing – BS to BS	4 dB
HPBW at BS	24 degrees
HPBW at MS	20 degrees
Frequency	1.9 GHz
Antenna aperture size – BS	0.3302 m
Antenna aperture size – MS	0.385 m
Number of iterations	10000

The results obtained from the *Max* {SIR} algorithm are shown in figure 4-6.

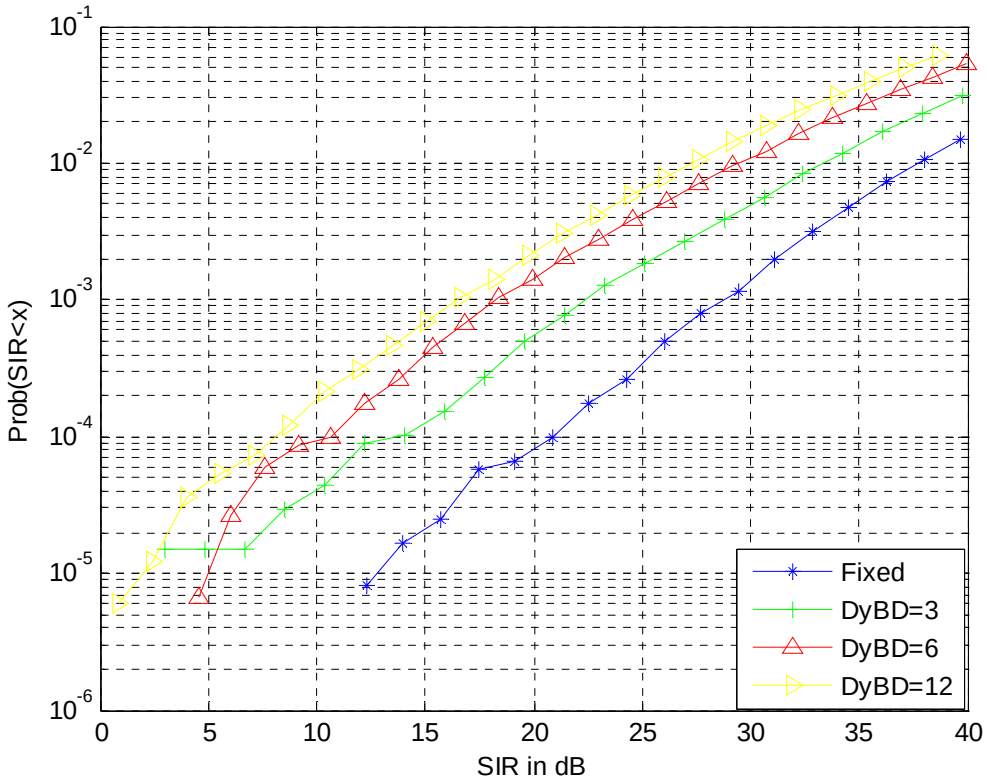

Figure 4-6: SIR outage using fifteen-sectored antennas and the Max {SIR} algorithm.

The results obtained when the multi-cell D-TDD allocation algorithm is used are shown in figure 4-7.

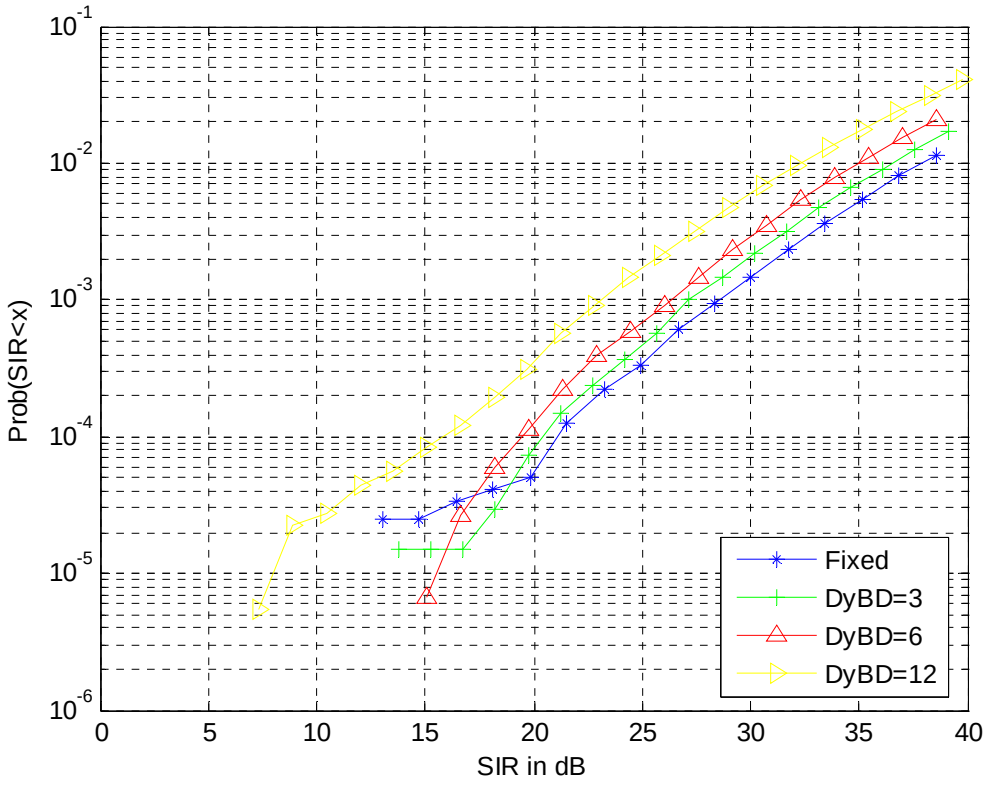

Figure 4-7: SIR outage using fifteen-sectored antennas and the multi-cell D-TDD allocation algorithm.

Comparing figures 4-6 and 4-7 there is a substantial improvement in the SIR outage performance. For example, at an outage of 1%, the achievable SIR from figure 4-6 is 27 dB and this increase to 32 dB when the number of extra UL TSs is 12 from figure 4-7.

As a next step of our research, the *Max* {SIR} algorithm is expanded and applied to a multi-cell environment. The algorithm is applied to cells that have extra UL TSs. The expanded *Max* {SIR} algorithm is explained with respect to figure 4-1. Each frame has 36 TSs in figure 4-1 and the first and last 12 TSs are used for UL transmission and DL reception respectively. TSs 13-18 and TSs 19-24 are extra UL and DL TSs respectively in the reference cell. Similarly, TSs 13-20 and TSs 21-24 are extra UL and DL TSs respectively in the co-channel cell #l. TSs 13-24 are extra DL TSs in the co-channel cell

#2. TSs 13-15 and TSs 16-24 are extra UL and DL TSs respectively in the co-channel cell #4. The highest TS number that is in UL is TS #20 in co-channel cell #1. The MS with the maximum SIR in the UL direction is placed in TS #20 and the MS with the second maximum SIR is placed in TS #19. In TS #18, the reference cell and co-channel cell#1 are in UL transmission. So the MS corresponding to the maximum SIR and the MS corresponding to the third maximum SIR is placed in TS #18 in the reference cell and co-channel cell #1 respectively. The execution of the algorithm proceeds in this manner until the first extra uplink TS, namely TS #13 for all the cells that have one or more extra UL TSs.

The flowchart of the steps involved in the expanded Max {SIR} algorithm is shown in figure 4-8.

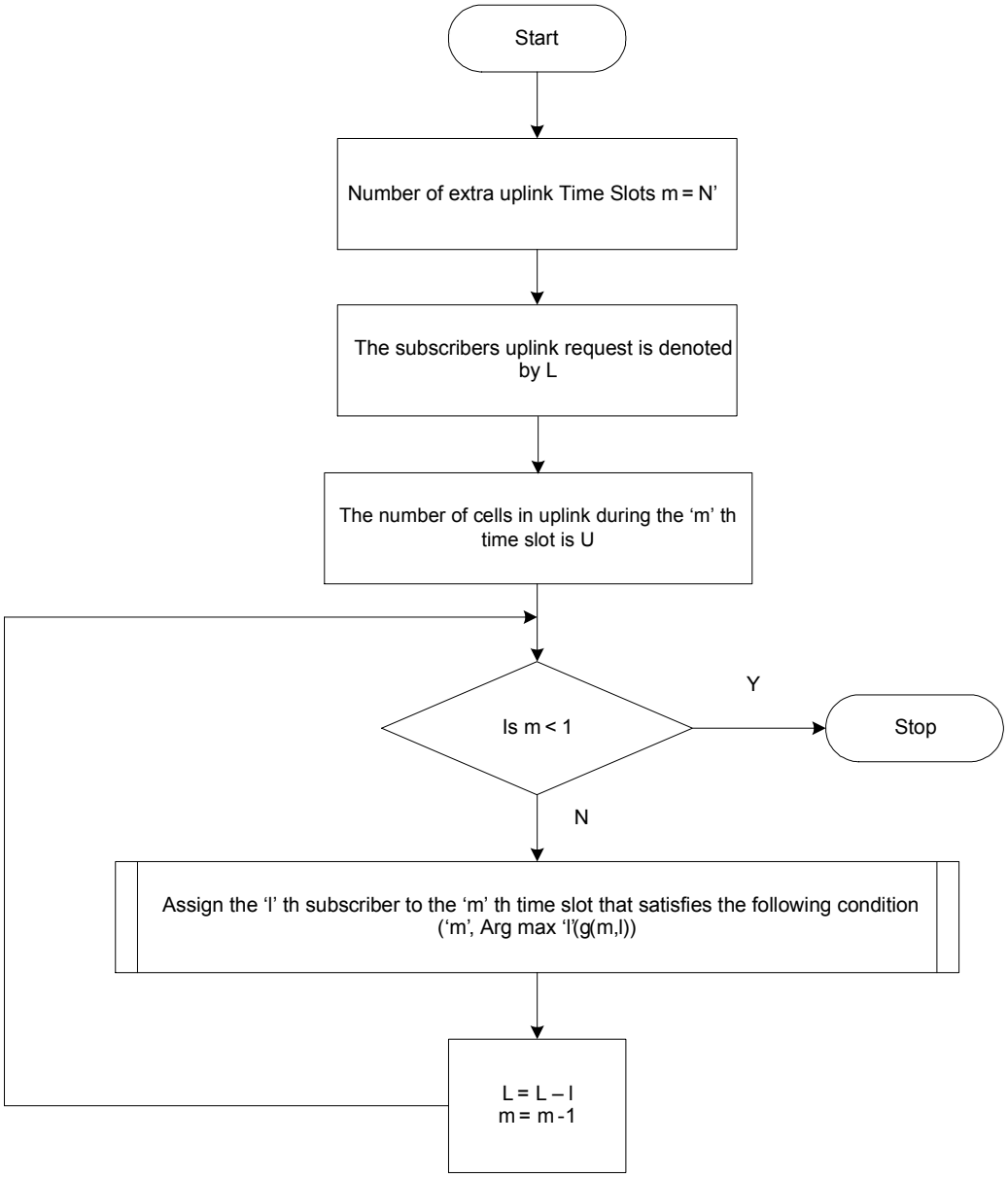

Figure 4-8: Flowchart of the extended D-TDD allocation algorithm.

The results obtained from the simulation are summarized. The results obtained with and without the application of the expanded *Max* {SIR} algorithm are compared. The comparison is based on the SIR of one of the cells chosen at random out of the 25 available cells. Fifteen-sectored antennas are used at the BS. The different parameters used in the simulation are given in table 4-3.

Table 4-3: Simulation parameters when fifteen-sectored antennas are used at the base station site.

Parameter	*Value*
Cell size	4000 m
Frequency reuse	25
Number of Co-channel cells	24 (First and second tier)
Number of users per cell	12
Path loss exponent – MS to BS	4
Path loss exponent – BS to BS	3
Lognormal shadowing – MS to BS	6 dB
Lognormal shadowing – BS to BS	4 dB
HPBW at BS	24 degrees
HPBW at MS	20 degrees
Frequency	1.9 GHz
Antenna aperture size – BS	0.3302 m
Antenna aperture size – MS	0.385 m
Number of iterations	10000

The results obtained without the application of the extended *Max* {SIR} algorithm are shown in figure 4-9.

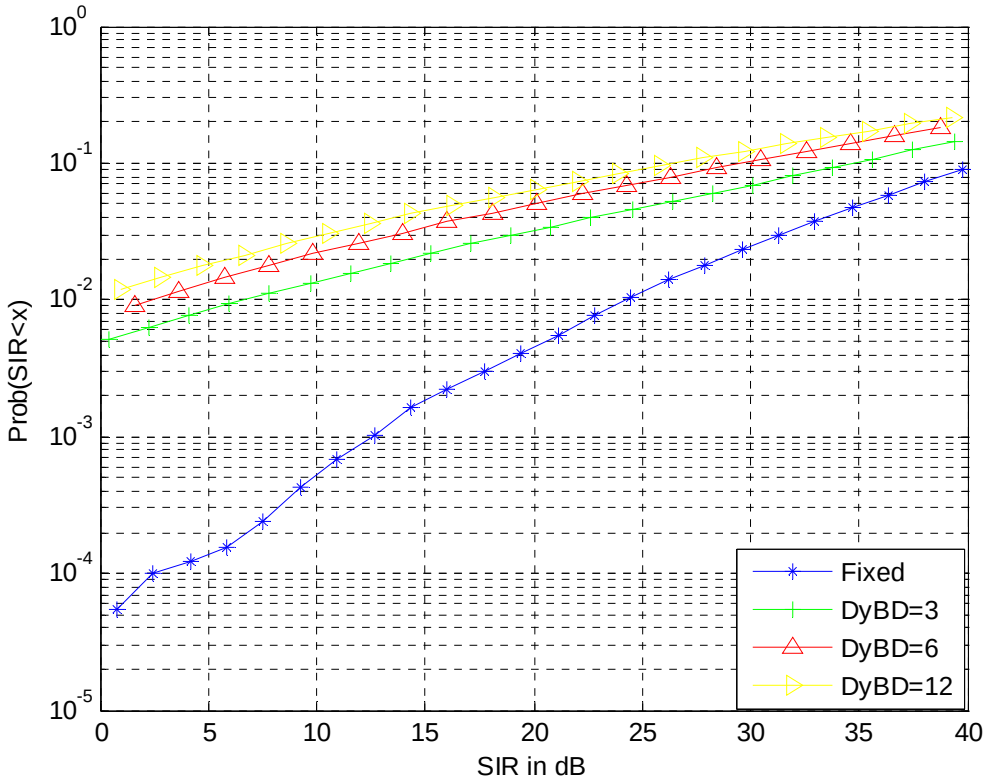

Figure 4-9: SIR outage using fifteen-sectored antennas.

The results obtained with the application of the extended *Max* {SIR} algorithm are shown in figure 4-10.

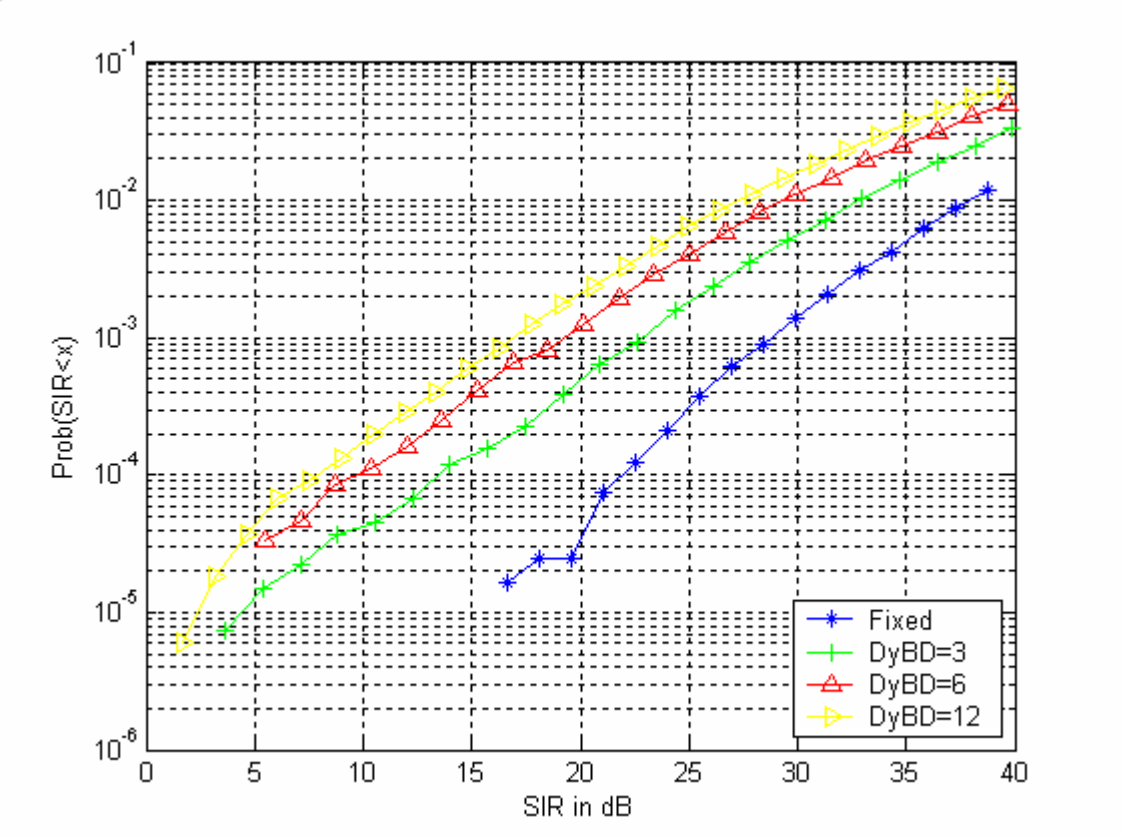

Figure 4-10: SIR outage using fifteen-sectored antennas and the extended Max {SIR} algorithm.

The application of the extended *Max* {SIR} algorithm provides a significant increase in the SIR outage performance as can be seen by comparing the figures 4-9 and 4-10. For example, at an outage of 1%, the achievable SIR is 7dB without the application of the extended *Max* {SIR} algorithm and this increases to 33 dB with the application of the extended *Max* {SIR} algorithm when the number of extra uplink TSs is 3.

4.2 Priority based D-TDD systems

The results obtained when the subscribers in a TDMA/D-TDD system were divided into different groups based on the priority assigned to each group are summarized next. A D-TDD frame having 36 TSs is considered and the first 12 TSs and the last 12

TSs are allocated to the 12 mobile stations (MSs) for uplink transmission and downlink reception respectively. The remaining 12 TSs – TS 13 to TS 24 – are allocated for uplink transmission in the reference cell and they can be allocated either for uplink transmission or downlink reception in a dynamic fashion in the co-channel cells. In the reference cell, the MS #1 is allocated to TS #13; MS #2 is allocated to TS #14 and so on. The MSs are uniformly and randomly distributed in TSs 13-24 for the co-channel cells. The MSs 1-6 are considered to belong to class one and the MSs 7-12 are considered to belong to class two. Figure 4-11 shows the result obtained when only the MSs belonging to class one are considered. The SIR outage probability is compared for the cases when there is no execution of the *Max* {SIR} algorithm and when the *Max* {SIR} algorithm is applied.

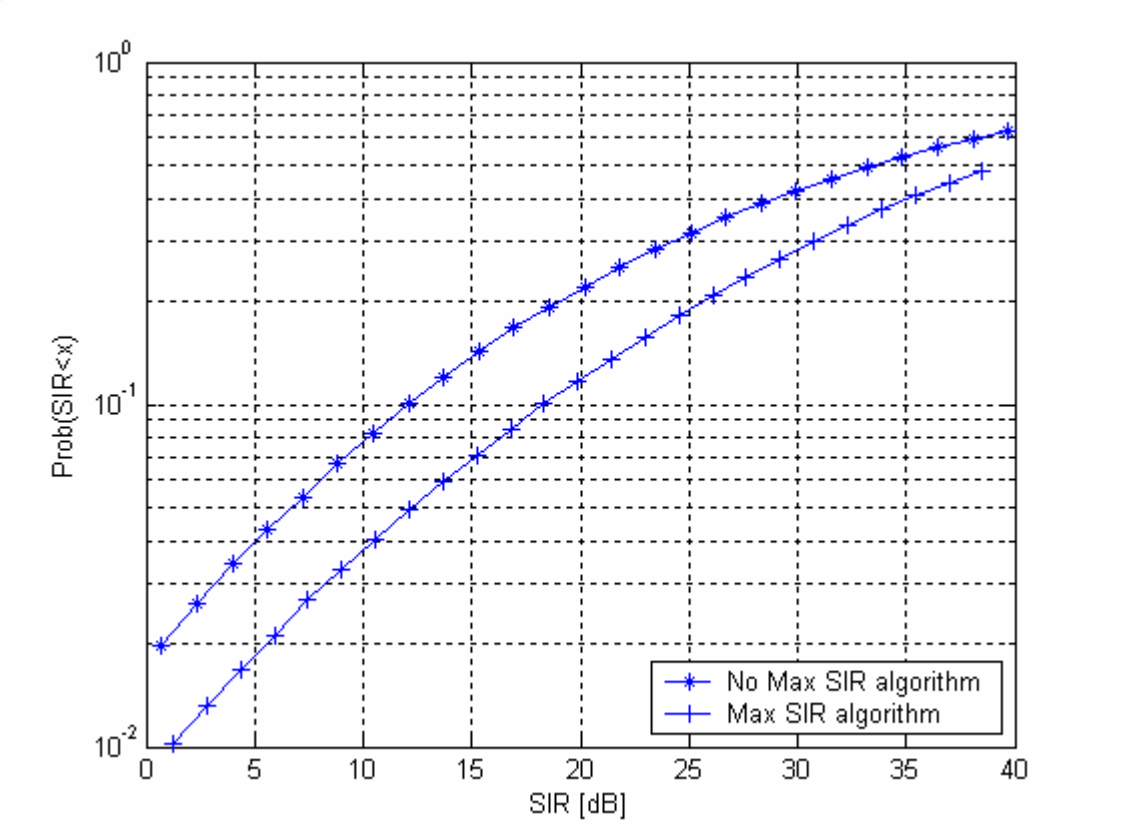

Figure 4-11: SIR outage probability of class one priority subscribers with and without the execution of the *Max* {SIR} algorithm.

From figure 4-11, it can be seen that the application of the *Max* {SIR} algorithm improves the SIR outage probability ratio. For example, at an outage of 10%, the achievable SIR increases from 12 dB with no application of the *Max* {SIR} algorithm to about 18 dB with the application of the *Max* {SIR} algorithm.

Figure 4-12 shows the result obtained when only the MSs belonging to class two are considered. The SIR outage probability is compared for the cases when there is no execution of the *Max* {SIR} algorithm and when the *Max* {SIR} algorithm is applied.

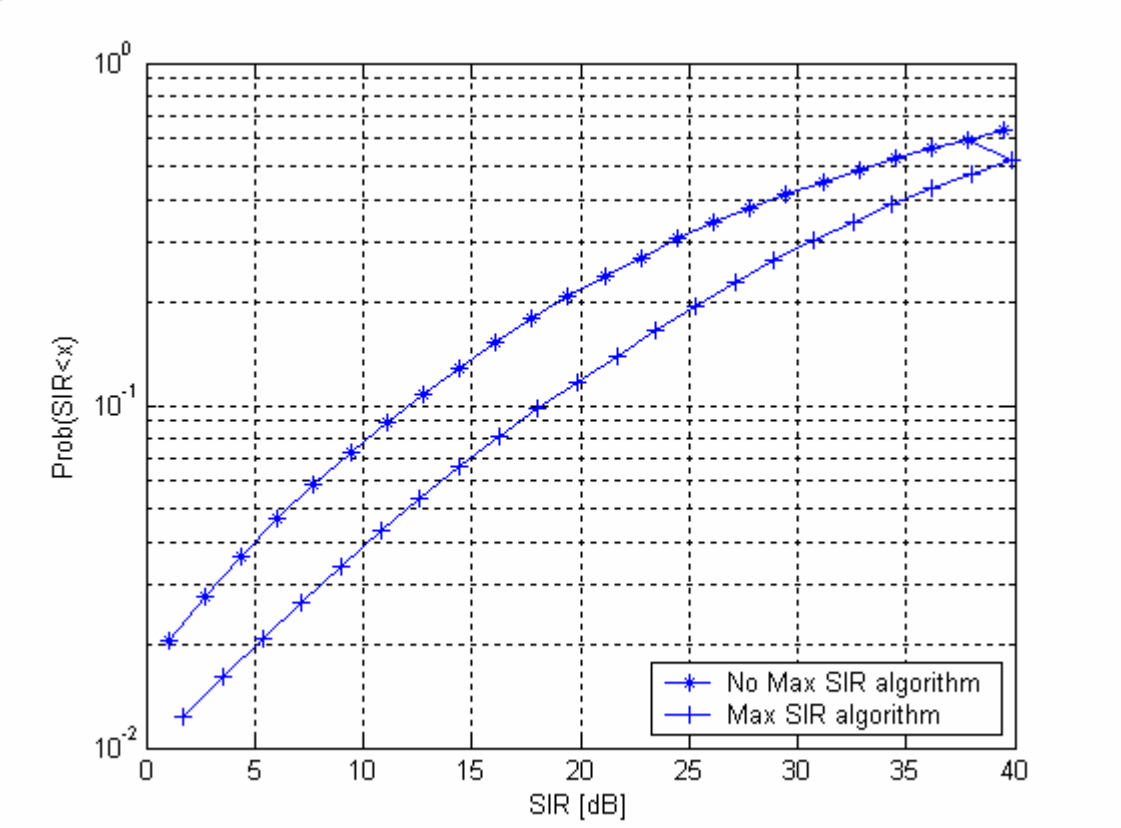

Figure 4-12: SIR outage probability of class two priority subscribers with and without the execution of the *Max* {SIR} algorithm.

From figure 4-12, it can be seen that the application of the *Max* {SIR} algorithm improves the SIR outage probability ratio. For example, at an outage of 10%, the

achievable SIR increases from 12 dB with no application of the *Max* {SIR} algorithm to about 18 dB with the application of the *Max* {SIR} algorithm.

As a final step, the subscribers belonging to both class one and class two are considered and the results obtained are shown in figure 4-13.

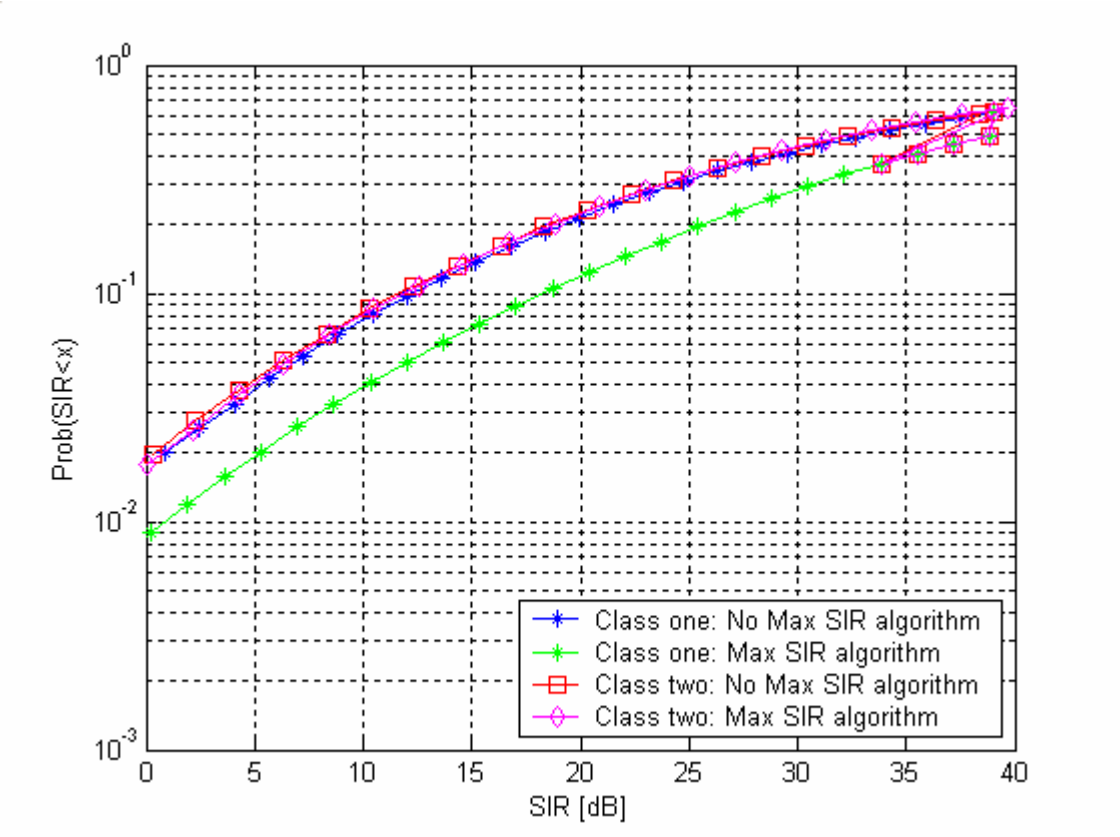

Figure 4-13: SIR outage probability of class one and class two priority subscribers with and without the execution of the *Max* {SIR} algorithm.

From figure 4-13, it can be concluded that the SIR outage probability improvement in class one subscribers is maintained but there is no improvement in the SIR outage probability of class two subscribers.

4.3 Conclusion

This chapter introduced the multi-cell D-TDD allocation algorithm and the simulations were performed when the algorithm was combined with an implementation of the sectored antennas at the BS. Four-sectored antennas and fifteen-sectored antennas were used. The results obtained showed an improvement in SIR outage probability when compared with the *Max* {SIR} algorithm. Then the analysis of D-TDDD systems with priority was carried and the results were documented.

5 SUMMARY AND FUTURE RESEARCH DIRECTIONS

5.1 Summary

The following is the list of research done in this thesis.

- D-TDD has a unique feature compared to FDD and S-TDD, in that it provides statistical multiplexing gain. The gain is due to the dynamic boundary between the uplink and downlink transmission bandwidth. The nature of emerging traffic is asymmetric and the need for D-TDD for future wireless systems was seen.
- D-TDD also causes additional interference mechanisms that are normally not present when employing FDD or S-TDD. Thus the need for DCA algorithms to suppress the additional interference in D-TDD was documented.
- The TS-opposing algorithm from [1] which is an example of a DCA algorithm was reviewed and this algorithm was found to reduce the interference in TD-CDMA/D-TDD systems and provide a corresponding increase in the capacity of the system.
- The poor performance of TDMA/D-TDD systems when omni-directional antennas are used at the BS and MS sites was explained.
    - The performance improvement in TDMA/D-TDD systems was obtained by making use of spatial filters like sectored antennas at the BS and MS sites and also by using DCA algorithms, namely the *Max* {SIR} algorithm.

- To provide a realistic performance analysis, real Ethernet data traffic must be applied. The two types of data sets used are:
    - Arrival of a million packets on an Ethernet at the Bellcore Morristown Research and Engineering facility [34].
    - Motion Picture Experts Group -4 (MPEG-4) video. The video is of a high quality *Jurassic Park 1* movie [35].

  The self-similar nature of the two data sets was proved.
- Data traffic was modeled using the simple Gaussian traffic model in S-TDD and D-TDD modes and the effect of the dynamic boundary on the spectral efficiency on these two modes was derived.

The following is the list of contributions from this research.

- Multi-cell coordinated D-TDD resource allocation for multi-cell environments was analyzed. The SIR outage probability was improved when the multi-cell D-TDD application algorithm was used when compared with the *Max* {SIR} algorithm.
- The *Max* {SIR} algorithm was expanded and applied to multiple cells. The algorithm is called the extended *Max* {SIR} algorithm. The analysis was done for the following four cases.
    - The boundary between the uplink and downlink traffic is fixed and there are no extra uplink time slots. This is similar to a FDD system
    - The boundary between the uplink and downlink traffic is made variable and the maximum number of extra uplink time slots is three.

- The boundary between the uplink and downlink traffic is made variable and the maximum number of extra uplink time slots is six.
- The boundary between the uplink and downlink traffic is made variable and the maximum number of extra uplink time slots is twelve.

- The multi-cell D-TDD application algorithm was combined with sectored antennas at the BS and high-gain antenna at the MS. The following cases were discussed.
  - Four-sectored antennas were used at the BS and high-gain antennas were used at the MS.
  - Fifteen-sectored antennas were used at the BS and high-gain antennas were used at the MS.

The extended *Max* {SIR} algorithm provides a significant increase in the SIR outage performance. For example, at an outage of 1%, the achievable SIR is 7dB without the application of the extended *Max* {SIR} algorithm and this increases to 33 dB with the application of the extended *Max* {SIR} algorithm when the number of extra uplink TSs is 3.

The significant improvement in the SIR outage performance (about 26 dB in the example case shown) might come with a small penalty. The extended *Max* {SIR} algorithm needs information from all the cells present in the system. The cells are the reference cell and the surrounding co-channel cells. The algorithm needs the signal transmission power of all the BSs and MSs in all the time slots and the path loss between the various entities. As the algorithm is executed at a higher layer in the architecture, some of the required information may be already required at this higher layer with or

without the execution of the extended *Max* {SIR} algorithm. The extended *Max* {SIR} algorithm is assumed to be executed at the Radio Network Controller (RNC) to which all the BSs are connected. The MSs report their transmission powers and path loss measurements to the BS which makes them available to the RNC. Also, the transmission powers of the BS are known and can be reported to the RNC as can be the path loss between BSs. Thus, the information needed for the execution of the extended *Max* {SIR} algorithm maybe already present at the RNC. The signaling overhead due to the execution of the *Max* {SIR} algorithm will be minimal and correspond to the number of extra uplink time slots in the cell in which the algorithm is executed. The execution of the extended *Max* {SIR} algorithm might introduce a slight latency in the system and this latency is due to the time involved in processing all the relevant information and arriving at a decision with respect to the extra uplink time slots. Also, the issue of handover between cells is not considered in our analysis.

- Priority of subscribers was introduced in the D-TDD systems. The subscribers in the D-TDD system were divided into groups based on priority and the SIR outage probability was compared with and without the application of the *Max* {SIR} algorithm.
- Traffic available from [34] was modeled as an ON-OFF traffic source and applied to a TDMA/D-TDD system employing the *Max* {SIR} algorithm. The results obtained were compared with the results obtained when the number of extra uplink time slots was modeled using the uniform density function. The results were comparable in both the cases.

5.2 Future research directions

Topics for future research in D-TDD systems are suggested in this section.

5.2.1 Call admission control for QoS guarantee

The *Max* {SIR} algorithm takes advantage of the degrees of freedom of the spatially distributed location of the subscribers. It was assumed that the subscribers were already resolved by a certain call admission control scheme. In wireless networks, a call admission control scheme allows a packet whose channel quality is good and delays a packet whose channel quality is bad. The call admission control and radio resource allocation schemes affect the QoS when both the delay-tolerant and delay-sensitive traffic are present in the network. Thus, careful consideration must be given to the design on call admission control and resource allocation schemes.

5.2.2 Algorithms for mobile networks

The strong co-channel interference is also present in mobile cellular networks. This thesis concentrated on reducing the BS-BS co-channel interference in fixed cellular networks. The SC-SC co-channel interference was suppressed by using high-gain antennas at the site of the subscriber. But mobility makes it almost impossible to deploy high-gain antennas at the subscriber in a mobile cellular network. Also, the power consumption is an important factor that must be considered in mobile networks. Thus, the simplest design suggests the deployment of omni-directional antennas at the subscriber site. But, omni-directional antennas create strong SC-SC co-channel interference when the SC in the reference cell is in downlink reception and the closest SC in the co-channel cell is in uplink reception. Thus, similar to fixed cellular networks, time slot allocation

algorithms must be considered in mobile cellular networks also. But due to the presence of SC-SC co-channel interference in the mobile networks, the objective of the time slot allocation algorithms must be modified to include the same.

5.2.3 Scalable algorithms

The *Max* {SIR} and the extended *Max* {SIR} perform the search procedure in an exhaustive fashion and hence the complexity of the algorithm increases as the number of extra uplink time slots increases. To reduce the complexity, a scalable non-exhaustive search based algorithms have to be developed.

6 REFERENCES

[1] H. Haas, and S. McLaughlin, "A Dynamic Channel Assignment Algorithm for a Hybrid TDMA/CDMA-TDD Interface using the Novel TS-Opposing Technique," *IEEE J. Select. Areas Commun.*, vol. 19, no. 10, pp. 1831-1846, Oct. 2001.

[2] H. Holma, G. J. R. Povey, and A. Toskala, "Evaluation of inference between uplink and downlink in UTRA/TDD," in *Proc. IEEE Vehic. Tech. Conf.,* vol. 5, Amsterdam, Netherlands, pp. 2616-2620, Sept. 1999.

[3] J. Li, S. Farahvash, and M. Kavehrad, "Dynamic time division duplex wireless local loop," in *Proc. IEEE Vehic. Tech. Conf.,* vol. 3, pp. 1078-1085, Sept. 2000.

[4] I. Forkel, "Performance Comparison of Radio Access technologies for the UMTS," in *Proc. Wireless Personal Multimedia Communication*, Yokosuka, Japan, Oct. 2003.

[5] Wuncheol Jeong, and M. Kavehrad, "Co-channel Interference Reduction in Dynamic-TDD Fixed Wireless Applications, Using Time Slot Allocation Algorithms," *IEEE Trans. Commun.,* vol. 50, no. 10, pp. 1627-1636, Oct. 2002.

[6] R. D. Yates, "A Framework for Uplink Power Control in Cellular Radio Systems," *IEEE J. Select. Areas Commun.,* vol. 13, no. 7, pp. 1341-1347, Sept. 1995.

[7] H. Haas, S. McLaughlin, and G. J. R. Povey, "Capacity-coverage analysis of the TDD and FDD mode in UMTS at 1920 MHz," in *Proc. IEE Commun.,* vol. 149, no. 1, pp. 51-57, Feb. 2002.

[8] H. Haas, S. McLaughlin, and G. J. R. Povey, "The Effects of Interference between the TDD and FDD node in UMTS at the boundary of 1920 MHz," in *Proc. 6th Int. Conf. Spread Spec. Tech. Appl.,* vol. 2, pp. 486-490, Sept. 2000.

[9] K.S. Gilhousen, I. M. Jacobs, R. Padovani, A. J. Viterbi, L. A. Weaver, Jr., and C. E. Wheatly, III, "On the capacity of a cellular CDMA system," *IEEE Trans. Vehic. Tech.,* vol. 40, no. 2, pp. 303-312, May 1991.

[10] H. Haas, S. McLaughlin, and G. J. R. Povey, "A novel interference resolving algorithm for the TDD TD-CDMA mode in UMTS," in *Proc. Int. Symp. Pers. Indoor and Mobile Radio Commun.,* vol. 2, pp. 1231-1235, Sept. 2000.

[11] ETSI 30.03, V3.2.0 (1998-04), "Universal mobile telecommunications system (UMTS); selection procedures for the choice of radio transmission technologies of the UMTS," TR 101 112 1998.

[12] 3rd Generation Partnership Project (3GPP), Technical Specification Group (TSG), Radio Access Network (Ran), Working Group4 (WG4), "Evaluation of up and downlink adjacent channel performance," TSGR4#2(99) 048, Feb. 1999.

[13] R. D. Yates, and C.Y. Huang, "Integrated Power Control and Base Station Assignment," *IEEE Trans. Vehic. Technol.*, vol. 44, no. 3, pp. 638-644, Aug. 1995.

[14] S. Ariyavisitakul, and L. F. Chang, "Signal and Interference Statistics of a CDMA System with Feedback Power Control," *IEEE Trans. Commun.*, vol. 41, no. 11, pp. 1626-1634, Nov. 1993.

[15] S. Ariyavisitakul, "Signal and Interference Statistics of a CDMA System with Feedback Power Control II," *IEEE Trans. Commun.*, vol. 42, no. 234, pp. 597-605, Apr. 1994.

[16] W. E. Leland, M. S. Taqqu, W. Willinger, and D. V. Wilson. "On the self-similar nature of Ethernet traffic," (extended version), *IEEE/ACM Trans. Networking*, vol. 2, no. 1, pp. 1–15, Feb. 1994.

[17] V. Paxson, and S. Floyd, "Wide-area traffic: The failure of Poisson modeling," *IEEE/ACM Trans. Networking*, vol. 3, no. 3, pp. 226–244, June 1995.

[18] M. E. Corvella, and A, Bestavros, "Self-similarity in World Wide Web traffic: evidence and possible causes," *IEEE/ACM Trans. Commun.*, vol. 5, no. 6, pp. 835-846, Dec. 1997.

[19] http://mathworld.wolfram.com/Self-Similarity.html

[20] W. Stallings, High-*Speed Networks and Internets*, 2nd ed. Pearson Education, Singapore, 2003.

[21] S. H. Hing, R. H. Park, and C. B. Lee, "Hurst parameter Estimation of Long-Range Dependent VBR MPEG Video Traffic in ATM Networks," *Journal of Visual Communication and Image Repersentation*, vo1. 12, pp. 44-65, 2001.

[22] F. H. P. Fitzek, and M. Reisslein, "MPEG-4 and H.263 video traces for network performance evaluation," *IEEE Network*, vol. 15, no. 6, pp. 40-54, Nov. 2001.

[23] J. C.-I. Chuang, "Performance limitations of TDD wireless personal communications with asynchronous radio ports," *Electron. Lett.*, vol. 28, pp. 532–534, Mar. 1992.

[24] T. S. Rappaport, *Wireless Communications—Principles and Practice*. Englewood Cliffs, NJ: Prentice-Hall, 1996.

[25] A. Papoulis, *Probability, Random Variables, and Stochastic Processes*, 3rd ed. NY: McGraw-Hill, 1991.

[26] P. Chaudhury, W. Mohr, and S. Onoe, "The 3GPP proposal for IMT-2000," *IEEE Commun. Mag.*, vol. 37, pp. 72 -81, Dec. 1999.

[27] C. You and K. Chandra, "Time series models for Internet data traffic," *Conf. on Local Computer Networks*, 1999, pp. 164-171 Oct 1999.

[28] M. Jiang, M. Nikolic, S. Hardy, and L. Trajkovic, "Impact of self-similarity on wireless data network performance," in *Proc. IEEE ICC'01*, vol. 2, pp. 11-14, June 2001.

[29] W. Willinger, M. S. Taqqu, W. E. Leland, and D. V. Wilson, "Self-similarity in high-speed packet traffic: analysis and modeling of Ethernet traffic measurements," *Statistical Science*, vol. 10, no. 1, pp. 67 - 85, 1995.

[30] C. Partridge, "The end of simple traffic models," *IEEE Network*, vol. 7, no. 5, p. 3, Sept. 1993.

[31] V. Paxson, "Empirically derived analytic models of wide-area TCP connections," *IEEE/ACM Trans. Networking*, vol. 2, no. 4, pp. 316 - 336, Aug. 1994.

[32] Y. Argyropoulos, S. Jordan, and S. P. R. Kumar, "Dynamic channel allocation in interference-limited cellular Systems with Uneven Traffic Distribution," *IEEE Trans. Vehic. Technol.*, vol. 48, no. 1, pp. 224-232, Jan. 1999.

[33] R. Beck, and H. Penzer, "Strategies for handover and dynamic channel allocation in micro-cellular mobile system," in *Proc. IEEE Vehic. Tech. Conf.*, vol. 1, San Francisco, pp. 178-185, May 1989.

[34] http://ita.ee.lbl.gov/html/contrib/BC.html

[35] http://www-tkn.ee.tu-berlin.de/research/trace/stat.html

[36] W. C. Y. Lee, "Overview of cellular CDMA," *IEEE Trans. Vehic. Tech.*, vol. 40, no. 2, pp. 291-302, May 1991.

[37] P. K. Saha, M. M. Hossain, M. F. M. Hossian, and S. A. Haider, "Reduction of co-channel interference in a mobile system by antenna parameter optimization," *Int'l Symp. On Electromagnetic Compatibility*, vol. 1, pp. 303-307, Aug. 2002.

[38] T. Mayer, C. Robertson, and T. T. Ha, "Co-channel interference reduction on the forward channel of a wideband CDMA system," in *Proc. IEEE MILCOM '99*, vol. 1, pp. 585-589, Nov. 1999.

[39] A. A. Saleeb, "Design of a smart antenna for reducing co-channel interference in cellular mobile communication," *Int'l Symp. On Antennas and Prop.*, vol. 3, pp. 1620-1623, July 1999.

[40] S. Moshave, "Multi-user detection for DS-CDMA communications," *IEEE Commun. Mag.*, vol. 34, pp. 124 -136, Oct. 1996.

[41] A. Duel-Hallen, J. Holtzman, and Z. Zvonar, "Multi-User Detection for CDMA systems," *IEEE Pers. Commun.*, vol. 2, no. 2, pp. 46-58, Apr. 1995.

[42] K-N. Chang, J-T. Kim, C-S. Yim, and S. Kim, "An efficient borrowing channel assignment scheme for cellular mobile systems," *IEEE Trans. Vehic. Tech.*, vol. 40, no. 2, pp. 602-608, May 1998.

[43] C. Mihailescu, X. Lagrange, and P. Godlewski, "Dynamic resource allocation for packet transmission in TDD TD-CDMA systems," in *Proc. IEEE Vehi. Tech. Conf.*, vol. 2, pp. 1737-1741, May 1999.

[44] L. Anderson, "A Simulation study of some dynamic channel assignment algorithms in a high capacity Mobile Telecommunication sustem ," *IEEE Trans. Commun.*, vol. 21, no. 11, pp. 1294-1301, Nov. 1973.

[45] S. M. Shin, C.-H. Cho, and D. K. Sung, "Interference-based channel assignment for DS-CDMA cellular systems," *IEEE Trans. Vehic. Tech.*, vol. 48, no. 1, pp. 233–239, Jan. 1999.

[46] W. C. Y. Lee, *Mobile Cellular Telecommunications Systems*. New York: McGraw-Hill, 1989.

[47] J. Zander, "Generalized reuse partitioning in cellular mobile radio," in *Proc. IEEE Vehic. Tech. Conf.*, 1993, pp. 181–184.

[48] Y. Argyropoulos, S. Jordan, and S. P. R. Kumar, "Dynamic channel allocation in interference-limited cellular systems with uneven traffic distribution," *IEEE Trans. Vehic. Tech.*, vol. 48, no. 1, pp. 224–232, Jan. 1999.

[49] H. Haas, S. McLaughlin, and G. J. R. Povey, "An investigation on capacity versus guard-bands in the TDD mode of UMTS," in *Proc. IEEE Vehic. Tech. Conf.*, vol. 4, pp. 1820-1824, Sept. 2000.

[50] J. Li, S. Farahvash, M. Kavehrad, and R. Valenzuela, "Dynamic-TDD and fixed cellular networks," *IEEE Commun. Lett.*, vol. 4, pp. 218–220, July 2000.

[51] Wuncheol Jeong, and M. Kavehrad, "Spectral efficiency of time division duplex fixed wireless cellular system for dynamic traffic," in *Proc. IEEE Vehic. Tech. Conf.*, vol. 2, pp. 907-911, Oct. 2003.

[52] E. A. Wolff, *Antenna Analysis*, 2nd ed. Norwood, MA: Artech House, 1988.

[53] Wuncheol Jeong, M. Kavehrad, and J. Yun, "Spectral Efficiency of Dynamic Time Division Duplex Fixed Wireless Cellular System for Asymmetric and Dynamic Multimedia Traffic," *Int'l J. Wireless Information Networks*, vol. 11, no. 4, pp. 173-185, Oct. 2004.

[54] M. –S. Alouini, and A. J. Goldsmith, “Area spectral efficiency of cellular mobile radio systems,” *IEEE Trans. Vehic. Technol.,* vol. 48, no. 4, pp. 1047-1066, July 1999.

[55] R. Muammar, and S. C. Gupta, “Co-channel interference in high-capacity mobile radio systems,” *IEEE Trans. Commun.,* vol. 30, pp. 1973 - 1978, Aug. 1982.

[56] P. Petrus, R. B. Ertel, and J. H. Reed, “Capacity enhancement using adaptive arrays in an AMPS system,” *IEEE Trans Vehic. Tech.,* vol. 47, no. 3. pp. 717-727, Aug. 1998.

[57] L. Fenton, “The sum of Lognormal Probability Distributions in Scatter Transmissions,” *IEEE Trans. Commun.,* vol. 8, pp. 42-52, March. 1960.

[58] S. C. Schwartz, and Y. S. Yeh, “On the Distributions and Moments of Power Sums with Lognormal Interferers, “ *Bell Sys Tech, Jnl.,* vol. 61, pp. 1441-1462, Sep. 1982.

[59] H. Michiel, and K. Laevens, “Teletraffic Engineering in a broad-band era,” in *Proc. IEEE,* vol. 85, no. 12, pp. 2007-2033, Dec. 1997.

[60] W. Willinger, M. S. Taqqu, R. Shermen, and D. V. Wilson, ”Self-Similarity Through High-Variability: Statistical Analysis of Ethernet LAN Traffic at the Source Level,” in *Proc. ACM SIGCOMM’ 95,* pp. 100-113, 1995.

[61] R, B. D’Agostino, and M. A. Stephens, *Goodness-of-fit-Techniques,* Marcel Dekker, 1986.

[62] D. C. Cox, “Universal Digital Portable Radio Communications,” in *Proc., IEEE,* vol. 27, no. 4, pp. 436-477, April 1987.

[63] C. E. Shannon, “A Mathematical Theory of Communication, “ *Bell Sys Tech, Jnl.,* vol. 61, pp. 379-423 and pp.623-656, July and Oct. 1948.

VITA

Rajpamal R. Pethuraj

Candidate for the Degree of

Doctor of Philosophy

Thesis: ADATIVE RESOURCE ALLOCATION STRATEGIES FOR DYNAMIC HETEROGENOUS TRAFFIC IN TD-CDMA/TDD SYSTEMS

Major Field: Electrical Engineering

Biographical:

Education: Received a Bachelor of Engineering degree in Electronics and Communication Engineering from the Bharathiar University, India in May 1999. Received a Master of Science degree in Electrical and Computer Engineering from the Oklahoma State University in August 2001. Completed the requirements for the Doctor of Philosophy degree with a major in Electrical and Computer Engineering at the Oklahoma State University in May 2006.

Experience: Employed as a Research Assistant by the ACSEL Laboratories at the School of Electrical and Computer Engineering, Oklahoma State University, Aug. 2000 to present.
Employed as a Teaching Assistant in the FORTRAN Lab at the School of Electrical and Computer Engineering, Oklahoma State University, Jan. 2000 to May 2001.
Employed as a Teaching Assistant in the Embedded System Design Lab at the School of Electrical and Computer Engineering, Oklahoma State University, Jan. 2000 to Dec 2000.
Employed as a Teaching Assistant for the courses of Stochastic Systems, Telecommunication Systems, and Communication Theory at the School of Electrical and Computer Engineering, Oklahoma State University, Jan. 2002 to May 2004.

Professional Membership: Student member of the honorary Institute of Electrical and Electronics Engineers, Inc. (IEEE) from the academic year of 2000.

Name: Rajpamal R. Pethuraj Date of Degree: May, 2006

Institution: Oklahoma State University Location: Stillwater, Oklahoma

Title of Study: ADATIVE RESOURCE ALLOCATION STRATEGIES FOR DYNAMIC HETEROGENOUS TRAFFIC IN TD-CDMA/TDD SYSTEMS

Pages in Study: 147 Candidate for the Degree of Doctor of Philosophy

Major Field: Electrical Engineering

Scope and Method of Study: The purpose of this study was to investigate the co-channel interference present in TD-CDMA/TDD systems and TDMA/TDD systems and propose methods to avoid the co-channel interference. Time Slot Opposing algorithm which avoids co-channel interference in TD-CDMA/D-TDD system is reviewed as part of background study. The interference scenarios in TDMA/D-TDD systems are then studied and methods to avoid co-channel interference are proposed. The algorithms are then tested using real Internet data traffic to obtain a realistic analysis.

Findings and Conclusions: Based on the background research, an extended *Max* {SIR} algorithm is proposed to avoid co-channel interference in TDMA/D-TDD systems. This algorithm is a centralized dynamic channel allocation algorithm that uses information from all the cells in the system to avoid co-channel interference and increase the signal power-to-interference power outage probability ratio. The proposed algorithm is then applied to a TDMA/D-TDD system that have subscribers grouped based on priority. As a last step of the research, traffic in TDMA/D-TDD systems is modeled using the ON-OFF traffic modeling and the *Max* {SIR} algorithm is applied. The results obtained using ON-OFF traffic modeling matched with the results obtained using analytical simulations.

ADVISOR'S APPROVAL Dr. Keith A Teague